

TITANIA NANOSTRUCTURES FOR CATALYTIC AND SOLAR CELL APPLICATIONS

*Thesis Submitted to the
Calicut University, Malappuram
in Partial Fulfillment of the requirements
for the award of the degree of
Doctor of Philosophy
in Chemistry
under the Faculty of Science*

by

VIJILA KALARIVALAPPIL

Under the supervision of
Dr. V. Kumar, Senior Scientist



Centre for Materials for Electronics Technology (C-MET)
(Scientific Society, Department of Information Technology,
Ministry of Communication and Information Technology, Govt. of India)
Shornur Road, M. G. Kavu, Athani P.O., Thrissur 680 581, Kerala, India.
Email: cmett@cmet.gov.in URL: wwwcmett.gov.in

May 2018

Titania Nanostructures for Catalytic and Solar Cell Applications

Ph D Thesis under the Faculty of Science

Submitted by

Vijila Kalarivalappil,
Sivasakthi, Malliyote
Kunhimangalam P.O.,
Kannur-670309
Kerala, India.
e-mail: vijilakv@gmail.com

Research Supervisor

Dr. V. Kumar
Scientist F
Centre for Materials for Electronics Technology (C-MET)
Thrissur- 680 581
Kerala, India
e-mail: vkumar@cmet.gov.in

May 2018

Format for plagiarism check certificate

UNIVERSITY OF CALICUT
CERTIFICATE ON PLAGIARISM CHECK

1.	Name of the research scholar	Vijila Katarivalappil		
2.	Title of thesis/dissertation	Tibania Nanostructures for Catalytic and Solar Cell Applications		
3.	Name of the supervisor	Dr. V. Kumar		
4.	Department/Institution	C-MET, Thrissur		
5.	Similar content (%) identified	Introduction/ Review of literature	Materials and Methods	Result/ Discussion/Summary/ Conclusion
		03%	05%	02%
	Acceptable maximum limit (%)	25/35	25	10
6.	Software used	iQkund		
7.	Date of verification	7.4.2018		

*Report on plagiarism check, specifying included/excluded items with % of similarity to be attached.



Checked by (with name, designation & signature)

Name & Signature of the Researcher *Vijila Katarivalappil*

Name & Signature of the Supervisor *Dr. V. Kumar*

Dr. ABDUL KADIR
University Librarian
C.H. Mohammed Koya Library
University of Calicut
Calicut University, I.C.O.
Kerala PIN- 673635

The Doctoral Committee* has verified the report on plagiarism check with the contents of the thesis, as summarized above and appropriate measures have been taken to ensure originality of the Research accomplished herein.

Name & Signature of the HoD/HoI (Chairperson of the Doctoral Committee)



डॉ. एन. राघु
Dr. N. RAGHU
Director
C-MET (MeitY, Govt. of India)
अथानि पोस्ट/Athani P.O., एम.जी. कावु /M.G. Kavu
त्रिश्शूर - 680 581 / Thrissur - 680 581
केरला/ Kerala

*In case of languages like Malayalam, Hindi, etc. on which no software is available for plagiarism check, a manual check shall be conducted by the Doctoral Committee, for which an additional certificate has to be attached.



सेन्टर फॉर मेटिरियल्स फॉर इलेक्ट्रॉनिक्स टेक्नोलॉजी (सी-मेट)

(वैज्ञानिक संस्था, इलेक्ट्रॉनिक्स और सूचना प्रौद्योगिकी मंत्रालय, भारत सरकार)

षोरनूर रोड, मुलंगुन्नतुकावु पोस्ट, अत्तानि, त्रिशूर - 680 581, केरला, भारत

CENTRE FOR MATERIALS FOR ELECTRONICS TECHNOLOGY

(Scientific Society, Ministry of Electronics and Information Technology, Government of India)

Shoranur Road, P.O. Mulangunnathukavu, Athani, Thrissur - 680 581, Kerala, India

Tel : EPABX : 91-487-2201156-59 (4 LINES). Fax : 91-487-2201347

E-mail : cmett@cmet.gov.in URL : www.cmet.gov.in

Dr. V. Kumar

Scientist F

Certificate

This is to certify that the thesis entitled “**Titania Nanostructures for Catalytic and Solar Cell Applications**” submitted to Calicut University in partial fulfilment of the requirements for the award of the degree of *Doctor of Philosophy in Chemistry* under the Faculty of Science, Calicut University, Malappuram is a record of the authentic work carried out by Smt. Vijila Kalarivalappil, at Centre for Materials for Electronics Technology, Thrissur, under my guidance. The work presented in this thesis has not been submitted for any other degree or diploma of this or any other University.

Thrissur

Dr. V. Kumar
(Supervising Guide)

Declaration

I hereby declare that the thesis entitled “**Titania Nanostructures for Catalytic and Solar Cell Applications**” submitted to Calicut University, is based on the original research work carried out by me under the guidance and supervision of Dr. V. Kumar, Senior Scientist, Centre for Materials for Electronics Technology, Thrissur. No part of this work has been presented for the award of any other degree from any other institution.

Thrissur

Vijila Kalarivalappil



सेन्टर फॉर मेटिरियल्स फॉर इलेक्ट्रॉनिक्स टेक्नोलॉजी (सी-मेट)

(वैज्ञानिक संस्था, इलेक्ट्रॉनिक्स और सूचना प्रौद्योगिकी मंत्रालय, भारत सरकार)

षोरनूर रोड, मुलंगुन्नतुकवु पोस्ट, अत्तानि, त्रिशूर - 680 581, केरला, भारत

CENTRE FOR MATERIALS FOR ELECTRONICS TECHNOLOGY

(Scientific Society, Ministry of Electronics and Information Technology, Government of India)

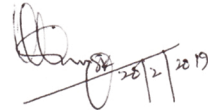
Shoranur Road, P.O. Mulangunnathukavu, Athani, Thrissur - 680 581, Kerala, India

Tel : EPABX : 91-487-2201156-59 (4 LINES). Fax : 91-487-2201347

E-mail : cmet@cmct.gov.in URL : www.cmet.gov.in

20-02-2019

This is to certify that all the corrections/ suggestions from the adjudicators have been incorporated in the thesis entitled "TITANIA NANOSTRUCTURES FOR CATALYTIC AND SOLAR CELL APPLICATIONS" submitted by Vijila Kalarivalappil to Calicut University. The content in CD and hard copy is same.


20/2/2019
Dr. V. KUMAR, Research Supervisor

Dr. V. Kumar
Scientist
Centre for Materials for Electronics
Technology (C-MET), DIT, Govt. of India
Mulangunnathukavu, Athani,
Thrissur-680 581

Dedicated to the loving memories of my father

Acknowledgments

I have great pleasure to express my deep sense of gratitude to Dr. V Kumar, my thesis supervisor, for suggesting the research problem and for his valuable guidance, leading to the successful completion of this work. I am greatly indebted to him for his keen interest in my work and guidance which served considerably to increase my level of confidence and freedom of thought.

I express my sincere thanks to former Executive Director of C-MET, Dr. D. P. Amelnerker, and former Director of C-MET, Thrissur, Dr. K. R. Dayas for allowing me to use the facilities in the institute. I wish to acknowledge Dr. N. Raghu, Director of C-MET, Thrissur for the encouragement and support given to me during my research.

I don't have enough words to express my gratitude to Dr. K.V. Baiju for the intellectual support and encouragement he has given to me throughout my research work. Also for the imotional support he extended to me as husband during the critical situations in my life.

I would like to express my sincere thanks to Dr. R. Ratheesh, Dr. N. C. Pramanik, Dr. S. N Potty, Dr. A. Seema, Dr. Radhika, Dr. Stanly Jacob, and Dr. K. P. Murali for their valuable suggestions and support. Also, I am grateful to all support staffs of C-MET, Thrissur for their constant support.

I am taking this opportunity to thank the Principal of Indian Naval Academy, Rear Admiral Amit Vikram for his encouragement and support during my research. I really inspired by his concern and care he extended to me. Also I remember with gratitude the Head of faculty of BSH Cmdr Arul G Selvam and Head of Department Cdr A.K.Desai, for their encouragement and support during my PhD work. I always cherished by the concern and support given by Oi/C Lt Jagriti Sharma. Also I would like to thank our new JSO S R Gangawane and my colleagues at Indian Naval Academy, Mrs Divya K, Mrs Aneetta Simon T, Mrs Sangeetha M, Mrs Manjula M K, Mr.Sreekanth B.

Patil, Mr Saneesh, Mrs Reshma Ravindran, Mrs Vidya Raveendran, Mrs Sharanya, Mr Shaji, Mr Sreenath S S, Mr Vivek VS and Miss Rohini T G. for their constant encouragement during my work.

I am extremely pleased to express my indebtedness to Dr. Suresh C Pillai Nanotechnology Research Group, Department of Environmental Sciences, Institute of Technology Sligo, Ireland and Steven J. Hinder, The Surface Analysis Laboratory, Department of Mechanical Engineering Sciences, University of Surrey, Guildford, Surrey GU2 7XH, U.K. for supporting the work with XPS analysis facility.

I take this opportunity to thank Mr. Anil Kumar A., administrative officer and Mr. Ramdas, Finance officer for their sincere help throughout the research work. It is with great pleasure that I would like to thank Administrative Staff for their constant support and care.

I also take this opportunity to express my sincere thanks towards Mrs. Priyadarsini V., Mr. Sivanandan, Dr. Anto Jhony T. and Dr. Ambika D. for their strong support and love. Also I would like to express my gratitude to Satheesan sir for true motivation and Mr. Sathyanarayanan for his care and support during my work.

Now I am taking this opportunity to thank my colleagues Dr. Vani K., Dr. Divya. A.S., Mr. Anil A., Mr. Manoj N. and Mrs Laxmi priya S. for their support and care throughout my work. I also extend my thanks to Mrs Rahana N.B., Mrs Unnimaya N., Prabeesh P. and Suresh, Mrs. Shalet A.B., S Gopakumar, Mr. Vinoj and Mr. Rohith, who helped me directly or indirectly during the tenure of my work.

Above all I remember Almighty who gave me internal strength and knowledge to fulfill the work and finally, I remember with gratitude my parents and all other family members who were always a source of strength and support especially my mother and my son Sidharth who suffered a lot during my research work.

Vijila Kalarivalappil

PREFACE

In the present era, environmental pollution and depletion of conventional energy resources are the two major problems for human beings. Semiconductor-based photocatalysis and solar cells have received considerable attention as alternative approaches for solar energy harvesting. The wide band gap semiconducting oxide acts as the photoanode for dye sensitized and quantum dot sensitized solar cells, which provides the scaffold for light harvesters (either dye molecules or quantum dots) and electron collection. The performance of these semiconductors as photocatalyst and photoanode is closely related to the design of these materials at the nanoscale. Among various nanostructures, one-dimensional (1D) nanostructured photocatalysts and photoelectrodes have attracted increasing interest owing to their distinct optical, structural, and electronic advantages. Optimization of the functional properties relies with modulation of the shape and structure of the photoanode, as well as on application of different materials (TiO_2 , ZnO , SnO_2) and/or composite systems, which allow fine tuning of electronic band structure. This aspect is critical because it determines exciton and charge dynamics in the photoelectrochemical system and is strictly connected to the photoconversion efficiency of the solar cell. Being an ecofriendly and chemically stable material, TiO_2 nanostructures have been widely studied for the last several years. However, the wide band gap (>3.0 eV) of TiO_2 restricts its utilization of the visible light in the solar spectrum, and the low charge-mobility often leads to the high recombination rate of photogenerated electrons and holes in TiO_2 nanoparticles. So the one-dimensional (1D) nanostructures including nanorods, nanoneedles, nanotubes, nanofibers and nanowires of titania can be used for the efficient electron transportation by serving as an electron express way along the axial direction with a shorter collection time. Nowadays Titania nanotubes (TNT) are widely used in dye sensitized solar cells because of its peculiar properties such as high transport rate of electrons from the adsorbed photo excited dye to the Ti electrode onto which TNT are attached compared to titania nano particle (TNP). So it is expected that the peculiar and regular texture of TNT definitely improve the photocatalytic efficacy for pollutant removal in air and water with respect to TNP. There are different methodologies

for improving the activity of photocatalyst and photoanode efficiency. The various methods of photocatalyst engineering include synthesis of heterojunctions of semiconductors with correct band alignment, which enhance charge separation by electron or hole transfer from one semiconductor to another (or to a metal), facet engineering strategies such that electrons and holes are driven toward different surfaces, doping with different elements such as metals and nonmetals and another important methodology is the quantum confinement which is purely a size effect.

First chapter describes general introduction to nanomaterials, titania the most widely experimented photocatalyst and photoanode material. Then it describes the process of photocatalysis and factors affecting photocatalysis and different synthesis methods for titania nanotubes. Also it covers the literatures related to titania nanotube as a photocatalyst and chalcogenide sensitized titania nanotube for solarcell applications. Finally it explains the advantages of chalcogenide quantum dots and importance of one dimensional nano structures for channeled electron flow. At the end motivation of the present work is also included.

Chapter-2 discusses the various synthesis methods and characterization techniques used to characterize the photocatalyst and photoanode materials. Also, this chapter discusses the theory of some of the important characterization techniques like X-ray powder diffraction (XRD), Raman spectroscopy, UV- Visible absorption spectroscopy, Photoluminance Spectroscopy, BET surface area analysis, surface characterization techniques such as SEM, TEM and X-ray Photoelectron spectroscopy (XPS) .

Third chapter describes the role of titania nanotube, as a catalyst support for Pd metal particle. One of the major limitations of the catalytic reaction is the separation and distribution of the catalyst. These issues are effectively addressed by using various catalyst support to immobilize the particle in heterogeneous catalysis. In our study Pd nanoparticles decorated titania nanotubes are prepared by hydrothermal technique, also we investigated the role of palladium nanoparticle loading on titania nanotubes on the catalytic reduction of p-nitophenol. The catalytic properties of palladium loaded titania

nanotubes were systematically examined by studying the reduction of p-nitrophenol with sodium borohydride (NaBH_4) to p-aminophenol. The current investigation revealed that there is an optimum loading for metal nanoparticles to be more catalytically active. Also the morphology as well as the crystalline phase of the titania nanotube is found to play an important roles in their catalytic activity.

The major factors which restrict many practical applications of widely used semiconductor titania are the rapid charge recombination of the electron-hole pairs, thereby suppressing the quantum efficiency, and the wide band gap of the material, which restricts light absorption only to UV region of solar spectrum. In this scenario sensitisation of wide band gap semiconductors with those having a smaller band gap is receiving considerable attention for enhanced solar cell and photocatalytic applications through the effective utilization of solar radiation. Here the fourth chapter describes the synthesis of PbS sensitized titania nanotube by SILAR method and the effect of coating cycle on its photocatalytic and solarcell applications. Also it studied the stability of PbS sensitized titania as a photocatalyst by studying the recyclability of the photocatalyst and we correlated the results of photocatalytic activity to the observed changes in XPS results.

In chapter five we reported titania nanotubes sensitized with CdS nanoparticles of different sizes prepared using the successive ionic layer (SILAR) deposition method. The red shift in the UV/visible spectra indicates CdS absorption upon increasing the number of SILAR cycles may be due to an increase in CdS particle size. The stability of CdS particle sensitized on the surface of titania nanotubes were monitored using X-ray photoelectron spectroscopy (XPS). The formation of CdSO_4 species on the surface of CdS particles was evident from the XPS analysis. Smaller CdS particles, formed using a lower number of SILAR cycles, are more prone to oxidation than the larger particles formed using a greater number of SILAR cycles. The photocatalytic activity and solar cell efficiency are found to be dependent on the number of SILAR cycles employed.

CONTENTS

Chapter 1: Introduction to Titania Nanostructures -----	1-52
1.1 Introduction -----	2
1.2 Titanium Dioxide -----	3
1.2.1 TiO ₂ Photocatalysis -----	6
1.2.2 TiO ₂ as Catalyst Support -----	8
1.3 Anatase – Rutile Phase Transformation -----	8
1.4 1D-Nanostructures -----	10
1.4.1 Titania Nanotubes -----	10
1.4.2 Methods for Synthesis of Titania Nanotubes -----	11
1.4.2.1 Hydrothermal Method -----	11
1.4.2.2 Template Assisted Synthesis -----	12
1.4.2.3 Anodized Titania Nanotubes -----	13
1.5 Semiconductor Photocatalysis -----	17
1.6 Influence of Operational Parameters -----	20
1.6.1 Light Intensity -----	20
1.6.2 Nature and Concentration of the Substrate -----	21
1.6.3 Nature of the Photocatalyst -----	22
1.6.4 Influence of Particle Size on Band-gap Modulation -----	22
1.6.5 Concentration of Photocatalyst -----	23
1.6.6 Effect of pH -----	23
1.6.7 Reaction Temperature -----	24
1.7 Literature Review: Titania Nanotube as Photocatalyst -----	25
1.8 1D-Nanostructures in Dye Sensitized Solar Cells (DSSC) -----	29
1.9 Chalcogenide Sensitized Titania for Solar Cell Applications -----	31
1.9.1 Advantages of Quatumdots as Sensitizers -----	34

1.9.1.1	Tunable Energy Gaps-----	35
1.9.1.2	Multiple Exciton Generation -----	36
1.10	Motivation of the Present Study -----	37
	References-----	39
Chapter 2:	Experimental and Characterization Techniques -----	53-75
2.1	Hydrothermal Synthesis of Titania Nanotube -----	55
2.2	Anodization Process -----	56
2.3	SILAR Method of Deposition-----	57
2.4	Photoactivity Evaluation Study -----	58
2.5	Fundamental Characterisation Techniques-----	62
2.5.1	X- ray Diffraction- Determination of Crystalline Structure-----	62
2.5.2	Raman Spectroscopy -----	65
2.5.3	UV-Visible Spectroscopy -----	66
2.5.4	XPS Spectroscopy -----	68
2.5.5	PL Spectroscopy -----	69
2.5.6	BET – Surface Area Analysis -----	70
2.5.7	Scanning Electron Microscopy -----	72
2.5.8	Transmission Electron Microscopy -----	73
	References-----	75
Chapter 3:	Pd loaded TiO₂ Nanotubes for the Effective Catalytic Reduction of p-Nitrophenol -----	77-106
3.1	Introduction-----	78
3.2	Experimental -----	80
3.3	Results and Discussion-----	83
3.4	Conclusions-----	100
	References-----	102

Chapter 4: PbS Sensitised TiO₂ Nanotube Arrays for Visible Light Photocatalytic Applications	107-134
4.1 Introduction	108
4.2 Experimental	110
4.2.1 Deposition of PbS on Titania Nanotube	110
4.3 Result and Discussions	113
4.4 Conclusions	129
References	130
Chapter 5: CdS Sensitized TiO₂ Nanotube Arrays for Enhanced Photocatalytic Applications	135-171
5.1 Introduction	136
5.2 Experimental	138
5.3 Results and Discussion	142
5.4 Conclusions	164
References	166
Highlights of the Present Work	173-174
List of Research Publications	175-176

LIST OF TABLES

Table 1.1	Typical properties of TiO ₂ -----	6
Table 3.1	Comparitive evaluation of catalytic activity of Pd loaded titania nanotube samples-----	92
Table 4.1	Comparison of the photoactivity of PbS sensitised semiconductor system-----	126
Table 4.2	Parameters obtained from J-V curve of the PbS sensitized titania nanotube-----	128
Table 5.1	Parameters obtained from J-V curve of the CdS sensitized titania nanotubes-----	161

LIST OF FIGURES

Figure 1.1	Unit cells of anatase and rutile titania -----	4
Figure 1.2	Crystal structure of anatase and rutile titania -----	5
Figure 1.3	Electron-hole separation in anatase/ rutile heterostructure and their band alignment-----	7
Figure 1.4	The anodization setup for titania nanotube synthesis -----	14
Figure 1.5	Features of titania nanotubes with reported dimensions -----	16
Figure 1.6	SEM images of titania nanotubes synthesized by anodization of titania metal sample at 40V -----	17
Figure 1.7	Schematic diagram of photocatalytic process initiated by photon on the semiconductor-----	19
Figure 1.8	Schematic diagram of DSSC-----	29
Figure 1.9	Schematic of electron diffusion between (A) sintered spherical nanoparticles and (B) one-dimensional (1-D) nanostructures. (C) shown in the box explains how reduction of diameter of the 1-D structure make the electron flow more channelled -----	31
Figure 1.10	Multiple-carrier generation in QDs: a high-energy photon is absorbed at a high energy level in the QD, which then decays into two or more electron-hole pairs at the first confined energy level-----	36
Figure 2.1	Hydrothermal setup for the synthesis of titania nanostructures-----	55
Figure 2.2	Anodization setup for the synthesis of titania nanotubes -----	56
Figure 2.3	Schematic representation for sensitization of titania nanotube with chalcogenide by SILAR method-----	58
Figure 2.4	Chemical structure of methylene blue and degradation profile of MB in presence of photocatalyst -----	59
Figure 2.5	Schematic representation of the photocatalytic reactor -----	60
Figure 2.6	The transmittance spectra of the polycarbonate sheet along with glass sheet -----	61
Figure 2.7	Emission spectra of the mercury lamp after the filtration with polycarbonate and glass sheet -----	61
Figure 2.8	X-ray Diffractometer -----	62

Figure 2.9	X-ray diffraction from different crystal planes-----	63
Figure 2.10	Raman Spectrometer-----	65
Figure 2.11	UV-Visible Spectrophotometer-----	66
Figure 2.12	Basic components of a monochromatic XPS system-----	68
Figure 2.13	Principle of Photoluminance Spectroscopy -----	70
Figure 3.1	XRD pattern of pure and Pd loaded titania nanotube calcined at 400 °C (a) unloaded TNT (b) 0.1Pd (c) 1Pd (d) 5Pd and (e) 10Pd -----	84
Figure 3.2	Raman spectra of Pd loaded and unloaded titania nanotube (a) unloaded TNT (b) 0.1Pd (c) 1Pd, (d) 5Pd and (e) 10Pd-----	85
Figure 3.3	SEM images of pure and Pd loaded titania nanotubes calcined at 400 °C (a) NT (b) 0.1Pd (c) 1Pd, (d) 5Pd and (e) 10Pd-----	86
Figure 3.4	TEM images of Pd loaded titania nanotubes calcined at 400 °C (a) 0.1Pd (b,c) 1Pd (d) 5Pd -----	87
Figure 3.5	XPS spectra of Pd doped titania nanotube samples (A) Ti 2p (B) O 1s, Pd 3d of (C) Pd loaded titania nanotube and (D) 10Pd sample fitted for Pd and PdO -----	89-91
Figure 3.6	The diffusion of p-nitrophenol through TNT -----	93
Figure 3.7	(A) Time dependent absorption spectra of the reaction solution in the presence of the Pd loaded titania nanotube (0.1Pd) (B) A typical plot of $-\ln(C/C_0)$ against time for the determination of rate constant for reduction of p-nitrophenol by NaBH_4 in presence of Pd loaded titania nanotube catalyst (a) 0.1Pd (b) 1Pd (c) 5Pd and (d) 10Pd -----	95
Figure 3.8	Plot of C/C_0 for the catalytic reduction of 4-nitrophenol by sodium borohydride in presence of pure titania nanotube-----	96
Figure 3.9	Time dependent absorption spectra of the reaction solution in the presence of the 1Pd sample (A) 2 nd cycle (B) 3 rd cycle -----	99
Figure 3.10	A typical plot of $-\ln(C/C_0)$ against time for the determination of rate constant for reduction of p-nitrophenol by NaBH_4 in presence of 1Pd (recyclability) (■) 1 st cycle (●) 2 nd cycle and (▲) 3 rd cycle -----	100
Figure 4.1	XRD patterns of (a) TiO_2 nanotube calcined at 400 °C, PbS sensitised TiO_2 nanotube (b) 1PT (c) 3PT (d) 5PT and (e) 10PT -----	113

Figure 4.2	SEM images of (A,A1) titania nanotube calcined at 400 °C (B,B1) PbS sensitised titania nanotube -----	114
Figure 4.3	Diffuse reflectance spectra of (a) TiO ₂ nanotube calcined at 400 °C, PbS sensitised TiO ₂ nanotube (b) 1PT (c) 3PT (d) 5PT and (e) 10PT-----	115
Figure 4.4	Photocatalytic degradation of methylene blue under visible light with freshly prepared PbS sensitized titania nanotube (1 st cycle) (a) TiO ₂ nanotube calcined at 400 °C, PbS sensitised TiO ₂ nanotube (b) 1PT (c) 3PT (d) 5PT and (e) 10PT -----	116
Figure 4.5	Photocatalytic degradation of methylene blue under visible light by PbS sensitized titania nanotube which once used for a photocatalytic reaction (2 nd Cycle) (a) TiO ₂ nanotube calcined at 400 °C, PbS sensitised TiO ₂ nanotube (b) 1PT (c) 3PT (d) 5PT and (e) 10PT -----	118
Figure 4.6	Rate constant of methylene blue degradation of PbS sensitised titania nanotube under irradiation with visible light (a) 1 st cycle (b) 2 nd Cycle-----	118
Figure 4.7A	XPS spectra of Ti 2p peak of (a) TiO ₂ nanotube calcined at 400 °C, PbS sensitised TiO ₂ nanotube (b) 1PT (c) 3PT (d) 5PT and (e) 10PT-----	120
Figure 4.7B	XPS spectra of O 1s peak of (a) TiO ₂ nanotube calcined at 400 °C, PbS sensitised TiO ₂ nanotube (b) 1PT (c) 3PT (d) 5PT and (e) 10PT-----	122
Figure 4.7C	XPS spectra of Pb 4f peak of PbS sensitised TiO ₂ nanotube (a) 1PT (b) 3PT (c) 5PT and (d) 10PT -----	123
Figure 4.7D	XPS spectra of Pb 4f peak of 10PT fitted for PbS particle with different size -----	123
Figure 4.7E	XPS spectra of Pb 4f peak of PbS sensitised TiO ₂ nanotube sample after photocatalytic reaction (a) 1PT (b) 3PT (c) 5PT and (d) 10PT -----	124
Figure 4.8	J-V curve of PbS sensitised solar cell under 1sun (AM1.5) illumination-----	128
Figure 5.1	The band alignment CdS sensitized titania nanotube and charge carrier separation -----	136
Figure 5.2	Reaction of Coumarine with OH radical to form umbelliferon-----	141

Figure 5.3	X-ray diffraction pattern of (a) TNT (b) T1 (c) T3 (d) T5(e) T10 (f) T15 (g) T20 and (h) T30 -----	144
Figure 5.4	SEM images of (A)unsensitized TNT (B) T15-----	145
Figure 5.5	TEM and HRTEM images of (A, C) T15 (B, D) T30-----	145
Figure 5.6	Raman spectra of (a) unsensitized TNT (b) T1 (c) T3 (d) T5 (e) T10 (f) T15 (g) T20 and (h) T30-----	147
Figure 5.7	Diffuse reflectance spectra of (a) TNT (b) T1 (c) T3 (d) T5 (e) T10 (f) T15 (g) T20 and (h) T30 -----	148
Figure 5.8	Tauc plot of titania nanotubes and CdS sensitized titania nanotubes (a) TNT (b) T10 (c) T15 (d) T20 and (e) T30-----	148
Figure 5.9	XPS survey scan of T15 -----	151
Figure 5.10A	XPS spectra of Cd 3d peak of CdS sensitized titania nanotubes (a) T1 (b) T3 (c) T5 (d) T10 (e) T15 (f) T20 and (g) T30 -----	152
Figure 5.10B	XPS spectra of S 2p peak of CdS sensitized titania nanotubes (a) T3 (b) T5 (c) T10 (d) T15 (e) T20 and (f) T30 ---	153
Figure 5.10C	XPS spectra of O 1s peak of CdS sensitized titania nanotubes (a) TNT (b) T1 (c) T3 (d) T5 (e) T10 (f) T15 (g) T20 and (h) T30 -----	154
Figure 5.11	Photocatalytic degradation of methylene blue under visible light (a) TiO ₂ nanotubes calcined at 400 °C, CdS sensitized TiO ₂ nanotubes (b) T1 (c) T3 (d) T5 (e) T10 (f) T15 (g) T20 and (h) T30 (A) 1 st cycle (B) 2 nd Cycle-----	156
Figure 5.12	Rate constant of methylene blue degradation of CdS sensitized titania nanotubes under irradiation with visible light (a) 1 st cycle (b) 2 nd Cycle-----	157
Figure 5.13	Fluorescence spectra for (a) 0.5 mM coumarin solution, after visible light irradiation in presence of (b) T5 (c) T15 (d) T30 ---	158
Figure 5.14	XPS spectra of S 2p peak of CdS sensitized titania nanotubes (a) T3 (b) T5 (c) T10 (d) T15 (e) T20 and (f) T30 after first cycle -----	159
Figure 5.15	X-ray diffraction pattern of after first cycle (reused for photocatalysis) (a) TNT (b) T1 (c) T3 (d) T5 (e) T10 (f) T15 (g) T20 and (h) T30 -----	161

Figure 5.16	J-V curve of CdS sensitized solar cell under 1sun (AM1.5) illumination-----	162
Figure 5.17	XPS valence band spectra of the samples (a) TNT (b) T10 (c) T15 (d) T20 and (e) T30 -----	163
Figure 5.18	Band diagram versus Fermi level, valence band positions with reference to their Fermi levels are labeled -----	164

Introduction to Titania Nanostructures

● Contents ●	1.1 Introduction
	1.2 Titanium Dioxide
	1.3 Anatase – Rutile Phase Transformation
	1.4 1 D-Nanostructures
	1.5 Semiconductor photocatalysis
	1.6 Influence of operational parameters
	1.7 Literature review: Titania nanotube as photocatalyst
	1.8. 1 D-nanostructures in Dye Sensitized Solar Cells (DSSC)
	1.9 Chalcogenide sensitized titania for solar cell applications
	1.10 Motivation of the present study
References	

1.1 Introduction

Nanotechnology and nanomaterials have attracted a great deal of attention in the last few years having huge potential to bring benefits to many areas of research and applications including drug delivery, micro/nano electromechanical systems, development of smart fabrics etc.¹⁻³ Nanotechnology is the technique of manipulating the matter on an atomic and molecular level having scale and size in the nanometer range. Generally it deals with structures sized between 1 to 100 nanometers, and involves developing materials or devices possessing at least one dimension in that size regime. An important aspect of nanotechnology is the vastly increased ratio of surface area to volume associated with nanomaterials, which makes possible new quantum mechanical effects. Thus the change in properties from macro scale to nanoscale can be due to the increase in surface energy with the overall surface area which in turn is strongly dependent on the dimension of material. Nanoparticles can adopt a range of different morphologies including nanotubes, nanowires, nanofibres, nanodots and a range of spherical or aggregated dendritic forms of different fractal dimensions. Structures that are having at least one dimension in nanometer scale are receiving considerable attention because of their peculiar and fascinating properties, and applications superior to their bulk counterparts.⁴⁻⁵ There are two main streams for the synthesis of nanomaterials. One is bottom-up approach and second one is top-down approach. Bottom-up approaches, use the chemical properties of single molecules to cause single-molecule components to self organize or self assemble into some useful conformation, or rely on positional assembly. These approaches utilize the concepts of molecular self-assembly and/or molecular recognition. In top-down approach, nano objects are constructed from larger entities without atomic-level control. Recently, one dimensional (1D)

nanostructures such as wires, rods, belts and tubes have also become the focus of intensive research owing to their unique applications especially in the fabrication of nanoscale devices.⁶ It is generally accepted that 1D nanostructures provide a good system to investigate dependence of electrical and thermal transport or mechanical properties on dimensionality and size reduction (quantum confinement). They are also expected to play an important role as both interconnects and functional units in fabricating electronic, optoelectronic, electrochemical and electromechanical devices with nanoscale dimensions apart from their huge application potential in energy and environment.

1.2 Titanium Dioxide

Titanium dioxide is a member of transition metal oxides known for many years as a constituent of naturally occurring mineral ilmenite ($\text{FeO}\cdot\text{TiO}_2$). Presently titanium dioxide is well recognized as a valuable material with application as a white pigment in paints, as filler in paper, textile and in rubber/plastics.⁷ Titania has received great attention due to its chemical stability, non-toxicity and low cost. The very high refractive index (2.4) and low visible absorptivity favour in the field of anti-reflection coatings and in thin film optical devices, but the wide band gap (3.2 eV) combined with the high ultraviolet absorption could be exploited in the field of optical coatings. Further, it finds use as wastewater purification⁸ inorganic membranes and as catalyst support.⁹⁻¹⁰ Titanium dioxide is also being used in heterogeneous catalysis, as a photocatalyst, for the production of hydrogen and oxygen by water splitting, and electrical energy in solar cells.¹¹⁻¹⁴ Because of the excellent biocompatibility titania is widely used in bone implants and also finds applications in the area of Li based batteries¹⁵ and electrochromic devices.¹⁶

Titania mainly exists in three polymorphic forms rutile, anatase and brookite. Anatase (Tetragonal, D_{4h} -141/amd, $a=b=3.7845 \text{ \AA}$, $c=9.5143 \text{ \AA}$), rutile (tetragonal, D_{4h} -P42/mnm, $a=b=4.5937 \text{ \AA}$, $c=2.9587 \text{ \AA}$) and brookite (rhombohedral, D_{2h} -Pbca, $a=5.436 \text{ \AA}$, $b=9.166 \text{ \AA}$).¹⁶⁻¹⁸ Anatase and rutile are in tetragonal structure and brookite is orthorhombic. In all three TiO_2 structures, the stacking of the octahedra results in threefold coordinated oxygen atoms.¹⁹ Thermodynamically rutile structure is most stable. Brookite has an orthorhombic crystal structure and spontaneously transforms to rutile at $\sim 750 \text{ }^\circ\text{C}$.²⁰ Its mechanical properties are very similar to those of rutile, but it is the least common of the three phases and is rarely used commercially. In all the three crystalline forms each of the Ti^{4+} ions is surrounded by an irregular octahedron of oxygen atoms. Both in rutile and anatase the six oxygen atoms that surround the Ti^{4+} ions can be grouped into two. The two oxygen atoms are farthest from Ti^{4+} and the other four oxygen ions are relatively closer to Ti^{4+} . In rutile these distances are 0.201 nm and 0.192 nm respectively and in the anatase they are 0.195 nm and 0.191 nm (Figure 1.1). Anatase transforms irreversibly and exothermally to rutile in the temperature range 600-800 $^\circ\text{C}$.²¹ The schematic diagram of unit cells for rutile and anatase is shown in figure 1.1

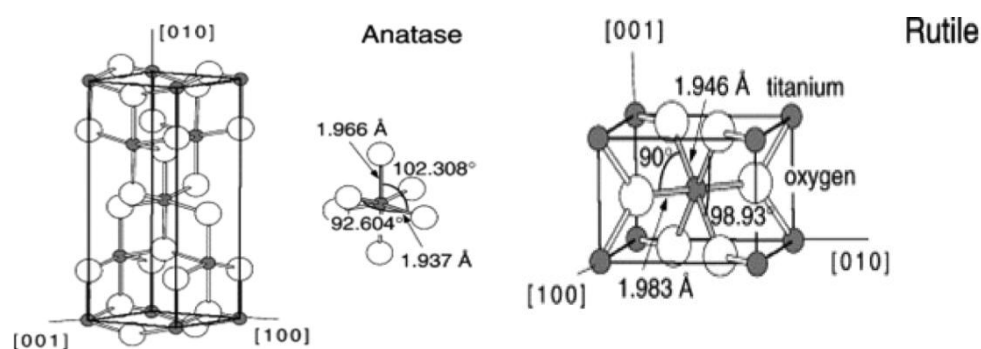


Figure 1.1 Unit cells of anatase and rutile titania.

[Source: L. Li, et al. In *Advanced Catalytic Materials - Photocatalysis and Other Current Trends*; Norena, L. E., Wang, J.-A., Eds.; InTech: Rijeka, 2016, p Ch. 07.]

The distortion is greater in anatase than rutile. The structures of anatase and rutile crystals have been described in terms of chains of TiO_6 octahedra having common edges. Two or four edges are shared in rutile and anatase, respectively. In the third form of titanium dioxide, brookite, the inter-atomic distances and the O-Ti-O bond angles are similar to those of rutile and anatase. The essential difference is that there are six different Ti-O bonds ranging from 0.187 to 0.204 nm. The tetragonal crystal structure of anatase and rutile are shown in figure 1.2. A comparison of layers in figure 1.2 shows that the rutile structure is more densely packed than anatase. As a point of reference, the densities of the anatase and rutile phases are known to be 3.83 g/cm^3 and 4.24 g/cm^3 respectively.²² Typical properties of the major two crystal forms of titania are provided in Table 1.1

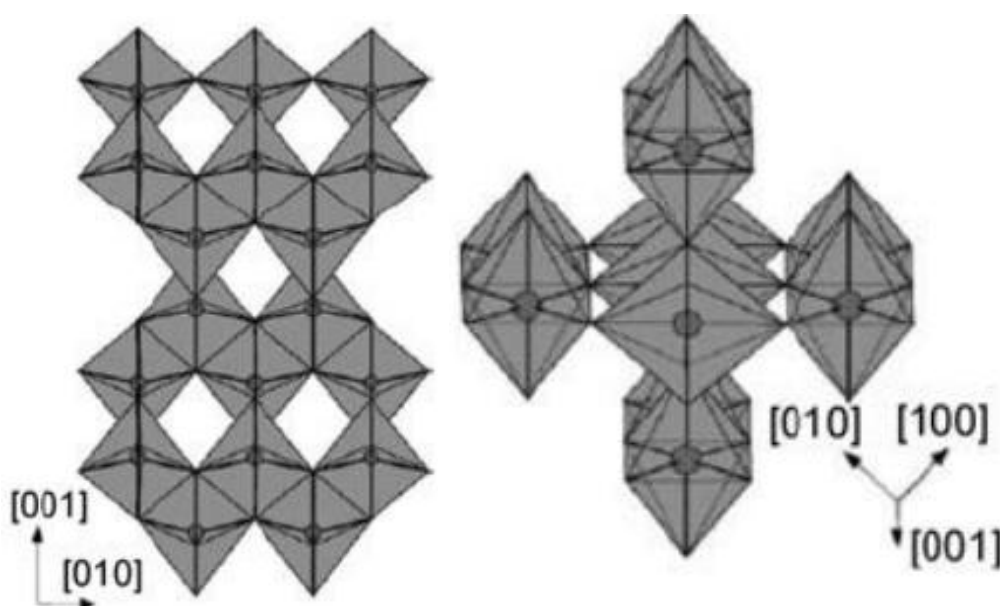


Figure 1.2 Crystal structure of anatase and rutile titania.

[Source : Li, L.; Wang, M. In *Advanced Catalytic Materials - Photocatalysis and Other Current Trends*; Norena, L. E., Wang, J.-A., Eds.; InTech: Rijeka, 2016, p Ch. 07.]

Table 1.1 Typical properties of TiO₂

Crystal form	Anatase	Rutile
Density(g/cm ³)	3.83	4.24
Hardness(moh)	5-6	6-7
Crystal structure	Tetragonal, Uniaxial, negative	Tetragonal, Uniaxial, positive
Dielectric constant	48	114
Band-gap energy(eV)	3.2	3.0

1.2.1 TiO₂ Photocatalysis

Photocatalytic applications of titania gained considerable emphasis in the 1990s with the emerging demands on clean energy and protecting the environment. Other important semiconducting oxides for such applications include zinc oxide, cadmium sulphide and zinc sulphide. Zinc oxide is also a reasonable substitute for titania, except for its property of undergoing incongruent dissolution resulting in formation of zinc hydroxide coating on the ZnO particles which in turn leads to slow catalyst inactivation. Ideally, a semiconductor photocatalyst should be chemically inert, stable under light illumination, efficiently activated by sunlight, to act as a catalyst, cheap and environment friendly. Titanium dioxide can be considered as an ideal photocatalyst, displaying almost all the above properties. The single exception is that it does not absorb visible light owing to its wide band-gap of 3.2 eV. Both anatase and rutile, are commonly used as photocatalysts²³⁻²⁶, with anatase showing a greater photocatalytic activity for most reactions.²⁷⁻²⁸ This increased photoreactivity is due to anatase's slightly higher Fermi level, lower capacity to adsorb oxygen and higher degree of hydroxylation (i.e., number of hydroxyl groups on the surface).²⁹⁻³¹ There is considerable scatter in data in the literature with regard to the reactivity of the different crystalline modifications of TiO₂. Reactions in which both crystalline phases have the same photoreactivity have been reported³² where as higher reactivity for rutile is

also reported.³³ Furthermore, there are also studies which claim that a mixture of anatase (70-75%) and rutile (25-30%) is more active than pure anatase.³⁴⁻³⁶ The disagreement of the results may be due to the intervening effects of various coexisting factors, such as specific surface area, pore size distribution, crystalline size, preparation methods etc. Degussa P25, a commercial photocatalyst, consisting of an amorphous phase together with a mixture of anatase and rutile in an approximate proportion of 80/20, has been reported to be more active than both the pure crystalline phases for many reactions.³⁷ The enhanced activity arises from the increased efficiency of the electron-hole separation due to the multiphase nature of the particles. Another commercial TiO₂ photocatalyst, Sachtlebem Hombikat UV 100, consisting only of anatase, has been reported to have high photoreactivity due to fast interfacial electron-transfer rate.³⁸

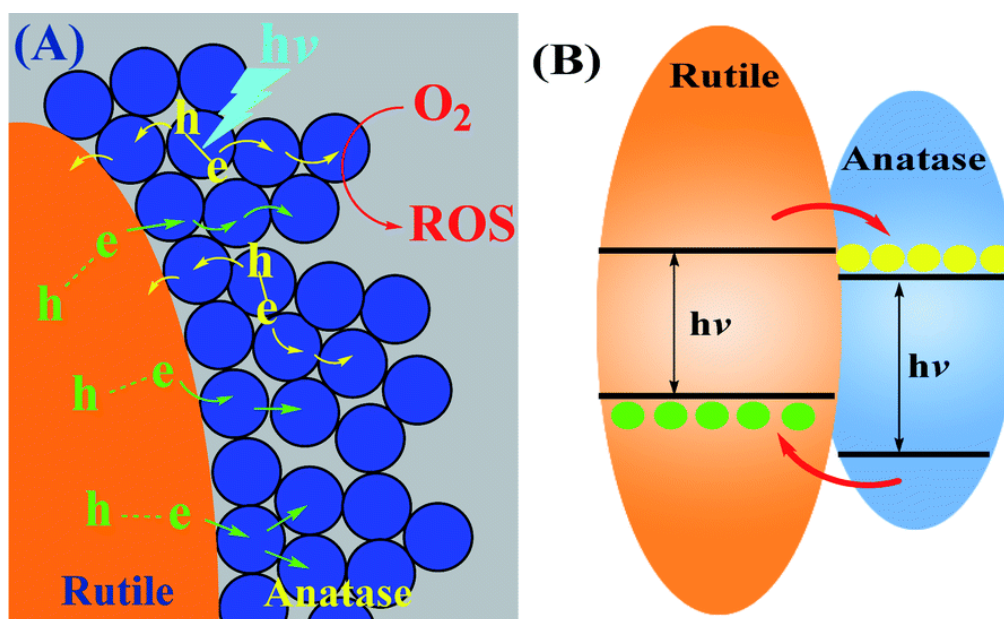


Figure 1.3 Electron-hole separation in anatase/ rutile heterostructure and their band alignment

[Source: Xiong et.al. *Journal of Materials Chemistry A* **2014**, 2, 9291]

1.2.2 Titania as a Catalyst Support

Today's chemical industry largely depends on catalyst and catalytic reactions. The attractive future evolution of this industry involves attaining more selective products, energy-efficient processes, use of environment friendly products and a better use of raw materials. The major challenge for most heterogeneous catalysts is lack of stability and agglomeration of particles during operations which block the active sites of the catalyst, leading to its instability. Therefore, the selection of an appropriate catalyst's support material has been of great interest. For choosing a catalyst support the main idea is that the catalyst should be dispersed on a suitable support to make the catalytic nanoparticles stable and obtain optimal performance and decrease the amount of costly metal being utilized, which accordingly decrease the total catalyst expenses. Also in the case of heterogeneous catalysis, the problem of catalyst separation and recovery from the reaction matrix are addressed by using various catalyst supports to immobilize them. Therefore, heterogeneous catalysts with supports such as Al_2O_3 , TiO_2 , ZrO_2 , ZnO and others are applied based on their processability and cost-effective modes of synthesis. In this scenario TiO_2 based heterogeneous catalysts have become a crucial part of many industrial activities, such as organic synthesis, oil refining, and pollution control.³⁹⁻⁴⁰ Due to its non toxicity, long-term photo stability, high effectiveness, good mechanical resistance and stabilities in acidic and oxidative environments, TiO_2 has become a prime candidate for heterogeneous catalyst support.

1.3 Anatase – Rutile Phase Transformation

Anatase and rutile are the two polymorphs of titania at atmospheric pressure. The room temperature phase is anatase and the high temperature

phase is rutile. Anatase transforms irreversibly and exothermically to rutile in the range 600 °C to 1200 °C⁴¹ depending on parameters such as the method of preparation, grain size, morphology, degree of agglomeration, nature of impurities and reaction atmosphere.⁴²⁻⁴⁴ At atmospheric pressure the transformation is time and temperature dependent and is also a function of impurity concentration. The complexity of the transition is typically attributed to the reconstructing nature. The transition is a nucleation-growth process and follows the first order rate law with an activation energy of ~90 kcal/mol.⁴⁵

The anatase – rutile transformation involves an overall contraction of oxygen and movement of ions so that a cooperative rearrangement of Ti⁴⁺ and O²⁻ occur. The transformation implies that two of the six Ti-O bonds of anatase structure break to form a rutile structure. The removal of the oxygen ions, which generate lattice vacancies, accelerate the transformation and inhibit the formation of interstitial titanium. The impurities that have most pronounced inhibiting action are chloride, sulphate and fluoride ion. Those ions with valency greater than four reduce the oxygen vacancy concentration and will retard the reaction.⁴⁶

The effect of reaction atmosphere such as vacuum conditions, atmosphere of hydrogen, static air, flowing air, oxygen, argon, nitrogen and chlorine will also have effect on anatase – rutile phase transformation. It is found that the transformation rate in hydrogen atmosphere is greater than in air and under vacuum, the rate of transformation decreases as oxygen partial pressure increases.⁴⁷ Oxygen vacancies are formed in hydrogen atmosphere whereas the interstitial Ti³⁺ ions are generated under vacuum. The rate constant of the transformation in hydrogen was 10 times larger than in air.⁴⁸ Similarly the nature of dopant and the site where the dopant is going in the lattice also have effect on anatase – rutile phase transformation.⁴⁹

1.4 1D-Nanostructures

One dimensional (1D) nanostructures became the focus of extensive studies worldwide due to their unique physical properties and potential to revolutionize broad areas of nanotechnology. Importance of 1D nanostructures is that it represent the smallest dimension structure that can efficiently transport electrical carriers, and thus are ideally suited to the critical and ubiquitous task of moving charges in integrated nanoscale systems. Secondly, 1D nanostructures can also exhibit device function, and thus can be exploited as both the wiring and device elements in architectures for functional nanosystems. In this regard semiconductor nanostructures have shown particular promise. One dimensional nanostructures of metal oxides can act as a better sensitive and selective chemical or biological sensors compared to their thinfilm counterparts, because of large surface-to-volume ratios and Debye length comparable to their small size, and also the electronic property of 1-D nanostructures is strongly influenced by the surface processes, such as charge transfer.⁵⁰⁻⁵¹ Currently bottom-up method has become one of the important strategy for the synthesis of one dimensional nanostructures. 1-D nanostructures, such as nanowires, nanotubes, nanorods, nanobelts, nanorings, and hetero-nanowires, can be produced for a variety of materials, including metal oxides, III-V and II-VI group semiconductors, metals, polymers, by using techniques like solution methods, template-assisted methods, vapor-phase methods, hydrothermal, electrochemical, electrospinning etc.⁵²⁻⁵³

1.4.1 Titania Nanotubes

One-dimensional (1D) nanostructures including nanorods, nanoneedles, nanotubes, nanofibers, and nanowires have been used in field effect transistors (FET)'s to enhance the electron transport. Titania nanotubes (TNT) are widely

used in dye sensitized solar cells because of its unique properties such as high transport rate of electrons from the adsorbed photo excited dye to the Ti electrode onto which TNT are attached when compared with that of titania nano particle (TNP).⁵⁴⁻⁵⁶ So it is expected that the unique morphology of TNT would significantly improve the photocatalytic efficacy in many reactions with respect to TNP. Studies show that the TNT prepared by different synthesis routes have different activity. It is widely accepted that TNT prepared by anodic oxidation exhibit better performance. Also there are numerous factors influencing the efficacy of TNT and the interrelations of these factors are more complex and more important in the context of their photocatalytic applications.

1.4.2 Methods for Synthesis of Titania Nanotubes

1.4.2.1 Hydrothermal Method

Hydrothermal is a widely used synthesis technique for the titania nanotubes. It is normally conducted in steel pressure vessels called autoclaves with or without teflon liners under controlled temperature or pressure with the reaction in aqueous solutions. The temperature and the volume of solution added to the autoclave largely determine the internal pressure produced. It is a method that is widely used for the production of small particles in the ceramics industry. TiO₂-derived nanotubes were obtained when TiO₂ nanopowders were treated chemically with NaOH aqueous solution at various reaction temperatures and subsequently, washing with HCl aqueous solution. While increasing temperature, the morphology altered from spherical particles to sheets at initial stage and then to nanotubes when temperature became higher. Therefore, the reaction temperature is a key factor in elucidating the aspect ratio of tubes and specific surface area.

1.4.2.2 Template Assisted Synthesis

It has been demonstrated that template synthesis is a general and versatile method for preparing nanostructured materials of nanotubules and nanofibrils composed of conductive polymers, metals, semiconductors and other materials⁵⁷, which entails synthesizing the desired material within the pores of a mesoporous template membrane.⁵⁸⁻⁵⁹ Due to cylindrical pore geometry and monodisperse diameters, corresponding cylindrical and oriented nanostructured materials with a narrow diameter distribution are obtained. More recently, template synthesis of semiconductor nanostructures has been well developed and a broad range of semiconductor materials have been fabricated. There are mainly two kinds of templates such as ‘hard’ template and ‘soft’ template. The hard templates include inorganic mesoporous materials such as anodic aluminium oxides (AAO) and zeolites, mesoporous polymer membranes, carbon nanotubes, etc. The soft templates generally refer to surfactant assemblies such as mono-layers, liquid crystals, vesicles, micelles etc. Porous AAO membrane is formed via the anodization of aluminium metal in acidic solutions. AAO film possesses regular and highly anisotropic porous structure with pore diameter ranging from several to hundred nanometers. These characteristics allow the use of AAO as template for the growth of metal or semiconductor nanowires and tubes. Titania nanotube array films on Al substrates have been prepared from $(\text{NH}_4)_2\text{TiF}_6$ aqueous solution by immersing AAO templates on aluminum substrate via Liquid Phase Deposition method at ambient temperature. The nanotube array films’ morphology depends on the anodic aluminum oxide (AAO) structure and deposition time. When AAO was immersed into $(\text{NH}_4)_2\text{TiF}_6$ solution at room temperature, AAO was dissolved in the solution and the holes became wide. The hydrolysis reaction occurs and TiO_2 particles locked in-situ on the

inner surface of the anodic alumina pore induced by hydroxyl group, thus nanotube array film was obtained. However, the disadvantages associated with template-assisted method are the difficulties of prefabrication and post-removal of the templates and usually results in impurities.

1.4.2.3 Anodized Titania Nanotubes

Synthesis and processing of nanomaterials and nanostructures are very important. Studies on new physical properties and applications of nanomaterials and nanostructures are possible only when nanostructured materials are made available with desired size, morphology, crystal and microstructure and chemical composition. There are various methods such as electrochemical deposition in nanoporous alumina templates, sol-gel methods, seeded growth, electrospinning, and hydrothermal methods for the synthesis of titania nanotubes (TNT). However, the disadvantages associated with these complex, multistep methods involve the difficulties to scale up beyond lab scale and a low yield of nanotubes. Recently it was reported that TNT can be synthesized in a simple, cost effective manner by means of electrochemical anodization of titanium metal in fluoride-ion containing electrolytes. Now the anodization process has become the standard synthesis method for highly ordered arrays of vertically aligned nanotubes. The synthesis of TNT is initiated by the application of a DC bias voltage in the presence of the electrolyte containing both oxidizing and reducing agents to form an oxide layer on the surface of the metal anode (Al or Ti). This is followed by the field-enhanced dissolution of the oxide, which results in corrosion pits. When equilibrium between oxidation and dissolution is reached, the corrosion pits grow continuously into vertically aligned nanopores or nanotubes. Since the nanotubes produced by anodization are amorphous, the samples must be

annealed in air, oxygen, or a nitrogen atmosphere at 300–500 °C, with a slow heating and cooling rate (1–5 °C/min) to produce crystalline material.

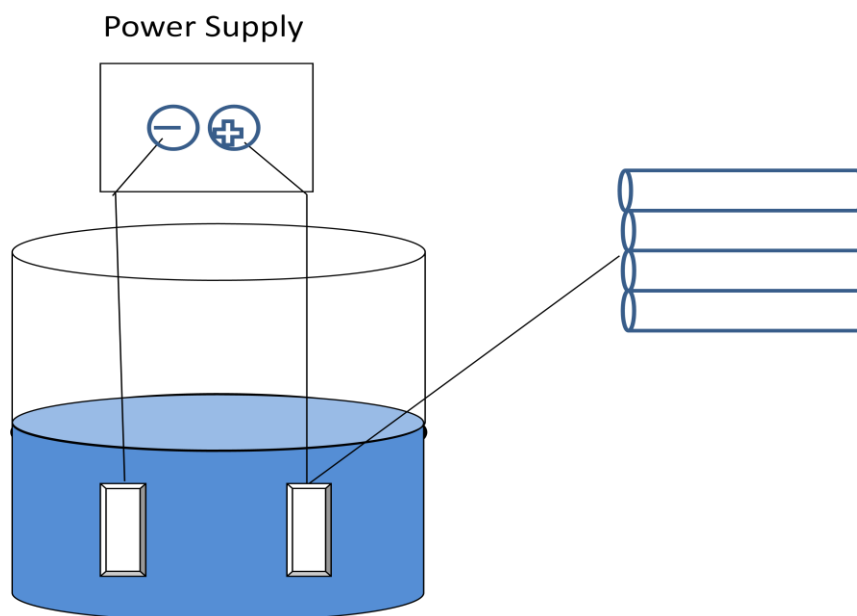


Figure 1.4 The anodization setup for titania nanotube synthesis

A significant advantage of anodization over other fabrication methods is that it offers precise control over the shape, structure, and morphology of the produced nanotubes simply by controlling different synthesis parameters. For instance, anodization voltage can be used to control nanotube diameter, while the time of anodization can be modified to control the average length of the tubes. The viscosity, pH, and concentration of fluoride ions within the solution influence the oxide dissolution and rate of chemical reaction. These parameters have a direct effect on the tube formation rate, maximum achievable tube length, and smoothness of the tube walls. The water content controls the strength of the attachment between the nanotube arrays and the original Ti substrate.

The properties of the nanotube arrays are dependent on their specific architecture, including length, wall thickness, wall roughness, pore diameter, and tube to tube spacing. The geometrical features of the nanotube arrays are controlled by a variety of parameters including anodization potential, electrolyte composition and properties thereof (conductivity, viscosity), as well as anodization time and temperature. It is possible to make identical tubes in dissimilar electrolytes by the control of different anodization variables.⁶⁰⁻⁶¹ Control of fabrication parameters has enabled titania nanotubes with different pore size, outer diameter, wall thickness and tube to tube spacing. In general it is observed that for getting very long titania nanotube arrays, polar organic electrolytes should be used with minimum water content. With organic electrolytes the donation of oxygen is more difficult in comparison to water and results in a reduced tendency to form oxide, while the reduction in water content allows for thinner or lower quality barrier layer through which ionic transport may be enhanced. From earlier reports it is confirmed that there occurs an optimal length and geometric area for titania nanotubes for photocatalytic and photoelectrolysis applications where the absorption of the incident light is balanced by recombination of the photogenerated charge carriers. That is low light absorption will take place with titania nanotubes which are too short in length. Also low photoconversion efficiency is reported with titania nanotubes which are too long in size because of the recombination of the photogenerated electron-hole pairs. A large surface area ensures the availability of a larger number of active sites for chemical reaction to occur and allows photogenerated holes to access a large number of solution ions. Also greater nanotube length enables higher absorption of incident photons and results in larger surface area for fixed nanotube pore size and outer diameter. Therefore the maximum photocurrent is a measure of the generation,

and subsequent collection of charge carrier and correlates well with the surface area of the nanotubes. Another important factor on which photoconversion efficiency depends on is the separation process of the photogenerated electron-hole pairs, that is its recombination characteristics, which for the nanotube arrays are a complex function of the temperature and extent of crystallization, the wall thickness of the nanotubes, barrier layer thickness and the incorporation of dopants from the electrolyte during anodization. Figure 1.5 indicates the various dimension ranges of titania nanotubes most frequently reported by various research groups.⁶²⁻⁶³ It is found that one can vary the thickness, width and length of TNT by making suitable changes in the preparation conditions.

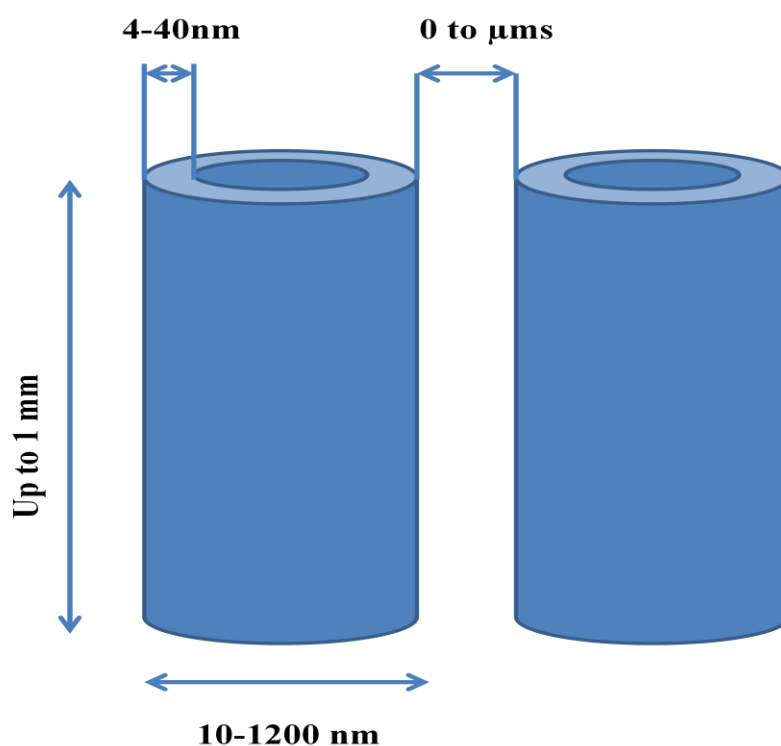


Figure 1.5 Features of titania nanotubes with reported dimensions

Main expectations for improved photocatalytic pollutant removal by using TNT is as follows. The texture will be most often irregular in the case of titania nanoparticles (TNP) so that a part of the TiO_2 surface is not easily accessed by the reactants. On the contrary, the reactants are expected to diffuse easily in the straight tubes of TNT, secondly the increased recombination rate of photoproduced charge carriers due to the large interparticular connection in the case of TNP compared to TNT. In addition to this a higher light harvesting is expected because of scattering within the tubes.

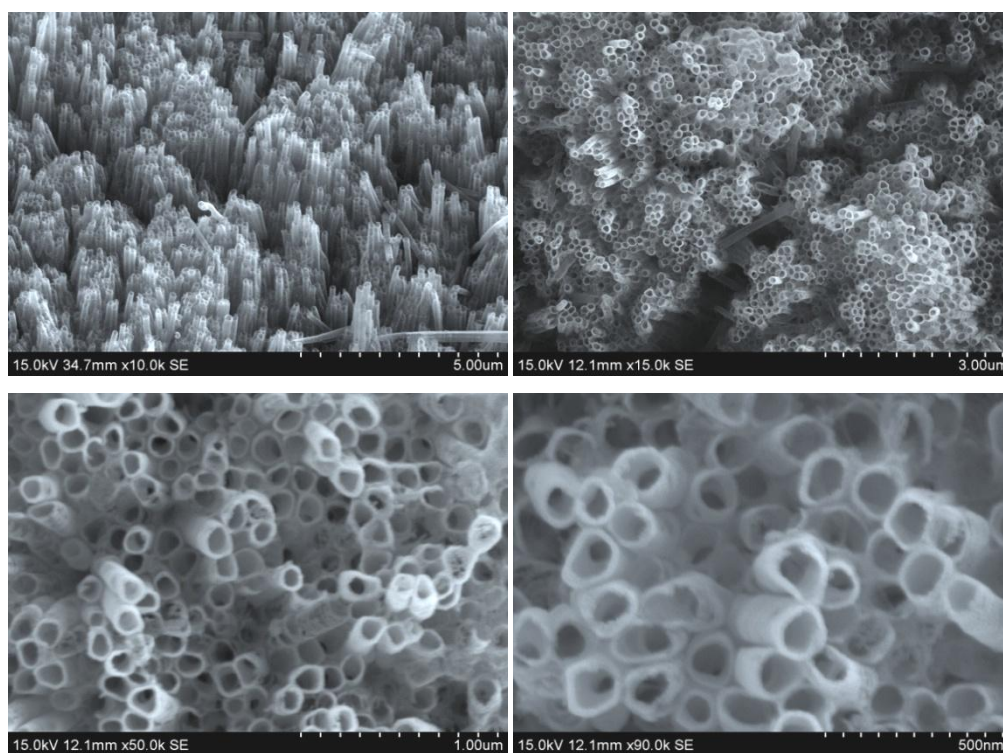
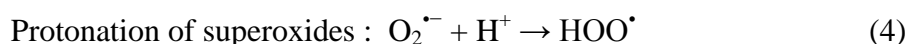
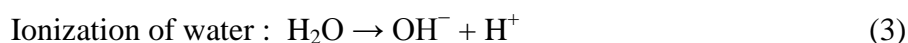
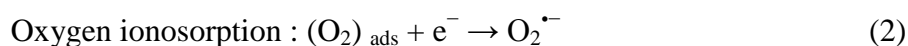
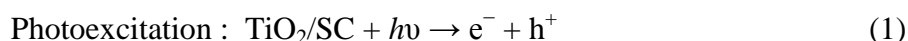


Figure 1.6 SEM images of titania nanotubes synthesized by anodization of titania metal sample at 40V

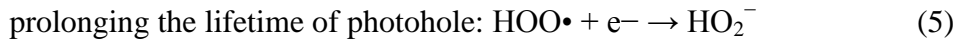
1.5 Semiconductor Photocatalysis

Photocatalysis can be defined as a photoinduced reaction which is accelerated by the presence of a catalyst.⁶⁴ These types of reactions begin with the absorption of a photon with sufficient energy corresponding or higher than

the band-gap energy (E_{bg}) of the catalyst. The absorption of energy leads to a charge separation due to promotion of an electron (e^-) from the valence band of the semiconductor catalyst to the conduction band, thus generating a hole (h^+) in the valence band. Schematic diagram of the process is presented in Fig.1.7.⁶⁵ The recombination of these generated electron-hole must be prevented for their effective reactions. The ultimate goal of the process is to have a reaction between the activated electrons with an oxidant to produce a reduced product, and also a reaction between the generated holes with a reductant to produce an oxidized product. The photogenerated electrons could reduce the dye or react with electron acceptors such as O_2 adsorbed on the Ti(III)-surface or dissolved in water, reducing it to superoxide radical anion $O_2^{\bullet-}$.⁶⁶ Sameway the photogenerated holes can oxidize the organic molecule to form R^+ , or react with OH^- or H_2O oxidizing them into OH^\bullet radicals. The resulting $\bullet OH$ radical, being a very strong oxidizing agent (standard redox potential +2.8 V) can oxidize most azo dyes to the mineral end-products. Along with other highly oxidant species (peroxide radicals) they are reported to be responsible for the heterogeneous TiO_2 photodecomposition of organic substrates and dyes. According to this, the relevant reactions at the semiconductor surface causing the degradation of dyes can be expressed as follows⁶⁶: The widely accepted chain reactions are as follows:



The hydroperoxyl radical formed in (4) has also scavenging properties similar to O_2 thus



Both the oxidation and reduction can take place at the surface of the photoexcited semiconductor photocatalyst. Recombination between electron and hole occurs unless oxygen is available to scavenge the electrons to form superoxides ($\text{O}_2^{\cdot-}$), its protonated form the hydroperoxyl radical (HO_2^{\cdot}) and subsequently H_2O_2 . Major disadvantage of the photocatalytic reacting system is the energy-wasting back-electron transfer reaction to give back the starting material. In fact for a heterogeneous semiconductor system, the inhibition of $\text{e}^- - \text{h}^+$ recombination process has become a formidable obstacle for realizing high efficiency. Thus the generated $\text{e}^- - \text{h}^+$ can be used to drive chemical reactions provided. From the point of view of the materials, photocatalyst require a series of characteristic properties depending on their applications including particle size, specific surface area or space between the electronic levels etc. among others.

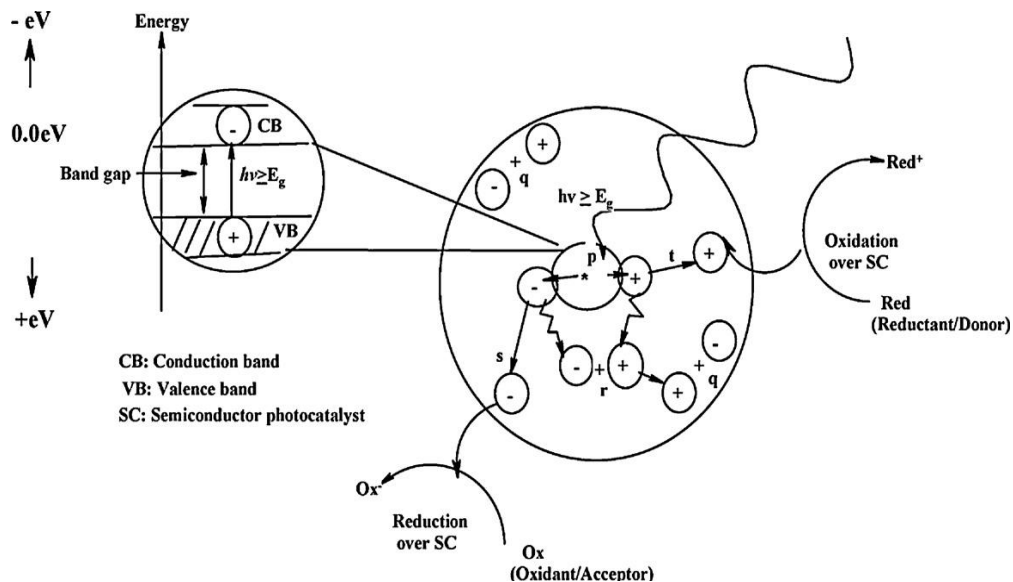


Figure 1.7 Schematic diagram of photocatalytic process initiated by photon on the semiconductor

[Source : Colmenares et. al. *Materials* 2009, 2, 2228]

1.6 Influence of Operational Parameters

1.6.1 Light Intensity

Light intensity is an important factor in photocatalytic degradation because electron-hole pairs are produced by light energy. TiO_2 has a wide band gap in the UV region, which limits its absorption only in UV region of solar spectrum.⁶⁷ The wavelength and intensity of the UV light irradiation source affects the degradation of dye in aqueous solution using TiO_2 catalyst powder in photocatalytic reactor. The artificial UV irradiation is more reproducible than sunlight and can bring higher efficiency in the degradation of textile dyes. However, because of its abundance and non-hazardous nature, solar energy, is expected to emerge as an alternative cost effective light source. The studies reported for the effect of light intensity on the kinetics of the photocatalysis process was reviewed by Ollis et al. and stated that⁶⁸:

- 1) At low light intensities ($0\text{--}20 \text{ mW/cm}^2$), the rate would increase linearly with increasing light intensity (first order).
- 2) At intermediate light intensities beyond a certain value (approximately 25 mW/cm^2), the rate would depend on the square root of the light intensity (half order).
- 3) At high light intensities the rate is independent of light intensity since at increased light intensity electron-hole pair separation competes with recombination, thereby causing lower effect on the reaction rate. However, as the light intensity increases, the number of activation sites remains the same thus the reaction rate only reaches a certain level even when the light intensity continues to increase. The photocatalytic reaction rate is largely dependent on the radiation absorbed by the photocatalyst. Recent reports revealed increase in the degradation rate

with increase in light intensity during photocatalytic degradation. Unfortunately, only 5% of the total irradiated natural sunlight has sufficient energy to cause effective photosensitization. Furthermore energy losses due to light reflection, transmission and transformation into heat are inevitable in the photoprocess.

The overall quanta of light absorbed by any photocatalyst or reactant is given by ϕ_{overall} , the quantum yield:

$$\Phi_{\text{overall}} = \text{rate of reaction} / \text{rate of absorption of radiation}$$

where the rate of reaction (mol/time) accounts for moles of reactants consumed or product formed in the bulk phase and the rate of absorption of radiation (Einstein /time) relates to the amount (mol or Einstein) of photons at wavelength λ absorbed by the photocatalyst.

The light scattering in solid-liquid regimes is particularly significant. As metal oxides in a heterogeneous regime including TiO_2 cannot absorb all the incident radiation due to refraction, so it is difficult to determine Quantum yield experimentally. Another factor which limits photonic efficiency is the thermal recombination between electrons and holes.

1.6.2 Nature and Concentration of the Substrate

Organic molecules which can effectively adsorb on the surface of the photocatalyst will be more susceptible to direct oxidation.⁶⁹ Thus, the photocatalytic degradation of aromatics depends on the substituent group. Nitrophenol has been reported to be a much stronger adsorbing substrate than phenol and therefore degrades faster.⁷⁰ Hugul et al. reported that monochlorinated phenol degrades faster than di- or tri- chlorinated derivatives in the degradation of chloroaromatics.⁷¹ In general molecules with electron withdrawing groups including nitrobenzene and benzoic acid have been found

to significantly adsorb in the dark compared to those with electron donating groups.⁷² The concentration of organic substrates in time is also dependent on photonic efficiency during photocatalytic oxidation.⁷³ At high-substrate concentrations, however, the photonic efficiency decreases and the titanium dioxide surface becomes saturated, thus leading to catalyst deactivation.⁷⁴

1.6.3 Nature of the Photocatalyst

There is direct correlation between the surface of organic reagents and surface coverage of TiO₂ photocatalyst.⁷⁵ Kogo et al. reported that the number of photons hitting the photocatalyst actually controls the rate of the reaction.⁷⁶ The latter is an indication that the reaction takes place only in the adsorbed phase of the semiconductor particle. A very important parameter influencing the performance of nanomaterials in photocatalytic oxidation is the surface morphology, namely particle and agglomerate size.⁷⁷ Numerous forms of TiO₂ have been synthesized by different methods with the aim to achieve materials exhibiting desirable physical properties, activity and stability for photocatalytic applications.⁷⁸ There exist a clear connection between the surface properties, the rational development of improved synthesis routes and the potential usefulness of the material prepared for particular applications.⁷⁹⁻⁸⁰ For instance, smaller nano-particle sizes have been reported to give higher activities in gaseous phase photomineralisation of organic compounds employing nanostructured titanium dioxide.⁸¹

1.6.4 Influence of Particle Size on Band-gap Modulation

A single atom of semiconductor material has a bandgap equal to the distance between ground state and first excited state, while in the bulk both levels are broadened and they have band structure instead of discrete energy levels. This broadening leads to narrowing of the bandgap. In a nanoparticle

broadening must be less than in the bulk. In the nanoscale phenomena, as the size of the particle approaches the size of the electron-hole distance known as the Bohr radius, the energy level spacing of electronic states of atom increases with reduction in dimensionality of particle and is called Quantum Confinement (QC). That is electronic states of an atom are typically characterized by discrete energy levels that are often separated by electron volts. At the nanoscale, the dimension of energy states resides between these limits. This can be easily understood by considering an electron confined within a one-dimension (1-D) box of size 'L'. The lowest energy level of this system is given by $E = \frac{h^2}{8mL^2}$, where 'h' is the Planck's constant and 'm' is the mass of the particle (electron). Since, if size of the box (particle diameter) is reduced, then E increases, hence a drastic variation occurs in its bulk properties.

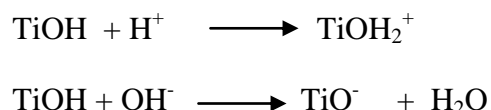
1.6.5 Concentration of Photocatalyst

The rate of photocatalytic reaction is strongly influenced by the photocatalyst concentration, as expected. Heterogeneous photocatalytic reactions are known to show proportional increase in photodegradation with increasing catalyst loadings.⁸² Generally in any given photocatalytic application, the optimum catalyst concentration must be determined, in order to avoid excess catalyst and ensure total absorption of efficient photons.⁸³ This is due to the observation of unfavourable light scattering and reduction of light penetration into the solution with an excess of photocatalyst.⁸⁴

1.6.6 Effect of pH

Another important parameter that affects the photocatalyst activity is the pH of the solution as it controls the surface charge properties of the photocatalyst and size of the formed aggregates. It was reported that the acid-

base properties of the metal oxide surface can have considerable implications upon their photocatalytic activity.⁸⁵ The surface of titania can be protonated or deprotonated under acidic or alkaline conditions, respectively, according to the following reaction :



Thus a titania surface will remain positively charged in acidic medium (pH less than 6.9) and negatively charged in alkaline medium (pH greater than 6.9). Titanium dioxide is reported to have higher oxidizing activity at lower pH, but excess H^+ at very low pH can decrease reaction rates because the TiO_2 particles tend to agglomerate leading to reduction in surface area available for dye adsorption and photon absorption.⁸⁶ Therefore pH changes influence the adsorption of dye molecules onto the TiO_2 surfaces, an important step for the photocatalytic oxidation to take place. Thus pH changes can result in enhancement of the efficiency of photoremoval of organic pollutants in presence of titanium dioxide without affecting the rate equation. So an optimized condition is required for improved degradation of compounds.

1.6.7 Reaction Temperature

The dependence of the reaction rate with temperature is widely experimented in the area of organic compounds degradation since 1970s. Many researchers reported experimental evidences for temperature dependency of photocatalytic activity.⁸⁷⁻⁹⁰ Generally, the increase in temperature enhances recombination of charge carriers and desorption process of adsorbed reactant species, resulting in a decrease of photocatalytic activity. These facts are in good agreement with the Arrhenius equation, for which the apparent first order rate constant LnK_{app} should increase linearly with $\exp(-1/T)$.⁹¹

1.7 Literature Review: Titania Nanotube as Photocatalyst

Nowadays titania nanostructures have gained much attention due to their unique properties such as high surface area, ion exchange ability and better electrical properties. There are numerous reports related to photocatalytic applications of titania nanotubes. The influence of structural parameters of titania nanotubes (TNTs) including pore diameters, length, inter nanotube-distances and crystallinity on their photocatalytic properties was studied by Mohammed et al.⁹² Composites of rutile nanoparticles and titania-nanotubes exhibits enhanced photocatalytic activities toward the decomposition of nitric oxide and the degradation of methylene blue compared with commercial P25 TiO₂.⁹³ Hierarchical porous TiO₂ nanotubes were synthesized through a facile and efficient template synthesis strategy exhibited higher dye degradation effect.⁹⁴ The photocatalytic study of TiO₂ nanotube array films with highly dispersed Pt nanoparticles showed that an optimum calcination temperature occurs for higher activity.⁹⁵ Liang et al reported higher photocatalytic activity for double walled titania nanotubes fabricated by electrochemical anodization at low temperature with subsequent annealing compared to single walled titania nanotube due to higher surface area associated with them.⁹⁶ Post annealing effect on synthesized titania nanotubes was studied and it was found that annealing beyond 400 °C leads to decreased activity because of the reduced surface area associated with collapsed nanotubes at that temperatures. Titania nanotubes (TNT) functionalized with fullerenes (C₆₀) have been successfully synthesized through a simple impregnation method using ethanol and toluene as co-solvents. C₆₀-sensitizing was found to effectively enhance the photocatalytic degradation of an organic molecule in the gas phase. Photocatalytic decomposition of isopropanol was carried out and showed high degradation in the visible region, where the TNT

samples loaded with 5 wt% C60 showed the best activity.⁹⁷ Titania nanotubes and Titania nanowires (TNW) were fabricated via a sonication-hydrothermal combination approach using TiO₂ Degussa P25 nanoparticle as precursors. The titania nanotube shows higher photocatalytic activity than TNW and titania precursor sample. Results showed that activity of the catalyst not only depends on the morphology of the catalysts, but also on the crystallinity and surface area.⁹⁸ Phosphorus-doped titania nanotubes fabricated using a facile wet chemical method shows higher activity. Eventhough the surface area is reduced with phosphorus doping band gap shifting occurs towards visible region that increases the quantum efficiency.⁹⁹ Pore structure analysis of titania nanotube aggregates synthesized by hydrothermal method shows that pores of smaller sizes are mainly contributed by the nanotubes while those of larger sizes are contributed by the inter space region of the aggregates. The study shows that both the hydrothermal treatment temperature and washing conditions affect the properties of the titania nanotubes.¹⁰⁰ Xue et al reported cerium impregnated titania nanotubes with enhanced photocatalytic activity. Photodeposition of copper on the surface of titania nanotube arrays exhibited better photocatalytic activity than the titania nanotube arrays due to the strong synergistic interactions between titania and copper.¹⁰¹ Single crystalline titania nanotubes prepared by hydrothermal method shows enhanced photocatalytic phenol degradation. Kim et al. reported enhanced photocatalytic activity in composites of titania nanotubes and CdS nanoparticles. Titania nanotubes with Fe,Cr,Co,Ce having enhanced photocatalytic activity have also been reported by several authors. Silver decorated titanium dioxide nanotube arrays with improved photocatalytic activity for visible light irradiation was reported by Chen et al.¹⁰² Lin et al reported a cost-effective way for the synthesis of TiO₂ nanotube (NT) powders using anodic oxidation and ultrasonication. They

prepared highly crystalline NT powders with intact tube structures and pure anatase phase, without the substrate effect arising from underlying Ti metals, using high-temperature heat treatment. The application of NTs with different crystallinity for the photocatalytic decomposition of methylene blue (MB) was then demonstrated. The results showed that with increasing annealing temperature, the photocatalytic decomposition rate was gradually enhanced, and the NT powder electrode annealed at 650 °C showed the highest photoactivity. Compared to typical NTs annealed at 450 °C, the rate constant increased by 2.7-fold, although the surface area was 21% lower. These findings indicate that the better photocatalytic activity was due to the significantly improved crystallinity of anatase anodic NTs resulting in a low density of crystalline defects.¹⁰³ In the case of TiO₂ nanotubes synthesized by the solvothermal process at low temperature in a highly alkaline water–methanol mixture. The ratio of methanol and water, as well as calcination temperature, affected the morphology, nanostructure and photocatalytic performance. Kontos et al used self assembled titania nanotubes with tailored morphological properties such as vertical arrangement, variable thickness prepared by electrochemical anodization. The NTs exhibited significant UV photocatalysis against toluene and benzene at ppb concentrations, under normal conditions of temperature and pressure. The photocatalytic activity depends on the length and thickness of the NT arrays. The optimum NT structures show enhanced activity compared to standard Degussa P25 films.¹⁰⁴ A novel TiO₂ nanotube photocatalyst was prepared by Chen et al that has a p–n junction. The photocatalyst particle surface is physically divided into reduction and oxidation surfaces, which possess a potential driving force for the transport of photogenerated charge carriers.¹⁰⁵ Vijayan et al studied the effect of calcination temperature on the photocatalytic reduction and oxidation

process of hydrothermally synthesized titania nanotubes.¹⁰⁶ Highly oriented titania nanotube arrays with $\{1\ 0\ 1\}$ crystal face were prepared on the surface of titanium substrate by liquid chemical deposition method.¹⁰⁷ The semiconductor quantum dots (QDs) can be effectively used to tune the response of photocatalyst TiO_2 nanotube to visible light. In this study, CdS QDs formed in situ onto the surfaces of TiO_2 nanotubes (TNTs) to form TNTs/CdS QDs nanocomposites by use of a simple bifunctional organic linker, thiolactic acid.¹⁰⁸ The effect of sandwiched Ag in the wall of TiO_2 nanotube on the photocatalytic performance was studied by Liu et al.¹⁰⁹ Ag and Au loaded titania nanotube shows enhanced photocatalytic activity.¹¹⁰ Tang et al reported efficient removal of herbicide 2,4-diphenoxyacetic acid from water using Ag/reduced graphene oxide co-decorated titania nanotube arrays produced by combining electrodeposition and photoreduction processes.¹¹¹ A series of Nd– TiO_2 powders have been prepared by hydrothermal method and the doped samples show enhanced visible light activity.¹¹² Gd^{3+} , N-codoped trititanate nanotubes have been prepared by hydrothermal and ion-exchanging method. The photocatalytic activity of TiO_2 has been enhanced significantly under visible light irradiation after Gd^{3+} , N-codoping.¹¹³ Liu et al reported the degradation of 4,4'-dibromobiphenyl, one of polybrominated biphenyls, through photoelectrocatalytic process with TiO_2 , Zr/ TiO_2 and Zr, N/ TiO_2 nanotube arrays. Study shows that photoelectrocatalytic process was more efficient than photocatalytic and electrolytic process alone.¹¹⁴ Copper sulfide quantum dots functionalized TiO_2 nanotubes were successfully prepared by a stepwise crystallization of CuS nanoparticles onto the nanotubes, using cysteine linkers. The effect of CuS QDs was investigated by studying the photodecomposition of malachite green and phenol.¹¹⁵ Surface modification of TiO_2 nanotube arrays with CuInS_2 nanoparticles for photocatalytic

degradation of 2,4-dichlorophenoxyacetic acid was reported.¹¹⁶ photocatalytic degradation of anthracene-9-carboxylic acid was investigated by using a new ZnTe modified TiO₂ nanotube array catalyst prepared by pulse potential electrodeposition of ZnTe nanoparticles onto TiO₂ NT arrays.¹¹⁷

1.8. 1 D-Nanostructures in Dye Sensitized Solar Cells (DSSC)

Third generation solar cells include nanocrystal based solar cells, Polymer based solar cells, dye sensitized solar cells and concentrated solar cells. Dye-sensitized solar cell is a promising candidate, that realizes the optical absorption and the charge separation processes by the association of a sensitizer as light-absorbing material having a wide band gap semiconductor of nanocrystalline morphology.

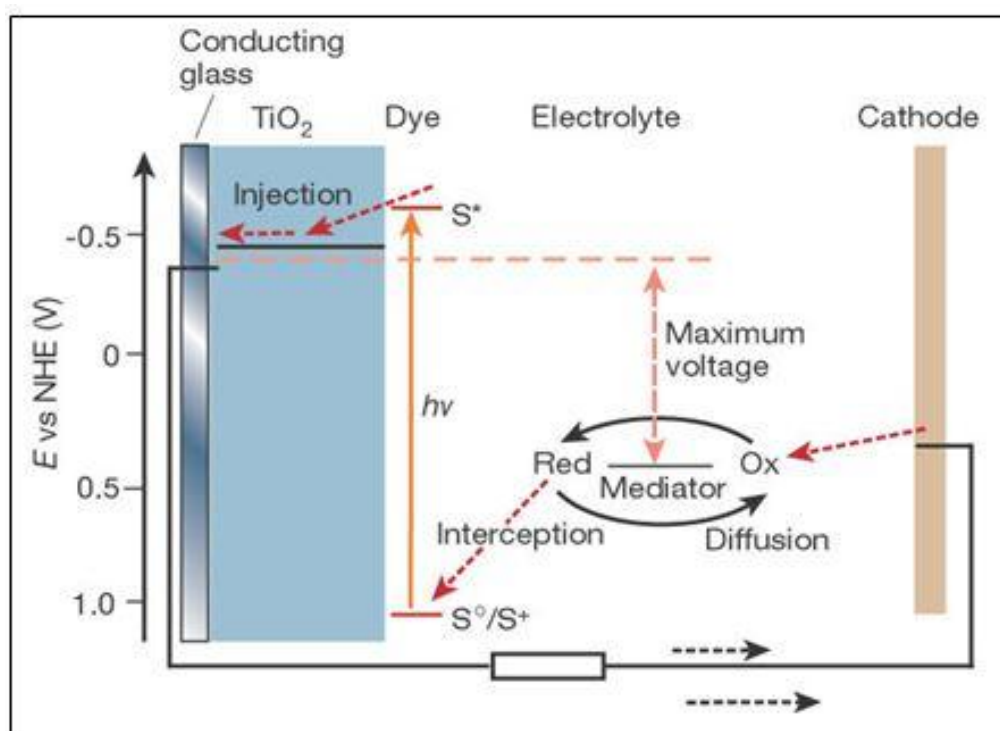


Figure 1.8 Schematic diagram of DSSC

[Source: Highfield, *J. Molecules* **2015**, 20(4), 6739]

To date the maximum efficiency reported for these cells is 11%.¹¹⁸ The d block binary metal oxides such as titania, zinc oxide and Nb₂O₅ are the best candidates as photoanode due to the dissimilarity in orbitals constituting their conduction band and valence band. This dissimilarity decreases the probability of charge recombination and enhances the carrier lifetime in these materials. So far, the most impressive DSSCs are the ones based on TiO₂ nanoscopic crystalline particle films loaded with a ruthenium-polypyridine complex dye (such as N3 and N719 dyes). Unfortunately, the record high conversion efficiency of DSSCs (11%) plateaued in an unchanged level over the last 15 years. Further increase in conversion efficiency is difficult due to large energy loss from recombination between electrons and either oxidized dye molecules or electron-accepting species in the electrolyte during the charge-transport process. Such a recombination is related to the lack of a depletion layer on TiO₂ nanocrystallite surfaces, and becomes comparatively serious as the thickness of TiO₂ photoanode film increases. Various morphologies such as nanotube, nanorod and nanofibers need to be explored for enhancing the energy conversion efficiency of DSSC, as enhanced grain boundary density and random network of nanoparticles increase the loss in DSSC due to carrier recombination. For the usual nanoparticle network used in DSSC, with porosity ~60%, the average diffusion length has been estimated to be 15-20 μm.¹¹⁹ This inferior electron transport limits the electrode thickness for DSSC and adversely affects the final conversion efficiency. One possible way to improve the diffusion coefficient, and therefore, transport properties is to grow the electrode materials as one dimensional nanostructures such as nanotubes, nanorods, nanowires and nanofibers.¹²⁰ Figure 1.9 explains this concept of channeled electron transport through one dimensional nanostructures. In other words the electrons are constrained to move unidirectionally in nanotubular structure.

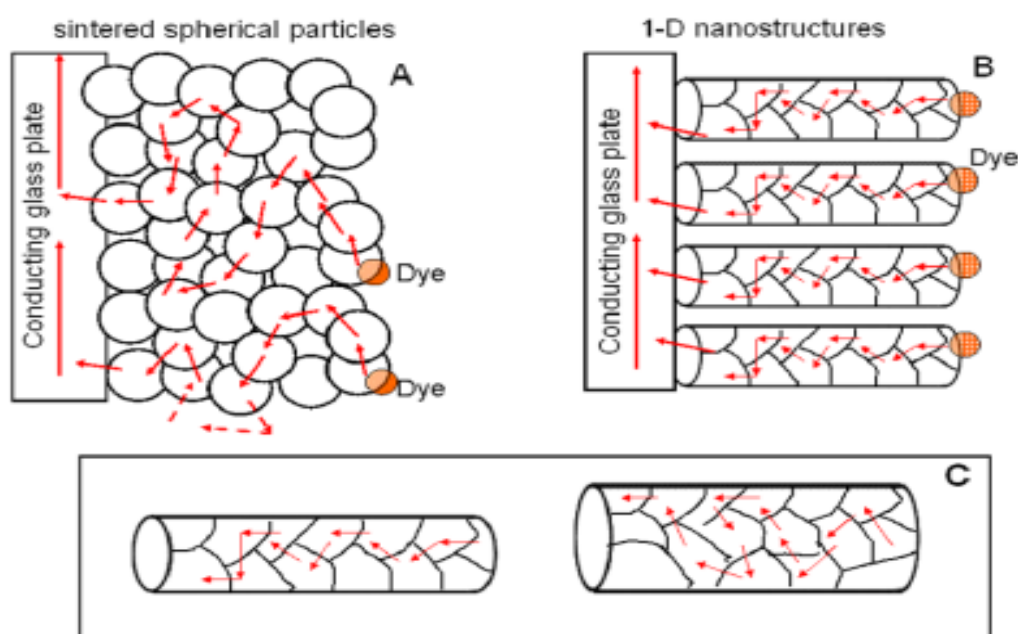


Figure 1.9 Schematic of electron diffusion between (A) sintered spherical nanoparticles and (B) one-dimensional (1-D) nanostructures. (C) shown in the box explains how reduction of diameter of the 1-D structure make the electron flow more channelled.

[Source: Jose et. al. *Journal of the American Ceramic Society* 2009, 92, 289]

1.9 Chalcogenide Sensitized Titania for Solar Cell Applications

Nowadays nanostructured materials and quantum dots (QDs) light harvesting assemblies have emerged as highly promising building blocks for the development of photocatalyst and third generation solar cells making efficient utilization of solar energy. Light harvesting through photocatalysis¹²¹ (PC) and dye sensitized solarcells (DSSC) are related to excited state charge transfer across nanostructured oxide surfaces. Photocatalysis consists of the absorption of photons at the oxide surfaces with the consequent generation of electron/hole pairs and eventual reduction/oxidation of adsorbed contaminant species. On the other hand in the case of DSSC the photogenerated electron/hole pairs at the oxide surface migrate to the external circuit for

photocurrent generation through an electrical load. With the advantages of low cost, transparency and flexibility, among different technologies, dye sensitized solar cells (DSCs) ¹²² hold great promise as an alternative renewable energy system.¹²³ In DSCs the efficient harvesting of solar energy is done by making use of nanocrystalline semiconducting electrodes sensitized with molecular dyes (the most efficient being polypyridyl ruthenium(II) complexes). The working principle of DSC involves the charge separation at the photoelectrode/sensitizer interface via electron injection from the dye into the conduction band of the semiconductor, followed by diffusive electron transport through the interpenetrated mesoporous network of the TiO₂ semiconductor to the charge collector, while dye regeneration occurs via a redox electrolyte. Even though such devices have reached high performance and stability standards ¹²⁴, the need for developing inorganic hybrid heterojunctions with enhanced selectivity, efficiency and robustness offering cost reduction and simplification in the area of DSCs manufacturing is attracting a great deal of attention. One of the most attractive approaches for the utilization of inorganic heterojunctions in DSCs is the exploitation of the exceptional electronic properties of chalcogenides such as CdS, CdSe, PbSe, PbS and CdTe nanocrystals as light harvesting antennas.¹²⁵⁻¹²⁷ Because of the unique quantum confinement effects, QDs offer unique high extinction coefficients and band gap tunability from the visible to the infrared spectral range by size control. Also the QDS have the property of multiple exciton generation (MEG) with single-photon absorption.¹²⁸⁻¹³⁰ The theoretical power conversion efficiency (PCE) of QDSCs can reach up to 42% in view of MEG effect of QDs, which is much higher than that of semiconductor solar cells (31%) according to Shockley-Queisser limit.¹³¹⁻¹³² Moreover, they can form favourable heterojunctions such as QDs/TiO₂ and QDs/dye/TiO₂ for efficient

charge extraction.¹³³⁻¹³⁶ A major drawback underlying the relatively low light harvesting ability and the associated reduction in photocurrents in quantum dot sensitized solar cell devices is the amount of QDs adsorbed on the TiO₂ electrode. Two main approaches have been so far employed for the sensitization by QDs, one is *in situ* growth of QDs on TiO₂ by chemical bath deposition (CBD)¹³⁷ and the other is successive ionic layer adsorption and reaction (SILAR)¹³⁸⁻¹³⁹ or attachment of preformed colloidal QDs to the TiO₂ mesoporous structure by means of bifunctional linker molecules or direct adsorption using a suitable solvent in the colloidal solution.¹⁴⁰⁻¹⁴¹ Linker-assisted and direct QD adsorption onto TiO₂ allows fine control of the QD size, exploiting colloidal synthesis. However these systems are associated with disadvantages such as low QD loading and relatively weaker electronic coupling between QDs and TiO₂. Eventhough chemical bath deposition permits enhanced electron transfer to the wide band gap TiO₂ electrode, QD aggregation occurs at significantly higher loading that finally deteriorates solar cell performance. In view of these things, direct growth of QDs by SILAR has recently emerged as a promising deposition route combining high QD loading together with low degree of aggregation and efficient electron transfer to TiO₂.

Krbal et al. studied the effect of tube diameter on the photoelectrochemical property of Sn-S-Se chromophore attached titania nanotubes using titania nanotubes of different diameter. The increased photocurrent with increasing tube diameter can be ascribed to the better interfacial contact and improved charge transport facilitated between the chromophore and nanotube walls.¹⁴² The photocurrent enhancement of heat treated composite materials of CdSe nanoparticle /titania nanotube arrays were studied by varying the annealing temperature from 200 to 350 °C. The study shows that the increment in annealing temperature has resulted in greater

amount of CdSe deposition and also a suitable annealing temperature can enhance the particle interaction leading to considerable improvement in photoelectrochemical performance.¹⁴³ CdSe decorated titania nanorods by hydrothermal method with enhanced efficiency was reported by Bang et al.¹⁴⁴ Green synthesis route for carbon quantum dots embedded titania nanowires was reported.¹⁴⁵ Solar cells based on a mesoporous structure of TiO₂ and the polysulfide redox electrolyte were prepared by direct adsorption of colloidal CdSe quantum dot light absorbers onto the oxide without any particular linker.¹⁴⁶ By optimizing the CdSe deposition time and the length of the nanotube, a power conversion efficiency of 3.18% has been achieved by a fibrous quantum dot sensitized solar cell, designed and fabricated by using CdS and CdSe co-sensitized TiO₂ nanotubes on Ti wire as the photoanode and highly active Cu₂S as the counter electrode.¹⁴⁷ Nanocomposites with different Cd to Ti molar ratio were synthesized from P25- nanopowder using microwave-assisted hydrothermal method. The results of the photocatalytic tests under high-intensity discharge lamp revealed that CdS/titania powders with low Cd to Ti molar ratios exhibited much higher activities than P25.¹⁴⁸ Zhou et al reported PbS quantum dots grown on mesoporous TiO₂ film using a successive ion layer adsorption and reaction (SILAR) method. The growth of QDs was found to be highly dependent on the concentration of the precursor solution.¹⁴⁹ The optical and structural properties of cadmium and lead sulfide nanocrystals deposited on mesoporous TiO₂ substrates via the successive ionic layer adsorption and reaction method was studied by Kontos et al.¹⁵⁰

1.9.1 Advantages of Quantumdots as Sensitizers

The major advantages of QDs compared to other dye materials widely used for solar cells are tunable energy gaps, ability of multiple exciton generation, photostability, low cost and high absorption coefficient, which is

known to reduce the dark current and increase the overall efficiency of solar cells.¹⁵¹ Out of these, tunable energy gaps and multiple exciton generation features are the most desirable characteristics of the QDs.^{125,152-153}

1.9.1.1 Tunable Energy Gaps

The ability of QDs as sensitizer in QDSSC is studied by various research groups.¹⁵⁴⁻¹⁵⁵ The main motivation of using QDs as sensitizers in solar cell is because of their tunable energy bandgaps, which can control their absorption range.¹⁵⁶ There are number of reports in the literature showing that CdS and CdSe with tunable bandgap are capable of converting visible light to electric energy.¹⁵⁷⁻¹⁵⁸ The efficient charge separation by tuning the size of the QD utilizing the quantization effect was achieved by Vogel et al.¹⁵⁶ . Kongkanand et al.¹⁵⁹ separately reported CdSe QDs with various size assembled on TiO₂ films, showed improvement in photoelectrochemical response and photoconversion efficiency. With the decrease of CdSe particle size, photocurrent increases due to the shift of the CB to more negative potentials which in turn increases the driving force for charge injection. As a result, higher Incident Photon Conversion Efficiency is obtained at the excitonic band. This size dependent effect is made possible because of the quantum confinement effect exhibited by the QD itself.¹⁶⁰⁻¹⁶¹ Quantum confinement effect can be observed when QDs in colloidal solution show different color corresponding to the change of particle size, which results in a different absorption band of light. When the QD particles are sufficiently small, the effective bandgap energy of the QD is wider. Subsequently, the optical absorptions and emissions in relation with excitations across the bandgap shift towards higher energies.¹⁵² Quantum size effects have been demonstrated by Gorer et al. with the observed blueshift of the optical spectra of CdSe films as the crystal size decreases.¹⁶² This phenomenon is also high-

lighted in CdS QDs, as reported by Thambidurai et al.¹⁶³ where the same blueshift was observed in the optical spectra of smaller CdS QDs. Therefore, a combination of different quantum dot sizes in a cell will have better efficiency due to wider absorption of light by the quantum dots having a range of bandgaps.

1.9.1.2 Multiple Exciton Generation

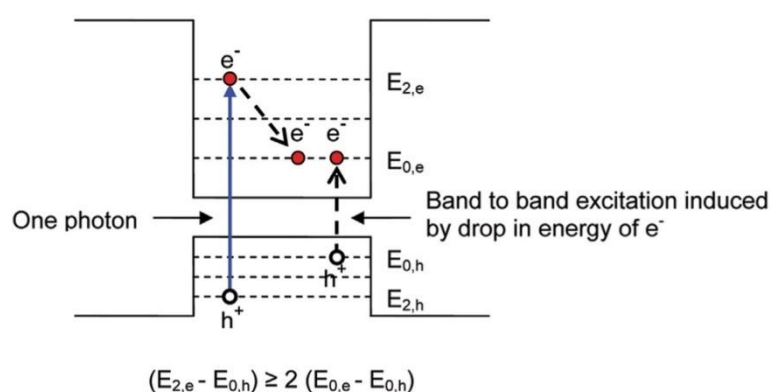


Figure 1.10 Multiple-carrier generation in QDs, a high-energy photon is absorbed at a high energy level in the QD, which then decays into two or more electron-hole pairs at the first confined energy level

[Source : Conibeer et. al. *Materials Today* 2007, 10, 42]

Carrier multiplication in solar cell research is the phenomenon where the absorption of a single photon leads to the excitation of multiple electrons from the valence band to conduction band. Conventional theory of solar cell suggests one photon excite only one electron across the band gap of the semiconductor, and if any excess energy is with the incident photon is dissipated as heat. But in material with carrier multiplication, high-energy photons excite more than one electron across the band gap, and so in principle the solar cell can produce more useful work. Multiple exciton generation (MEG) in QDs from a single photon have been reported by many research groups.¹⁶⁴⁻¹⁶⁵ In general, it is the

generation of more than one electron–hole pair upon the absorption of a photon. This phenomenon was first observed in PbS and PbSe QDs systems.¹⁶⁶ Upon absorption of solar radiation, photon with energies greater than the bandgap creates electrons and holes. At this point, the excess kinetic energy is equal to the difference between the photon energy and the bandgap, which creates an effective temperature condition for the carriers. The temperature of the carriers is higher than the lattice temperature. Thus, the term hot carriers (or hot electrons and hot holes) is used.

1.10 Motivation of the Present Study

The major factors which resist many practical applications of widely used semiconductor titania are the rapid charge recombination of the electron–hole pairs, thereby suppressing the quantum efficiency, and the wide band gap of the material, which restricts light absorption only to UV region of solar spectrum. In this scenario sensitisation of wide band gap semiconductors with those having a smaller band gap is receiving considerable attention for solar cell and photocatalytic applications. The effective use of the terrestrial solar spectrum is very important for the energy and environmental applications. Among the widely reported semiconductor photocatalysts, one dimensional titanium dioxide has attracted worldwide interest due to its strong oxidation activity and stability. One dimensional structures represent the smallest dimension structure that can efficiently transport electrical carriers. In recent years, because of the large band gap value (3.2 eV) the modification of TiO₂ photocatalysts for the enhancement of light absorption and photocatalytic activity under visible light irradiation has become the main research direction. To reach this goal, several modification techniques have been adopted that involve doping TiO₂ with metals and/or nonmetal elements such as Pd, Fe, Cu, C, and S, sensitization of TiO₂ by adsorbed dyes, and coupling TiO₂ with

semiconductors having lower band gaps and more cathodic conduction band (CB) such as CdS, PbS, CdSe due to their absorption characteristics in visible and near infrared region. In this regard titania nanostructures have shown particular promise as a support of such quantum dots for efficient charge transfer, due to its chemical inertness and appropriate band position. Eventhough chalcogenides have several advantages, the effectiveness has not reached upto the desired level because of the stability issues associated with them. Hence in this study we have chosen titania nanotubes sensitized with quantum dots of chalcogenides and metal nanoparticles for visible light driven photocatalytic activity and solar-cell applications. We have also followed the stability studies of such heterostructures through detailed XPS studies.

References

- [1] Gleiter, H. *Progress in Materials Science* **1989**, *33*, 223.
- [2] Mayo, M. J. *International Materials Reviews* **1996**, *41*, 85.
- [3] Suryanarayana, C. *International Materials Reviews* **1995**, *40*, 41.
- [4] *Chemistry of Materials* **1996**, *8*, 1569.
- [5] Zhang, X.; Jenekhe, S. A.; Perlstein, J. *Chemistry of Materials* **1996**, *8*, 1571.
- [6] Wang, Z. L. *Advanced Materials* **2000**, *12*, 1295.
- [7] Jalava, J.-P. *Particle & Particle Systems Characterization* **2006**, *23*, 159.
- [8] Li, X. Z.; Li, F. B. *Environmental Science & Technology* **2001**, *35*, 2381.
- [9] Kumar, K.-N. P.; Keizer, K.; Burggraaf, A. J. *Journal of Materials Chemistry* **1993**, *3*, 1141.
- [10] Kumar, K.-N. P.; Keizer, K.; Burggraaf, A. J.; Okubo, T.; Nagamoto, H. *Journal of Materials Chemistry* **1993**, *3*, 1151.
- [11] O'Regan, B.; Gratzel, M. *Nature* **1991**, *353*, 737.
- [12] Fujishima, A.; Rao, T. N.; Tryk, D. A. *Journal of Photochemistry and Photobiology C: Photochemistry Reviews* **2000**, *1*, 1.
- [13] Nakade, S.; Saito, Y.; Kubo, W.; Kitamura, T.; Wada, Y.; Yanagida, S. *The Journal of Physical Chemistry B* **2003**, *107*, 8607.
- [14] Kazuhito Hashimoto and Hiroshi Irie and Akira, F. *Japanese Journal of Applied Physics* **2005**, *44*, 8269.

- [15] Tian, Q.; Zhang, Z.; Yang, L.; Hirano, S.-i. *Electrochimica Acta* **2014**, *138*, 155.
- [16] Costa, E. D.; Avellaneda, C. O.; Pawlicka, A. *Journal of Materials Science* **2001**, *36*, 1407.
- [17] Krishnan, V. G.; Purushothaman, A.; Elango, P. *Journal of Materials Science: Materials in Electronics* **2017**, *28*, 11473.
- [18] Grant, F. A. *Reviews of Modern Physics* **1959**, *31*, 646.
- [19] Diebold, U. *Surface Science Reports* **2003**, *48*, 53.
- [20] Hadjiivanov, K. I.; Klissurski, D. G. *Chemical Society Reviews* **1996**, *25*, 61.
- [21] Wetchakun, N.; Incessungvorn, B.; Wetchakun, K.; Phanichphant, S. *Materials Letters* **2012**, *82*, 195.
- [22] Hanaor, D. A. H.; Sorrell, C. C. *Journal of Materials Science* **2011**, *46*, 855.
- [23] van der Meulen, T.; Mattson, A.; Osterlund, L. *Journal of Catalysis* **2007**, *251*, 131.
- [24] Xie, Y.; Zhao, Q.; Zhao, X. J.; Li, Y. *Catalysis Letters* **2007**, *118*, 231.
- [25] Kim, S.-Y.; Chang, T.-S.; Shin, C.-H. *Catalysis Letters* **2007**, *118*, 224.
- [26] Gimeno, O.; Rivas, F. J.; Beltran, F. J.; Carbajo, M. *Chemosphere* **2007**, *69*, 595.
- [27] Linsebigler, A. L.; Lu, G.; Yates, J. T. *Chemical Reviews* **1995**, *95*, 735.
- [28] Tanaka, K.; Capule, M. F. V.; Hisanaga, T. *Chemical Physics Letters* **1991**, *187*, 73.

- [29] Maruska, H. P.; Ghosh, A. K. *Solar Energy* **1978**, *20*, 443.
- [30] Gerischer, H.; Heller, A. *Journal of The Electrochemical Society* **1992**, *139*, 113.
- [31] Bickley, R. I.; Gonzalez-Carreno, T.; Lees, J. S.; Palmisano, L.; Tilley, R. J. D. *Journal of Solid State Chemistry* **1991**, *92*, 178.
- [32] Deng, X.; Yue, Y.; Gao, Z. *Applied Catalysis B: Environmental* **2002**, *39*, 135.
- [33] Mills, G.; Jonsson, H.; Schenter, G. K. *Surface Science* **1995**, *324*, 305.
- [34] Bacsá, R. R.; Kiwi, J. *Applied Catalysis B: Environmental* **1998**, *16*, 19.
- [35] Muggli, D. S.; Ding, L. *Applied Catalysis B: Environmental* **2001**, *32*, 181.
- [36] Ohno, T.; Sarukawa, K.; Tokieda, K.; Matsumura, M. *Journal of Catalysis* **2001**, *203*, 82.
- [37] Zhang, Q.; Gao, L.; Guo, J. *Applied Catalysis B: Environmental* **2000**, *26*, 207.
- [38] Martin, S. T.; Herrmann, H.; Choi, W.; Hoffmann, M. R. *Journal of the Chemical Society, Faraday Transactions* **1994**, *90*, 3315.
- [39] Wan, K. T.; Davis, M. E. *Nature* **1994**, *370*, 449.
- [40] Shibasaki-Kitakawa, N.; Honda, H.; Kuribayashi, H.; Toda, T.; Fukumura, T.; Yonemoto, T. *Bioresource Technology* **2007**, *98*, 416.
- [41] Shannon, R. D.; Pask, J. A. *Journal of the American Ceramic Society* **1965**, *48*, 391.
- [42] Hishita, S.; Mutoh, I.; Koumoto, K.; Yanagida, H. *Ceramics International* **1983**, *9*, 61.

- [43] Yijun Sun and Takashi Egawa and Liangying Zhang and Xi, Y. *Japanese Journal of Applied Physics* **2002**, *41*, L945.
- [44] Suresh, C.; Biju, V.; Mukundan, P.; Warriar, K. G. K. *Polyhedron* **1998**, *17*, 3131.
- [45] Gilbert, B.; Zhang, H.; Huang, F.; Finnegan, M. P.; Waychunas, G. A.; Banfield, J. F. *Geochemical Transactions* **2003**, *4*, 20.
- [46] Gamboa, J. A.; Pasquevich, D. M. *Journal of the American Ceramic Society* **1992**, *75*, 2934.
- [47] Riyas, S.; Krishnan, G.; Das, P. N. M. *Advances in Applied Ceramics* **2007**, *106*, 255.
- [48] Gennari, F. C.; Pasquevich, D. M. *Journal of the American Ceramic Society* **1999**, *82*, 1915.
- [49] Vargas, S.; Arroyo, R.; Haro, E.; Rodriguez, R. *Journal of Materials Research* **1999**, *14*, 3932.
- [50] Shen, G.; Cho, J. H.; Yoo, J. K.; Yi, G.-C.; Lee, C. J. *The Journal of Physical Chemistry B* **2005**, *109*, 9294.
- [51] Shen, G.; Chen, D. *Journal of the American Chemical Society* **2006**, *128*, 11762.
- [52] Kind, H.; Yan, H.; Messer, B.; Law, M.; Yang, P. *Advanced Materials* **2002**, *14*, 158.
- [53] Fan, X.; Meng, X. M.; Zhang, X. H.; Zhang, M. L.; Jie, J. S.; Zhang, W. J.; Lee, C. S.; Lee, S. T. *The Journal of Physical Chemistry C* **2009**, *113*, 834.

- [54] Mor, G. K.; Shankar, K.; Paulose, M.; Varghese, O. K.; Grimes, C. A. *Nano Letters* **2006**, *6*, 215.
- [55] Paulose M.; Shankar K.; and Oomman, K. V. *Nanotechnology* **2006**, *17*, 1446.
- [56] Varghese, O. K.; Paulose, M.; Grimes, C. A. *Nature Nanotechnology* **2009**, *4*, 592.
- [57] Martin, C. R. *Chemistry of Materials* **1996**, *8*, 1739.
- [58] Martin, C. R. *Science* **1994**, *266*, 1961.
- [59] Whitney, T. M.; Searson, P. C.; Jiang, J. S.; Chien, C. L. *Science* **1993**, *261*, 1316.
- [60] Shankar, K.; Basham, J. I.; Allam, N. K.; Varghese, O. K.; Mor, G. K.; Feng, X.; Paulose, M.; Seabold, J. A.; Choi, K.-S.; Grimes, C. A. *The Journal of Physical Chemistry C* **2009**, *113*, 6327.
- [61] Mor, G. K.; Varghese, O. K.; Paulose, M.; Shankar, K.; Grimes, C. A. *Solar Energy Materials and Solar Cells* **2006**, *90*, 2011.
- [62] Roy, P.; Berger, S.; Schmuki, P. *Angewandte Chemie International Edition*, **2011**, *50*, 2904.
- [63] Wong, C. L.; Tan, Y. N.; Mohamed, A. R. *Journal of Environmental Management* **2011**, *92*, 1669.
- [64] Mills, A.; Le Hunte, S. *Journal of Photochemistry and Photobiology A: Chemistry* **1997**, *108*, 1.
- [65] Gaya, U. I.; Abdullah, A. H. *Journal of Photochemistry and Photobiology C: Photochemistry Reviews* **2008**, *9*, 1.

- [66] Konstantinou, I. K.; Albanis, T. A. *Applied Catalysis B: Environmental* **2004**, *49*, 1.
- [67] Kuang, D.; Klein, C.; Ito, S.; Moser, J. E.; Humphry-Baker, R.; Evans, N.; Duriaux, F.; Gratzel, C.; Zakeeruddin, S. M.; Gratzel, M. *Advanced Materials* **2007**, *19*, 1133.
- [68] Ollis, D. F.; Pelizzetti, E.; Serpone, N. *Environmental Science & Technology* **1991**, *25*, 1522.
- [69] Tariq, M. A.; Faisal, M.; Muneer, M.; Bahnemann, D. *Journal of Molecular Catalysis A: Chemical* **2007**, *265*, 231.
- [70] Bhatkhande, D. S.; Kamble, S. P.; Sawant, S. B.; Pangarkar, V. G. *Chemical Engineering Journal* **2004**, *102*, 283.
- [71] Hugul, M.; Ercag, E.; Apak, R. *Journal of Environmental Science and Health, Part A* **2002**, *37*, 365.
- [72] Palmisano, G.; Addamo, M.; Augugliaro, V.; Caronna, T.; Di Paola, A.; Lopez, E. G.; Loddo, V.; Marci, G.; Palmisano, L.; Schiavello, M. *Catalysis Today* **2007**, *122*, 118.
- [73] Friesen, D. A.; Morello, L.; Headley, J. V.; Langford, C. H. *Journal of Photochemistry and Photobiology A: Chemistry* **2000**, *133*, 213.
- [74] Arana, J.; Martinez Nieto, J. L.; Herrera Melian, J. A.; Dona Rodriguez, J. M.; Gonzalez Diaz, O.; Perez Peria, J.; Bergasa, O.; Alvarez, C.; Mendez, J. *Chemosphere* **2004**, *55*, 893.
- [75] Guillard, C.; Lachheb, H.; Houas, A.; Ksibi, M.; Elaloui, E.; Herrmann, J.-M. *Journal of Photochemistry and Photobiology A: Chemistry* **2003**, *158*, 27.

- [76] Kogo, K.; Yoneyama, H.; Tamura, H. *The Journal of Physical Chemistry* **1980**, *84*, 1705.
- [77] Ding, H.; Sun, H.; Shan, Y. *Journal of Photochemistry and Photobiology A: Chemistry* **2005**, *169*, 101.
- [78] Gao, Y.; Liu, H. *Materials Chemistry and Physics* **2005**, *92*, 604.
- [79] Mohammadi, M. R.; Cordero-Cabrera, M. C.; Fray, D. J.; Ghorbani, M. *Sensors and Actuators B: Chemical* **2006**, *120*, 86.
- [80] Diebold, U. *Surface Science Reports* **2003**, *48*, 53.
- [81] Maira, A. J.; Yeung, K. L.; Soria, J.; Coronado, J. M.; Belver, C.; Lee, C. Y.; Augugliaro, V. *Applied Catalysis B: Environmental* **2001**, *29*, 327.
- [82] Krysa, J.; Keppert, M.; Jirkovsky, J.; Stengl, V.; Subrt, J. *Materials Chemistry and Physics* **2004**, *86*, 333.
- [83] Saquib, M.; Muneer, M. *Dyes and Pigments* **2003**, *56*, 37.
- [84] Chun, H.; Yizhong, W.; Hongxiao, T. *Chemosphere* **2000**, *41*, 1205.
- [85] Helz, G. R.; Zepp, R. G.; Crosby, D. G. *Aquatic and surface photochemistry*; Lewis Publishers: Boca Raton, 1994.
- [86] Fox, M. A.; Dulay, M. T. *Chemical Reviews* **1993**, *93*, 341.
- [87] Tunesi, S.; Anderson, M. A. *Chemosphere* **1987**, *16*, 1447.
- [88] Evgenidou, E.; Fytianos, K.; Poullos, I. *Applied Catalysis B: Environmental* **2005**, *59*, 81.
- [89] Muradov, N. Z.; T-Raissi, A.; Muzzey, D.; Painter, C. R.; Kemme, M. R. *Solar Energy* **1996**, *56*, 445.

- [90] Fu, X.; Clark, L. A.; Zeltner, W. A.; Anderson, M. A. *Journal of Photochemistry and Photobiology A: Chemistry* **1996**, *97*, 181.
- [91] Laidler, K. J. *Journal of Chemical Education* **1984**, *61*, 494.
- [92] Alsawat, M.; Altalhi, T.; Shapter, J. G.; Losic, D. *Catalysis Science & Technology* **2014**, *4*, 2091.
- [93] Huang, K.-C.; Chien, S.-H. *Applied Catalysis B: Environmental*, **2013**,*141*, 283.
- [94] Liu, H.; Zhang, Y.; Yang, H.; Xiao, W.; Sun, L. *Advances in Materials Science and Engineering* **2016**, *2016*, 10.
- [95] Zhang M.; Hou J.; Juan Wu J.; Jianjun, Y. *Japanese Journal of Applied Physics* **2014**, *53*, 115505.
- [96] Liang, K.; Tay, B. K.; Kupreeva, O. V.; Orekhovskaya, T. I.; Lazarouk, S. K.; Borisenko, V. E. *ACS Sustainable Chemistry & Engineering* **2014**, *2*, 991.
- [97] Grandcolas, M.; Ye, J.; Miyazawa, K. *Ceramics International* **2014**, *40*, 1297.
- [98] Kustiningsih, I.; ., S.; Purwanto, W. W. *International Journal of Technology* **2014**, *2*,133.
- [99] Asapu, R.; Palla, V. M.; Wang, B.; Guo, Z.; Sadu, R.; Chen, D. H. *Journal of Photochemistry and Photobiology A: Chemistry* **2011**, *225*, 81.
- [100] Tsai, C.-C.; Teng, H. *Chemistry of Materials* **2004**, *16*, 4352.
- [101] Momeni, M. M.; Ahadzadeh, I. *Materials Research Innovations* **2016**, *20*, 44.

- [102] Chen, K.; Feng, X.; Tian, H.; Li, Y.; Xie, K.; Hu, R.; Cai, Y.; Gu, H. *Journal of Materials Research* **2014**, *29*, 1302.
- [103] Lin, J.; Liu, X.; Zhu, S.; Liu, Y.; Chen, X. *Nanoscale Research Letters* **2015**, *10*, 110.
- [104] Kontos, A. G.; Stergiopoulos, T.; Tsiminis, G.; Raptis, Y. S.; Falaras, P. *Inorganica Chimica Acta* **2008**, *361*, 761.
- [105] Chen, Y.; Crittenden, J. C.; Hackney, S.; Sutter, L.; Hand, D. W. *Environmental Science & Technology* **2005**, *39*, 1201.
- [106] Vijayan, B.; Dimitrijevic, N. M.; Rajh, T.; Gray, K. *The Journal of Physical Chemistry C* **2010**, *114*, 12994.
- [107] Hou, Y.; Li, X.; Liu, P.; Zou, X.; Chen, G.; Yue, P.-L. *Separation and Purification Technology* **2009**, *67*, 135.
- [108] Zhou, Q.; Fu, M.-L.; Yuan, B.-L.; Cui, H.-J.; Shi, J.-W. *Journal of Nanoparticle Research* **2011**, *13*, 6661.
- [109] Liu, Z.; Chen, J.; Zhang, Y.; Wu, L.; Li, X. *Materials Chemistry and Physics* **2011**, *128*, 1.
- [110] Paramasivam, I.; Macak, J.; Schmuki, P. *Electrochemistry Communications* **2008**, *10*, 71.
- [111] Tang, Y.; Luo, S.; Teng, Y.; Liu, C.; Xu, X.; Zhang, X.; Chen, L. *Journal of Hazardous Materials* **2012**, *241*, 323.
- [112] Xu, Y.-H.; Chen, C.; Yang, X.-L.; Li, X.; Wang, B.-F. *Applied Surface Science* **2009**, *255*, 8624.
- [113] Liu, H.; Liu, G.; Xie, G.; Zhang, M.; Hou, Z.; He, Z. *Applied Surface Science* **2011**, *257*, 3728.

- [114] Liu, H.; Liu, G.; Fan, J.; Zhou, Q.; Zhou, H.; Zhang, N.; Hou, Z.; Zhang, M.; He, Z. *Chemosphere* **2011**, 82, 43.
- [115] Ratanatawanate, C.; Bui, A.; Vu, K.; Balkus, K. J. *The Journal of Physical Chemistry C* **2011**, 115, 6175.
- [116] Liu, R.; Liu, Y.; Liu, C.; Luo, S.; Teng, Y.; Yang, L.; Yang, R.; Cai, Q. *Journal of Alloys and Compounds* **2011**, 509, 2434.
- [117] Liu, Y.; Zhang, X.; Liu, R.; Yang, R.; Liu, C.; Cai, Q. *Journal of Solid State Chemistry* **2011**, 184, 684.
- [118] Jose, R.; Thavasi, V.; Ramakrishna, S. *Journal of the American Ceramic Society* **2009**, 92, 289.
- [119] Benkstein, K. D.; Kopidakis, N.; van de Lagemaat, J.; Frank, A. J. *The Journal of Physical Chemistry B* **2003**, 107, 7759.
- [120] Mor, G. K.; Varghese, O. K.; Paulose, M.; Shankar, K.; Grimes, C. A. *Solar Energy Materials and Solar Cells* **2006**, 90, 2011.
- [121] Fujishima, A.; Honda, K. *Nature* **1972**, 238, 37.
- [122] O'Regan, B.; Gratzel, M. *Nature* **1991**, 353, 737.
- [123] Meyer, G. J. *ACS Nano* **2010**, 4, 4337.
- [124] Likodimos, V.; Stergiopoulos, T.; Falaras, P.; Harikisun, R.; Desilvestro, J.; Tulloch, G. *The Journal of Physical Chemistry C* **2009**, 113, 9412.
- [125] Kamat, P. V. *The Journal of Physical Chemistry C* **2008**, 112, 18737.
- [126] Hodes, G. *The Journal of Physical Chemistry C* **2008**, 112, 17778.

- [127] Mora-Sero, I.; Gimenez, S.; Moehl, T.; Fabregat-Santiago, F.; Lana-Villareal, T.; Gomez, R.; Bisquert, J. *Nanotechnology* **2008**, *19*, 424007.
- [128] Bang, J. H.; Kamat, P. V. *Advanced Functional Materials* **2010**, *20*, 1970.
- [129] Gonzalez-Pedro, V.; Xu, X.; Mora-Sero, I.; Bisquert, J. *ACS Nano* **2010**, *4*, 5783.
- [130] Yu, X.-Y.; Liao, J.-Y.; Qiu, K.-Q.; Kuang, D.-B.; Su, C.-Y. *ACS Nano* **2011**, *5*, 9494.
- [131] Tian, J.; Gao, R.; Zhang, Q.; Zhang, S.; Li, Y.; Lan, J.; Qu, X.; Cao, G. *The Journal of Physical Chemistry C* **2012**, *116*, 18655.
- [132] Hines, D. A.; Kamat, P. V. *ACS Applied Materials & Interfaces* **2014**, *6*, 3041.
- [133] Shalom, M.; Dor, S.; Rahle, S.; Grinis, L.; Zaban, A. *The Journal of Physical Chemistry C* **2009**, *113*, 3895.
- [134] Lee, H.; Wang, M.; Chen, P.; Gamelin, D. R.; Zakeeruddin, S. M.; Gratzel, M.; Nazeeruddin, M. K. *Nano Letters* **2009**, *9*, 4221.
- [135] Guijarro, N.; Lana-Villarreal, T.; Mora-Sero, I.; Bisquert, J.; Gomez, R. *The Journal of Physical Chemistry C* **2009**, *113*, 4208.
- [136] Lee, H.; Wang, M. K.; Chen, P.; Gamelin, D. R.; Zakeeruddin, S. M.; Gratzel, M.; Nazeeruddin, M. K. *Nano Letters* **2009**, *9*, 4221.
- [137] Rauf, I. A.; Rezai, P. *Renewable and Sustainable Energy Reviews* **2017**, *73*, 408.

- [138] Lee, H. J.; Chen, P.; Moon, S. J.; Sauvage, F.; Sivula, K.; Bessho, T.; Gamelin, D. R.; Comte, P.; Zakeeruddin, S. M.; Seok, S. I.; Gratzel, M.; Nazeeruddin, M. K. *Langmuir* **2009**, *25*, 7602.
- [139] Barea, E. M.; Shalom, M.; Gimenez, S.; Hod, I.; Mora-Sero, I.; Zaban, A.; Bisquert, J. *Journal of the American Chemical Society* **2010**, *132*, 6834.
- [140] Leschkies, K. S.; Divakar, R.; Basu, J.; Enache-Pommer, E.; Boercker, J. E.; Carter, C. B.; Kortshagen, U. R.; Norris, D. J.; Aydil, E. S. *Nano Letters* **2007**, *7*, 1793.
- [141] Robel, I.; Subramanian, V.; Kuno, M.; Kamat, P. V. *Journal of the American Chemical Society* **2006**, *128*, 2385.
- [142] Krbal, M.; Sopha, H.; Podzemna, V.; Das, S.; Prikryl, J.; Macak, J. M. *The Journal of Physical Chemistry C* **2017**, *121*, 6065.
- [143] Ayal, A. K.; Zainal, Z.; Lim, H.-N.; Talib, Z. A.; Lim, Y.-C.; Chang, S.-K.; Holi, A. M. *Optical and Quantum Electronics* **2017**, *49*, 164.
- [144] Bang, J. H.; Kamat, P. V. *Advanced Functional Materials* **2010**, *20*, 1970.
- [145] Yen, Y.-C.; Lin, C.-C.; Chen, P.-Y.; Ko, W.-Y.; Tien, T.-R.; Lin, K.-J. *Royal Society Open Science* **2016**, *4*, 161051.
- [146] Sixto Gimenez , I. M.-S., Lorena Macor , Nestor Guijarro , Teresa Lana-Villarreal , Roberto Gomez , Lina, J. Diguna , Qing Shen , Taro Toyoda and Juan Bisquert *Nanotechnology* **2009**, *20*, 295204.
- [147] Huang S.; Zhang Q.; Huang X.; Guo X.; Deng M.; Li D. *Nanotechnology* **2010**, *21*, 375201.

- [148] Makama, A. B.; Salmiaton, A.; Saion, E. B.; Choong, T. S. Y.; Abdullah, N. *International Journal of Photoenergy* **2016**, *2016*, 14.
- [149] Zhou, R.; Zhang, Q.; Tian, J.; Myers, D.; Yin, M.; Cao, G. *The Journal of Physical Chemistry C* **2013**, *117*, 26948.
- [150] Kontos, A. G.; Likodimos, V.; Vassalou, E.; Kapogianni, I.; Raptis, Y. S.; Raptis, C.; Falaras, P. *Nanoscale Research Letters* **2011**, *6*, 266.
- [151] Shen Yu-Jen.; Yuh-Lang, L. *Nanotechnology* **2008**, *19*, 045602.
- [152] Rühle, S.; Shalom, M.; Zaban, A. *A European Journal of Chemical Physics and Physical Chemistry* **2010**, *11*, 2290.
- [153] Gonzalez-Pedro, V.; Xu, X.; Mora-Sero, I.; Bisquert, J. *ACS Nano* **2010**, *4*, 5783.
- [154] Jasim, K. E. In *Solar Cells - New Approaches and Reviews*; Kosyachenko, L. A., Ed.; InTech: Rijeka, 2015, p Ch. 11.
- [155] Torchynska, T.; Vorobiev, Y. In *Advanced Biomedical Engineering*; Gargiulo, G. D., McEwan, A., Eds.; InTech: Rijeka, 2011, p Ch. 09.
- [156] Vogel, R.; Hoyer, P.; Weller, H. *The Journal of Physical Chemistry* **1994**, *98*, 3183.
- [157] Kongkanand, A.; Tvrdy, K.; Takechi, K.; Kuno, M.; Kamat, P. V. *Journal of the American Chemical Society* **2008**, *130*, 4007.
- [158] Peng, Z. A.; Peng, X. *Journal of the American Chemical Society* **2001**, *123*, 183.
- [159] Kongkanand, A.; Tvrdy, K.; Takechi, K.; Kuno, M. K.; Kamat, P. V. *Journal of the American Chemical Society* **2008**, *130*, 4007.

- [160] Wang, X.; Koleilat, G. I.; Tang, J.; Liu, H.; Kramer, I. J.; Debnath, R.; Brzozowski, L.; Barkhouse, D. A. R.; Levina, L.; Hoogland, S.; Sargent, E. H. *Nature Photonics* **2011**, *5*, 480.
- [161] Gratzel, M. *Nature* **2001**, *414*, 338.
- [162] Gorer, S.; Hodes, G. *The Journal of Physical Chemistry* **1994**, *98*, 5338.
- [163] Thambidurai, M.; Muthukumarasamy, N.; Agilan, S.; Murugan, N.; Vasantha, S.; Balasundaraprabhu, R.; Senthil, T. S. *Journal of Materials Science* **2010**, *45*, 3254.
- [164] Nozik, A. J.; Beard, M. C.; Luther, J. M.; Law, M.; Ellingson, R. J.; Johnson, J. C. *Chemical Reviews* **2010**, *110*, 6873.
- [165] Schaller, R. D.; Klimov, V. I. *Physical Review Letters* **2004**, *92*, 186601.
- [166] Ellingson, R. J.; Beard, M. C.; Johnson, J. C.; Yu, P. R.; Micic, O. I.; Nozik, A. J.; Shabaev, A.; Efros, A. L. *Nano Letters* **2005**, *5*, 865.

Experimental and Characterization Techniques

• Contents •

- 2.1 Hydrothermal synthesis of Titania nanotube
- 2.2 Anodization Process
- 2.3 SILAR Method of Deposition
- 2.4 Photoactivity Evaluation Study
- 2.5 Fundamental Characterisation techniques
- References

Today the word nanotechnology implies design, fabrication and applications of nanostructures or nanomaterials and the fundamental understanding of the relationships between physical properties or phenomena and material dimensions. Similar to quantum mechanics on nanometer scale, materials or structures may possess new physical properties or exhibit new physical phenomena. A key challenge in exploiting the novel properties associated with nanomaterials is in the synthesis of nanoparticles with precisely controlled sizes and morphologies. Nanoscale properties of materials are size and shape dependent. Therefore there occurs an extensive effort to control size, shape and surface composition of materials. Nowadays environmental pollution and inadequate availability of non renewable energy sources became the two critical issues of human being. All these issues can be addressed by making use of two important technologies of science, photocatalysis and solar cells. In view of these things we developed different nanostructured titania, the most experimented semiconductor in the field of photocatalysis and solar cell technology. The major disadvantages of titania based photocatalysis includes the rapid charge recombination of the electron-hole pairs and the wide band gap of titania (3.0 eV for rutile and 3.2 eV for anatase) in the Ultra Violet region which restricts the efficient solar light harvesting. There are various strategies like dye sensitization, metal, or nonmetal doping and heterostructures of semiconductors have been developed to improve the visible light activity of titania. In our study we prepared titania nanotubes as base material. After that titania nanotubes were sensitized using chalcogenide quantum dots and Pd metal particles. And these photocatalysts were effectively used for photocatalytic, catalytic and solar cell applications.

2.1 Hydrothermal Synthesis of Titania Nanotube



Figure 2.1 Hydrothermal setup for the synthesis of titania nanostructures

Hydrothermal synthesis can be defined as a technique which involves crystallization of material from mineral dissolved in water at high temperature and pressure. Here the reaction was carried out inside a pressure vessel. In this method various parameters such as concentration of chemical constituents, temperature and the processing time are controlled for the development of required nanostructures. To achieve the targeted morphology it is proposed to

study different reaction conditions both in alkali and in acid conditions. Preparation of the nanotube and nanorod require the following steps. For the preparation of titania nanotube 50 ml of 10 M NaOH solution was added into the Teflon cup. Then 2 g of titanium dioxide was weighed and added into the cup and it was stirred well for one hour. Then it was placed under high pressure and kept in an oven at 120 °C for 48 hours. The reaction with sodium hydroxide leads to the breaking of two longer Ti-O bonds in the octahedrally coordinated titania, thus leads to the formation of sodium titanate, which is washed with HCl to form hydrogen titanate nanotube. These nanotubes are calcined to form anatase titania nanotube.

2.2 Anodization Process



Figure 2.2 Anodization setup for the synthesis of titania nanotubes

Anodic oxidation is a common method of choice to grow ordered nanostructures. This technique is simple, cheap, and provides a high degree of control over the dimensions of the nanostructures. By controlling the

anodization parameters of Ti such as applied voltage, temperature, concentration etc, different titanium oxide structures such as a compact oxide, a disordered porous layer or a self-organized nanotube structure can be produced. In the presence of fluorine in the electrolyte, a tubular titania layer forms instead of just a compact oxide layer. In the anodization process Ti is used as anode and Pt wire as cathode. Titania metal sheet (assay 99.7%, Sigma Aldrich) of dimension ($3 \times 1 \times 0.25 \text{ cm}^3$) is potentiostatically anodised under 40 V for 24 hours using platinum counter electrode in an electrolyte consists of 96.5 ml ethylene glycol (assay 99%, Merck), 3.5 ml water and 0.6 g ammonium fluoride (assay 98%, Sigma Aldrich). The resultant amorphous titania nanotube arrays formed on the surface of titanium metal surface was washed several times in distilled water to make free from fluoride ions. Then it was heated at 400 °C for one hour to form crystalline anatase phase of titania nanotube.

2.3 SILAR Method of Deposition

SILAR method is considered as one of the recent soft chemical solution methods for the deposition of thin films. It is relatively a new and less investigated method and based on sequential reaction at the substrate surface, rinsing follows each reaction, which enables heterogeneous reaction between the solid phase and the solvated ions in the solution. The features of the SILAR method include excellent material utilization efficiency, good control over the deposition process along with the film thickness, low cost and large-scale deposition capability on virtually any type of substrate. One SILAR cycle consists of four steps: (1) adsorption of cationic species for 1 minute, (2) rinsing with washing solvent for 5 s to remove excess adsorbed or loosely bounded cation species, (3) reaction with anionic precursor solution for 1 minute to form stable chalcogenide and (4) rinsing with purified washing solvent for 5 s to remove excess or unreacted species or powdery substance.

The higher concentration of precursor solutions will result higher growth rate but the quality of the film will be poor due to powdery deposit.

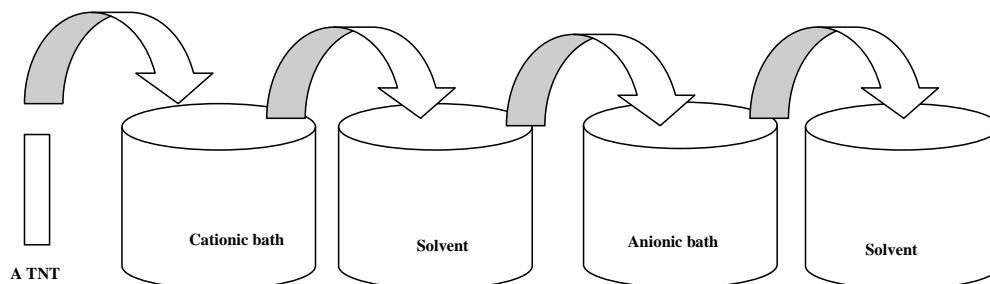


Figure 2.3 Schematic representation for Sensitization of titania nanotube with chalcogenide by SILAR method

2.4 Photoactivity Evaluation Study

The photocatalytic activity of the prepared photocatalyst were measured by determining the degradation of Methylene Blue (MB) dye. MB is a photostable dye having characteristic absorption at 663nm. The degradation experiments were performed in presence of UV or visible light in a photo reactor. In this experiment the concentration of MB is monitored at different time intervals. Before illumination the solution containing MB and photocatalyst was kept in dark for 2 hours in order to acquire adsorption-desorption equilibrium of dye over the catalyst. After this the initial absorption of the dye was recorded followed by irradiation of the solution in a UV/Visible chamber for different time intervals such as 10, 20, 30, 40, 50, 60, 90, 120, 150, 180, 210, 240 and 270 min using an UV visible spectrometer (Shimadzu, Japan, UV-2401PC). The degradation profiles were drawn by plotting the maximum absorbance of the main intensity peak (663 nm) of MB at regular intervals of light exposure. It was reported that the degradation of MB was found to follow the pseudo-first-order kinetic model, so the change in concentration of the dye, with respect to the initial concentration, was plotted

as a function of time. In a pseudo first order reaction, we can manipulate the initial concentration of the reactants. One of the reactants, A, for example would have significantly high concentration, while the other reactant B would have a significantly low concentration. We can then assume that reactant A concentration effectively remains constant during the reaction because its consumption is so small that the change in concentration becomes negligible. The kinetic model to predict rate constant for the reaction, in which the reaction rate for photocatalytic reactions are independent of hydroxyl ion concentration. Then the rate equation becomes $\frac{-dC_{MB}}{dt} = K * C_{MB}$ where C_{MB} represents the concentration of methylene blue. Then the rate equation can be written as $-\ln \frac{C_{dye}}{C_{dye 0}} = k_{obs} * t$ The reference methylene blue solution having same concentration without the photocatalyst, did not show any degradation under light illumination

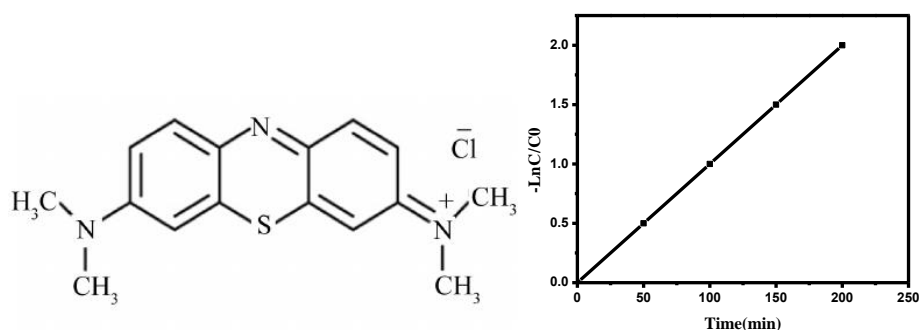


Figure 2.4 Chemical structure of methylene blue and Pseudo-first order kinetics of degradation of MB in presence of photocatalyst

The schematic representation of the photocatalytic reactor is provided in Figure 2.5. In a typical experiment, after adsorption-desorption equilibrium, the initial absorption of the methylene blue in the cuvette is monitored, followed by irradiation of the solution over different time intervals in a visible light chamber consisting of a 1000 W mercury lamp (Philips Belgium HPL-N)

with a polycarbonate sheet and glass as the UV radiation filter. The polycarbonate and glass filter out all the radiation below 400 nm and the light after filtration having intensity of $\sim 330 \mu\text{W}/\text{cm}^2$ was used for the photocatalytic reaction. The transmission spectra of the polycarbonate sheet along with a glass sheet and Emission Spectra of the mercury lamp after the filtration with polycarbonate and glass sheet are shown in Figure 2.6 and Figure 2.7. The change in concentration of the dye, with respect to the initial concentration, was plotted as a function of time. In certain cases, specific catalytic reactions were also studied to understand their efficacy for possible industrial applications.

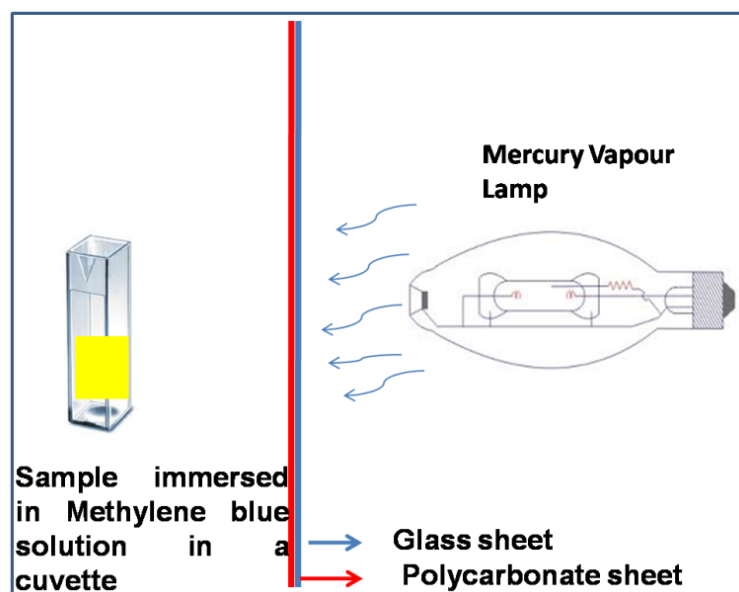


Figure 2.5 Schematic representation of the photocatalytic reactor

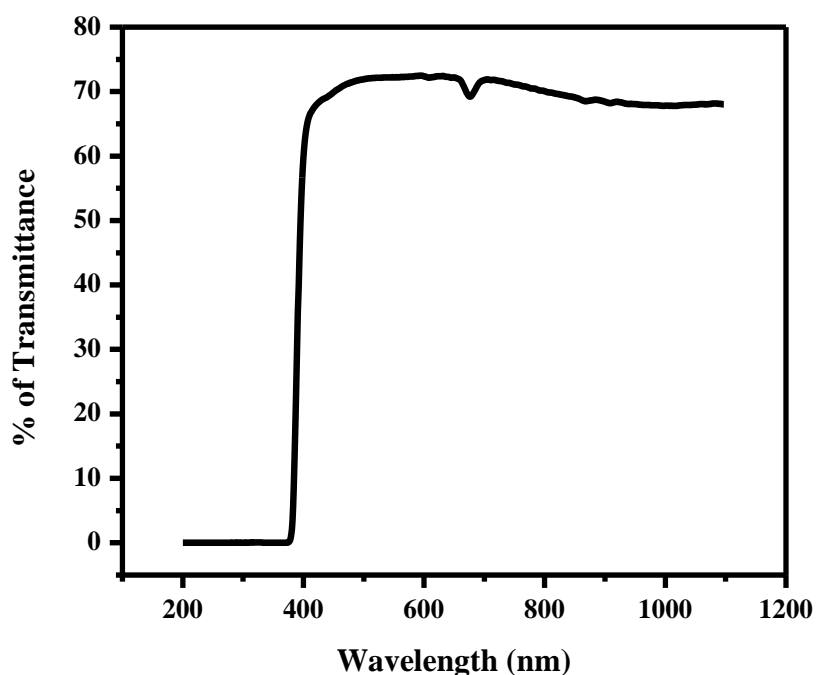


Figure 2.6 The transmittance spectra of the polycarbonate sheet along with a glass sheet

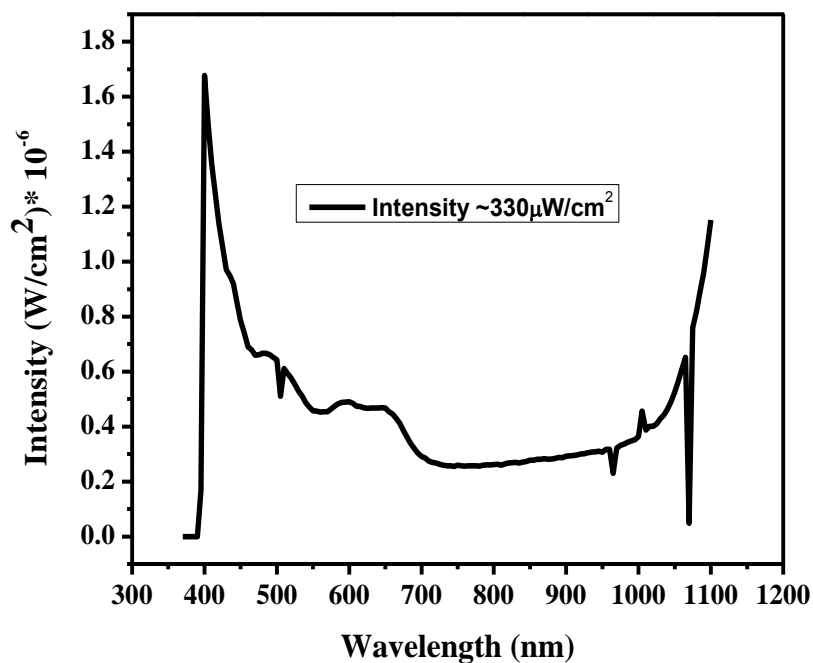


Figure 2.7 Emission Spectra of the mercury lamp after the filtration with polycarbonate and glass sheet

2.5 Fundamental Characterisation Techniques

Important techniques used for the characterization of prepared photocatalyst are X-ray diffraction technique (XRD), UV-Visible absorption spectroscopy, Raman Spectroscopy, X-ray Photoelectron Spectroscopy, PL spectroscopy, BET surface area analysis technique, SEM and TEM

2.5.1 X- ray diffraction- determination of crystalline structure



Figure 2.8 X-ray Diffractometer

X-ray diffraction is one of the most important non-destructive characterisation technique used in solid state chemistry and materials science. It is used for the investigation of the fine structure of matter and it also provides information about structures, phases, preferred crystal orientations, and other structural parameters, such as average grain size, crystallinity, strain,

and crystal defects etc.¹A crystal may be defined as a solid with periodic pattern of atoms arranged in three dimensions. X-ray diffraction technique had its beginnings with Von Laue's discovery in 1912. The regularly spaced atoms of crystals can act as scattering centers for X-rays, also the wave length of X-rays is in the order of interatomic distance in crystals. So the diffraction of X-rays can be done by means of crystals. Using X-ray diffraction we can identify the crystalline material and also its structure including how the atoms pack together in the crystalline state and what the interatomic distance and angle etc.² When a beam of monochromatic X-rays falls on a crystal, it is scattered by the individual atoms in parallel planes. These parallel planes are called Bragg planes. The basic principle in powder crystal method is that since millions of tiny crystals in the powder have random orientations, all possible diffraction planes will be available for Bragg reflection. By considering constructive interference, the path difference = $n\lambda$, then the Bragg law is

$$n\lambda = 2d\sin\theta \quad (2(1))$$

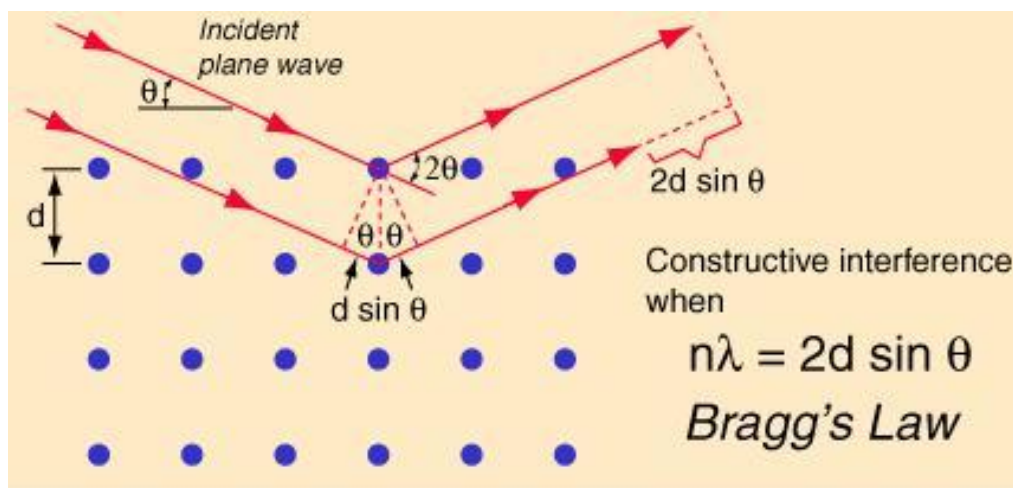


Figure 2.9 X-ray diffraction from different crystal planes

Also one can determine the size and the shape of the unit cell for any compound most easily using the diffraction of X-rays by applying Scherrer equation. This formula relates the size of sub-micrometre particles, or crystallites, in a solid to the broadening of the peak in diffraction pattern.

The Scherrer equation can be written as : $D = \frac{K\lambda}{\beta \cos\theta}$ 2(2)

where:

- D is the mean size of the ordered (crystalline) domains, which may be smaller or equal to the grain size
- K is a dimensionless shape factor, with a value close to unity.
- λ is the wavelength of X-ray;
- β is the line broadening at half the maximum intensity (FWHM), in radians.
- θ is the Bragg angle (in degrees)

Commonly in X-ray diffraction experiments the radiation used is that emitted by copper, whose characteristic wavelength for the K radiation is $\lambda = 1.5418 \text{ \AA}$. When the incident beam strikes a powder sample, diffraction occurs in every possible orientation of 2θ . XRD patterns of titania nanostructures synthesized by different routes were scanned in the 2θ range 10 to 80° with a step of 0.01° and a scan speed of $4^\circ/\text{min}$

2.5.2 Raman Spectroscopy



Figure 2.10 Raman Spectrometer

Reflection, absorption and scattering are the different processes occurs when a monochromatic radiation is incident up on a sample. According to raman scattering stoke's and anti-stoke's lines (with different wavelength) are observed along with Rayleigh scattering (with incident wavelength). Raman scattering gives information regarding chemical and structural property of the sample.³ Infrared spectroscopy deals with a change in the dipole moment of a molecule where as Raman spectroscopy arises from a change in polarizability of the molecule due to interaction of the light.⁴ The theory of Raman scattering shows that the phenomenon results from the same type of quantized vibrational changes that are associated with infrared absorption. Thus, the difference in wavelength between the incident and scattered visible radiation corresponds to wavelengths in the mid-infrared region. Raman spectra are acquired by irradiating a sample with a powerful laser source of visible or near-infrared monochromatic radiation. During irradiation, the spectrum of the scattered radiation is measured at some angle (often 90 deg) with a suitable spectrometer. The intensities of Raman lines are 0.001 % of the intensity of

the source; as a consequence, their detection and measurement are somewhat more difficult than the infrared spectra.

2.5.3 UV-Visible Spectroscopy



Figure 2.11 UV-Visible Spectrophotometer

The electronic transitions in a material can be studied in absorption/transmittance or reflectance mode by ultraviolet-visible spectroscopy. When a beam of radiation (light) passes through a substance or a solution, some of the light may be absorbed and the remainder transmitted through the sample. The ratio of the intensity of the light entering the sample (I_0) to that exiting the sample (I) at a particular wavelength is defined as the transmittance (T). The absorbance (A) of a sample is the negative logarithm of the transmittance.

$$A = -\log(T) \quad 2(3)$$

Beer- Lambert Law

The absorbance of a sample at a given wavelength is proportional to the absorptivity of the substance (a constant at each wavelength), the path length (the distance the light travels through the sample) and the concentration of the absorbing substance. In these cases the Beer- Lambert law holds:

$$A = a * b * c \quad 2(4)$$

where

a = the absorptivity of the substance

b = path length

c = concentration of the substance

When working in concentration units of molarity, the Beer-Lambert law is written as :

$$A = \epsilon * b * c \quad 2(5)$$

Where

ϵ is the wavelength-dependent molar absorptivity coefficient with units of $\text{mol}^{-1}\text{cm}^{-1}$. As ϵ and b, both are constant, then it can be written that $A \propto c$

2.5.4 XPS Spectroscopy

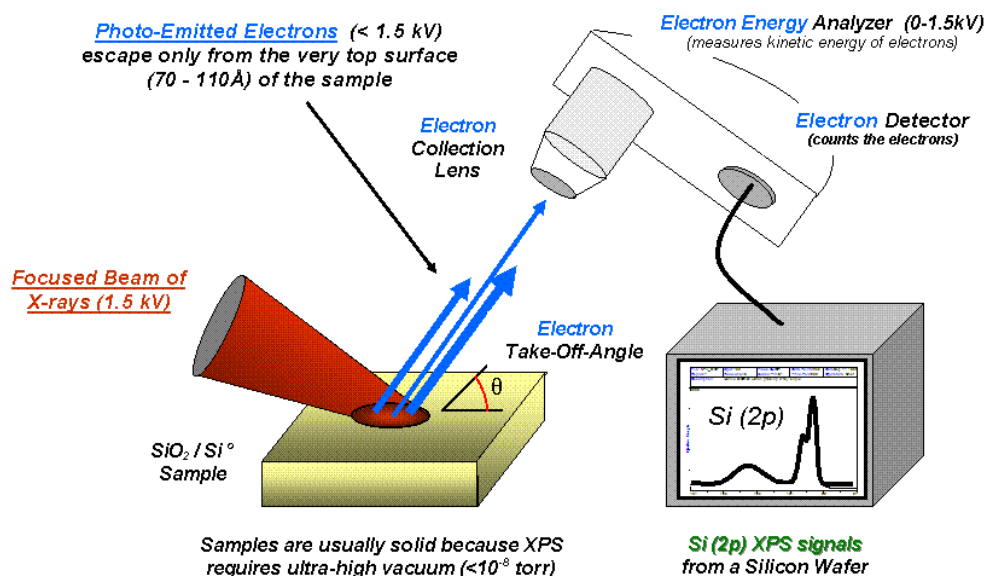


Figure 2.12 Basic components of a monochromatic XPS system

[Source: https://en.wikipedia.org/wiki/X-ray_photoelectron_spectroscopy]

The elemental composition of material is analysed by X-ray photoelectron spectroscopy (XPS). Using this technique the oxidation state, chemical and electronic state of the material can be evaluated.⁵⁻⁶ In this technique when the material is irradiated with a monochromatic X-ray, the kinetic energy of the escaping electrons will be evaluated from which the binding energy is estimated. This technique requires ultrahigh vacuum of the order of ($P \sim 10^{-8}$ to 10^{-9} millibar). The detection limits of XPS can be varied from parts per thousand to parts per million. Most of XPS analysis starts with a wide scan or survey spectrum because it allows one to set up high resolution XPS spectra acquisition by showing all elements present on the sample surface. In our work XPS analysis were carried out using a Thermofisher Scientific (East Grinstead, UK) K-Alpha spectrometer with a monochromated Al Kalpha X-ray source. The C1s peak at 285 eV is used for charge reference during acquisition. Quantitative surface chemical analysis

were calculated from the high resolution, core level spectra following the removal of a non-linear background. Also high resolution X-ray photo emission spectroscopy measurements are used to determine the valence band offset. Valence band spectra (VBS) give information about the density and occupancy of electronic states in the valence band of the material.

2.5.5 PL Spectroscopy

Photoluminescence spectroscopy is a non-contact and non destructive method for characterizing the electronic structure of materials. In this technique, when light is directed onto a sample, it is absorbed and photo-excitation occurs. The photo-excitation causes the electrons in the material to jump to a higher electronic state, and will then release energy or photons as it relaxes and returns back to a lower energy level. So the spontaneous emission of light from a material under photo excitation is known as photoluminescence. The difference in energy between the excited state and the equilibrium state level is related to the energy of the emitted light or amount of photoluminescence. Thus the intensity of this photoluminescence will give a measure of various material properties. The process involved in the photoluminance emission is as shown in **fig. 2.13**. In semiconductor systems, the most common radiative transition occurs between conduction and valence bands with photons having energy equal to its band gap. Radiative transitions in semiconductors may also involve localized defects or impurity levels therefore the analysis of the PL spectrum leads to the identification of these specific defects or impurities, and the magnitude of the PL signal can be a measure of their concentration also. Nonradiative recombination can be estimated from the variation of the PL intensity and decay time with temperature. At higher temperatures nonradiative recombination pathways are activated and the PL intensity decreases exponentially. In short photoluminescence is a process important for

determining band gap, purity, crystalline quality, and impurity defect levels of semiconducting material.

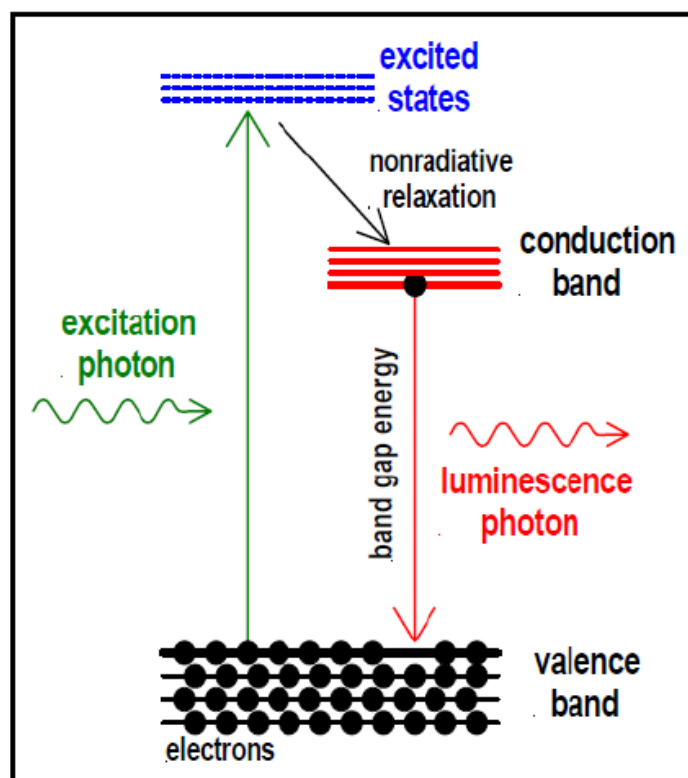


Figure 2.13 Principle of Photoluminescence Spectroscopy (PL)

2.5.6 BET – Surface Area Analysis

The specific surface area measurement of materials studied through the physical adsorption of gas molecules on a solid surface. The BET theory was developed by Stephen Brunauer, Paul Hugh Emmett, and Edward Teller in 1938. Also this theory is an extension of the Langmuir theory of monolayer molecular adsorption, to multilayer adsorption. The exposed surface area, temperature, gas pressure and strength of interaction between the gas and solid determines the amount of gas adsorbed on the material. In BET surface area

analysis, usually utilizes probing gases that do not chemically react with material surfaces as adsorbates to quantify specific surface area. Availability in high purity makes nitrogen as a suitable adsorbate in BET analysis. Since the interaction between gaseous and solid phases is usually weak, the surface is cooled using liquid N₂ to obtain detectable amounts of adsorption. Known amounts of nitrogen gas are then released stepwise into the sample cell. Relative pressures less than atmospheric pressure is achieved by creating conditions of partial vacuum. After the saturation pressure, no more adsorption occurs regardless of any further increase in pressure. Highly precise and accurate pressure transducers monitor the pressure changes due to the adsorption process. After the adsorption layers are formed, the sample is removed from the nitrogen atmosphere and heated to cause the adsorbed nitrogen to be released from the material and quantified. The measurement of surface area at different temperatures and measurement scales are possible with other probing adsorbates, such as argon, carbon dioxide, and water. Surface area of particles mainly varies with size, shape and porosity of material. Different methods for the measurement of surface area involves microscopic analysis, surface area from particle size distribution, small angle X-ray scattering, mercury porosimetry etc.

The data collected is displayed in the form of a BET isotherm, which plots the amount of gas adsorbed as a function of the relative pressure.

$$\frac{1}{\left[V_a \left(\frac{P_0}{P} - 1\right)\right]} = \frac{C - 1}{V_m C} \times \frac{P}{P_0} + \frac{1}{V_m C}$$

Where P = adsorbate gas partial vapour pressure in equilibrium at liquid nitrogen temperature (77.4 K) in pascals,

P₀ = saturated pressure of adsorbate gas, in pascals,

- V_a = volume of gas adsorbed at standard temperature and pressure (STP), in millilitres,
- V_m = volume of gas adsorbed at STP to produce an apparent monolayer on the sample surface, in millilitres,
- C = dimensionless constant that is related to the enthalpy of adsorption of the adsorbate gas on the powder sample.

2.5.7 Scanning Electron Microscopy

An electron microscope utilise electron beam for illuminating the sample and to get the image. The magnification and resolving power of electron microscope is much higher than that of a light microscope, which allows it to see smaller objects and greater details in these objects.⁷ In this system the control of illumination and imaging is done by using electrostatic and electromagnetic lenses. SEM can achieve resolution better than 1 nanometer. Specimens can be observed in high vacuum in conventional SEM, or in low vacuum or wet conditions in variable pressure in environmental SEM.

When high energy electrons impinge on the specimen, a number of signals are generated including backscattered electrons, secondary electrons and X-rays that contain information about the sample's surface topography and composition. Secondary electrons originate in the specimen itself, and have a much lower energy than the backscattered electrons.⁸⁻⁹ These secondary electrons are the basis for elemental analysis in Energy Dispersive X-ray system. Most of the SEM analysis system is having an integrated Energy dispersive X-ray analysis system and cannot operate on its own without the latter. When the specimen is collide with an electron beam inside the scanning electron microscope, knocks out some of the specimens own electron. Then the vacancy created by the ejected inner shell electron is occupied by a higher-

energy electron from an outer shell. These electron migration is accompanied by release of some amount of energy. The amount of energy released will depends on the shell from which it is transferring, as well as which shell it is transferring to.¹⁰ X-rays give information about the elemental composition of the sample.

2.5.8 Transmission Electron Microscopy

In transmission electron microscopy (TEM) the transmitted electrons are used to create an image of the sample. In this technique a beam of electron is transmitted through an ultra thin specimen, the transmitted electron beam after interaction with the specimen reaches the imaging system of the microscope. A series of electromagnetic lenses is used for magnifying and the spatial variation in the information until it is recorded by hitting a fluorescent screen, photographic plate, or light sensitive sensor such as a charge-coupled device (CCD) camera.¹¹ The advantages of TEM involve the following points that is real (image) and reciprocal space (diffraction pattern) information can be obtained from same region of sample and high resolution imaging is possible with TEM.¹² Also it is possible to obtain amplitude and phase contrast images. However some disadvantage is also associated with this technology. Among those first one is the high capital and running cost. Low sampling volume and rather slow process of obtaining information. Samples which are not stable in vacuum are difficult to study. At present high resolution transmission electron microscopy (HRTEM) allows the imaging of the crystallographic structure of a sample at an atomic scale. Because of its high resolution, it is an invaluable tool to study nanocrystalline materials.

The crystallographic information regarding a material can be obtained by selected area electron diffraction (SAED) analysis using transmission

electron microscope. During TEM analysis, a thin crystalline specimen is subjected to a parallel beam of high-energy electrons. The interatomic spacing between atoms in a solid is about hundred times larger than the high energy electron beam used for SAED analysis in a TEM instrument. Then the atoms act as a diffraction grating to electrons and they scattered the electron beam to different angles determined by the crystal structure of the sample. This makes a series of spots or selected area diffraction pattern on the screen of TEM. From these spots the crystal structure can be identified.

References

- [1] Bunaciu, A. A.; Udristioiu, E. g.; Aboul-Enein, H. Y. *Critical Reviews in Analytical Chemistry*, **2015**, *45*, 289.
- [2] Cullity, B. D. *Elements of X-ray diffraction. 2nd ed. Addison Wesley*, . **1978**.
- [3] Jones, W. J.; Stoicheff, B. P. *Physical Review Letters* **1964**, *13*, 657.
- [4] Tok makoff, A., Lang, M.J., Larsen, D.S. *Physical Review Letters*, **1997**, *79*, 2702.
- [5] Turner, D. W.; Jobory, M. I. A. *The Journal of Chemical Physics* **1962**, *37*, 3007.
- [6] Ray, S.; Shard, A. G. *Analytical Chemistry* **2011**, *83*, 8659.
- [7] Banerjee, A. N.; Chattopadhyay, K. K. *Journal of Applied Physics*, **2005**, *97*, 084308.
- [8] Joy, D. C.; Romig, A. D. *J. Goldstein, Springer, NY* **1986**.
- [9] Kundoo, S.; Banerjee, A. N.; Saha, P.; Chattopadhyay, K. K. *Materials Letters* **2003**, *57*, 2193.
- [10] Goldstein, J. *Scanning Electron Microscopy and X-Ray Microanalysis* , *Springer* **2003**.
- [11] Keller, D. J.; Chih-Chung, C. *Surface Science*, **1992**, 268,333.
- [12] Nag, A.; Sarma, D. D. *The Journal of Physical Chemistry C* **2007**, *111*, 13641.

Pd loaded TiO₂ nanotubes for the effective catalytic reduction of p-nitrophenol

● Contents ●	3.1 Introduction
	3.2 Experimental
	3.3 Results and discussion
	3.4 Conclusions
	References

Some of the contents of this chapter have appeared in the following research publication

- [1] **Vijila Kalarivalappil**, C.M.Divya, W.Wunderlich, Suresh C. Pillai, Steven J. Hinder, Manoj Nageri, V. Kumar and Baiju K. Vijayan “Pd Loaded TiO₂ Nanotubes for the Effective Catalytic Reduction of p-Nitrophenol”, *Catalysis Letters*, **146** (2016) 474

3.1 Introduction

Nowadays heterogeneous catalysts have become a crucial part of many industrial activities, such as organic synthesis, oil refining, and pollution control.¹⁻² The major challenge for most heterogeneous catalysts is lack of stability. The agglomeration of particles during operations may block the active sites of the catalyst, which is believed to lead to its instability. It is possible to improve the heterogeneous catalyst activity by modifying the support by approaches in nanotechnology and nanoscience which includes controlling the pore structure among other parameters.³⁻⁴ For heterogeneous catalysis, the problem of catalyst separation and recovery from the reaction matrix are addressed by using various catalyst supports to immobilize them.³ Therefore, heterogeneous catalysts with supports such as Al₂O₃, TiO₂, ZrO₂, ZnO and others are applied based on their processability and cost-effective modes of synthesis. Mesoporous titania finds applications in catalysis, photocatalysis, batteries, sensors and solar cells.⁵ Strong oxidation and reduction capabilities of photo generated reactive oxidation species (ROS) as a result of the photocatalytic reactions can effectively be used for decontamination and disinfection applications.⁶⁻¹² Titanium dioxide is identified as one of the most suitable candidates for catalytic reactions because of its chemical stability, nontoxicity and higher surface area.¹³ Palladium (Pd) supported titania has been employed as catalysts for various reactions such as oxidative destruction of dichloromethane in presence of water vapour, methane combustion and ethanol oxidation in alkaline medium etc.¹⁴⁻¹⁶ A cost effective method for the synthesis of iron doped titania loaded with noble metals using industrial waste was reported by Mahmoud *et al.*¹⁷ Dichloromethane oxidation using titania doped with Pd and Ni was also reported.¹⁴ Reduction of Pt(IV), Au(III) or Pd(II) doped titania under UV irradiation to metallic Pt, Au or Pd on the titania surface was reported.¹⁸

Liquid phase selective hydrogenation of long chain alkadienes is also dependent on the catalytic activity of polymorphic phase of titania.¹⁹ Palladium catalyst supported by anatase phase has shown higher selectivity compared with that of rutile phase supported materials.¹⁹ The Pd and Pt doped titania have been effectively used for the inactivation of bacteria.²⁰ Pt and Pd deposited on titanate nanotubes have also been reported to be effectively used for hydrogen sensor applications. The sensor prepared with Pd and Pt/titanate nanotubes displayed improved response compared to the conventional Pd and Pt catalysts.²¹ Pd deposited on titania nanofibers prepared by electrospinning technique have been reported to effectively catalyse the decomposition of NO and CO.²² Pd deposited on grapheneoxide nanosheet shows greater catalytic properties for the reduction of p-nitrophenol than Au and Ag deposited.²³ Au, Pt and Pd supported on SBA-15 (Santa Barbara Amorphous mesoporous silica) was used for catalytic reduction of p-nitrophenol. Among these Pd decorated material is more catalytically active than other metal nanoparticles.²⁴ However, a systematic study of Pd doping and its effect on the morphological stability and catalytic reduction of p-nitrophenol using Pd doped titania nanotubes has not yet been reported. In the current investigation Pd nanoparticles decorated titania nanotubes are prepared by hydrothermal technique. Various metal nanoparticles such as Ag, Au, Cu and Pd are used for the catalytic reduction of p-nitrophenol.²⁵ Pd is reported to be a better catalyst than the other similar metal.^{23-24,26} Catalytic properties of palladium loaded titania nanotubes were systematically examined by studying the reduction of p-nitrophenol with sodium borohydride (NaBH₄) to p-aminophenol. The present work also aims at investigating the role of palladium nanoparticle loading on titania nanotubes on the catalytic reduction of p-nitrophenol. The current investigation revealed that there is an optimum loading for metal nanoparticles to be more catalytically active.

3.2 Experimental

Titania nanotubes (TNTs) were synthesized by using an improved hydrothermal method. In a typical reaction, 2 g of anatase titania powder (assay 99%, Merck) were stirred with 50 ml of 10 M NaOH (assay 97%, Merck) solution in a 125 ml Teflon cup in a hydrothermal vessel (Paar Instrument Company, USA). This reaction system was retained in an oven for 48 h at 120 °C and the precipitate formed was washed with 1 M HCl (assay 35 %, Merck). The reaction mixture was washed several times using deionized water to attain a pH between 6 and 7. When nanocrystalline titania particles were reacted with highly concentrated NaOH solution some of Ti-O-Ti bonds were interrupted. Some Ti^+ ions were exchanged with Na^+ ions to form Ti-O-Na bonds. During the acid washing step the Na^+ ions is replaced by H^+ to form Ti-OH bonds in the washing process. Then the dehydration of Ti-OH bonds produced Ti-O-Ti bonds or Ti-O...H-O-Ti hydrogen bonds. The bond distance between one Ti and another on the photocatalyst surface consequently decreased, facilitating the sheet folding process. The electrostatic repulsion from Ti-O-Na bonds enabled a joint at the ends of the sheets to form the tube structure.²⁷ The titania nanotubes thus synthesized were dried in an oven at 110 °C overnight. The Pd nanoparticles were prepared by chemical reduction method. In a typical experiment, 25 mM palladium (II) chloride (assay 99%, Sigma Aldrich) was added drop-wise into a solution containing hyrazinemonohydrate (100 mM assay 98%, Sigma Aldrich) and CTAB (0.5 M, assay 99%, Sigma Aldrich). After the addition of PdCl_2 the colour of the resultant solution changed to dark brown indicating the formation of Pd nanoparticles. This mixture was stirred for 10 minutes, and is further used for loading the titania nanotubes with Pd nanoparticles. Palladium concentrations

of 0.1%, 1%, 5% and 10 mol.% were loaded over hydrogen titanate nanotubes by adding drop-wise the suspension of Pd nanoparticles into an aqueous suspension of hydrogen titanate nanotube under stirring. The resultant slurry was dried and further calcined at 400 °C for 1h. The samples were coded as 0.1Pd, 1Pd, 5Pd and 10Pd. This corresponds to 0.1 to 10 mol% of Pd loading in TNTS. The concentration of Pd in the respective samples was also determined using SEM EDAX analysis. The crystalline phase identification were carried out using an X-ray diffractometer (D5005, Bruker, Germany) using Cu K α radiation of 0.15406 nm at the scanning rate 0.05°/s in the 2 θ range from 5° to 80°. The amount of rutile in the sample was estimated using the method reported by Spurr from the intensities of the (101) and (110) reflections in the X-ray diffraction pattern as given below in equation 3.1.

$$\% \text{ Rutile} = \frac{1}{1+0.8[I_A(101)/I_R(110)]} \quad 3.1$$

Where I_A (1 0 1) and I_R (1 1 0) are the integrated main peak intensities of anatase and rutile respectively. The Scherrer formula was used to estimate the average crystalline size of the Pd nanoparticle (Eq3.2).

$$D = \frac{K\lambda}{\beta \cos\theta} \quad 3.2$$

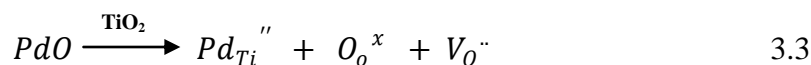
Where D is the average crystallite size (nm), K, the shape factor, λ the X-ray wavelength (0.15406 nm), β is the full width at half maximum (in radian) of (111) peak of metallic Pd and θ is the Bragg angle.

The morphology of the materials was studied using a field emission scanning electron microscope (Hitachi SU6600, USA) and high resolution transmission electron microscope (Hitachi HF 2200 TU (Japan). The catalytic performance of the titania nanotubes loaded with palladium was quantitatively

evaluated in the liquid-phase reduction of p-nitrophenol (4-NP) with sodium borohydride (NaBH_4). The reaction is known to be catalytically active in presence of metal nanoparticles at room temperature. In a typical experiment an aqueous solution of p-nitrophenol (0.01 M; 20 ml) and sodium borohydride (0.5 M; 20 ml) were prepared and from their mixture 0.12 ml is pipetted out to quartz cuvette and diluted with 3.8 ml water. 1 mg of each prepared sample of palladium loaded titania nanotubes (0.1 Pd, 1Pd, 5Pd and 10 Pd) is added into it and stirred. Then this mixture is transferred into a UV-Visible spectrometer (Perkin Elmer, Lambda 35, USA). p-nitrophenol exhibits an absorption peak at 317 nm. Addition of NaBH_4 deprotonates the OH group of p-nitrophenol, and subsequently the absorption peak shifts to 400 nm. When the catalytic reduction of p-nitrophenol is initiated the peak gradually reduces its intensity. In the mean time a small shoulder peak at 300 nm gradually rises, which is attributed to p-amino phenol.²⁶ The recyclability of the catalysts was also analyzed after the reaction. XPS analyses were performed on a ThermoFisher Scientific (East Grinstead, UK) Theta Probe spectrometer. XPS spectra were acquired using a monochromated Al K α X-ray source ($h\nu = 1486.6$ eV). An X-ray spot of ~ 400 μm radius was employed. All spectra were charge referenced against the C1s peak at 285 eV to correct for charging effects during acquisition. Quantitative surface chemical analyses were calculated from the high resolution, core level spectra following the removal of a non-linear (Shirley) background. The manufacturers Avantage software was used which incorporates the appropriate sensitivity factors and corrects for the electron energy analyser transmission function.

3.3 Results and Discussion

The X-ray diffraction patterns of the samples (Figure 3.1) calcined at 400 °C shows crystalline peaks corresponding to the anatase crystalline phase of titania. At higher loading of Pd such as 5 and 10 mol.%, crystallization of 32 and 85% of rutile phases respectively, were observed. In 5Pd and 10 Pd samples the peaks at $2\theta=40, 46.4, 68.2$ correspond to the (111), (200), (220) planes of fcc structured Pd particles.²⁸ It was reported that Pd in the titania matrix favours the anatase to rutile phase transformation.²⁹ The ionic radius of Pd²⁺ is 0.064 nm, which is almost similar to that of Ti⁴⁺ ion (0.068 nm). Therefore, the possibility to replace Ti⁴⁺ with Pd²⁺ in the lattice of anatase structure with the formation of oxygen vacancy can be according to the following equation.



However, the increase in oxygen vacancy in the titania lattice was reported to enhances the anatase to rutile phase transformation.²⁹⁻³⁰ Anatase to rutile transformation involves the rearrangement of the atoms in the anatase and rutile lattices. It is widely accepted that the most important factor affecting the phase transformation is the presence or amount of defect on the oxygen sublattice of TiO₂. So the increased presence of oxygen vacancy in the oxygen sublattice causes ease of rearrangement and transformation by reducing the structural rigidity. The average crystallite size of Pd is found to be 19.6, 20.3 nm in 5% and 10% Pd-loaded samples. The concentration of Pd in the titania matrix as determined using EDAX measurement are found to be 1.56, 2.70, 3.22 and 6.07 wt% respectively for 0.1Pd, 1Pd, 5Pd, 10Pd samples.

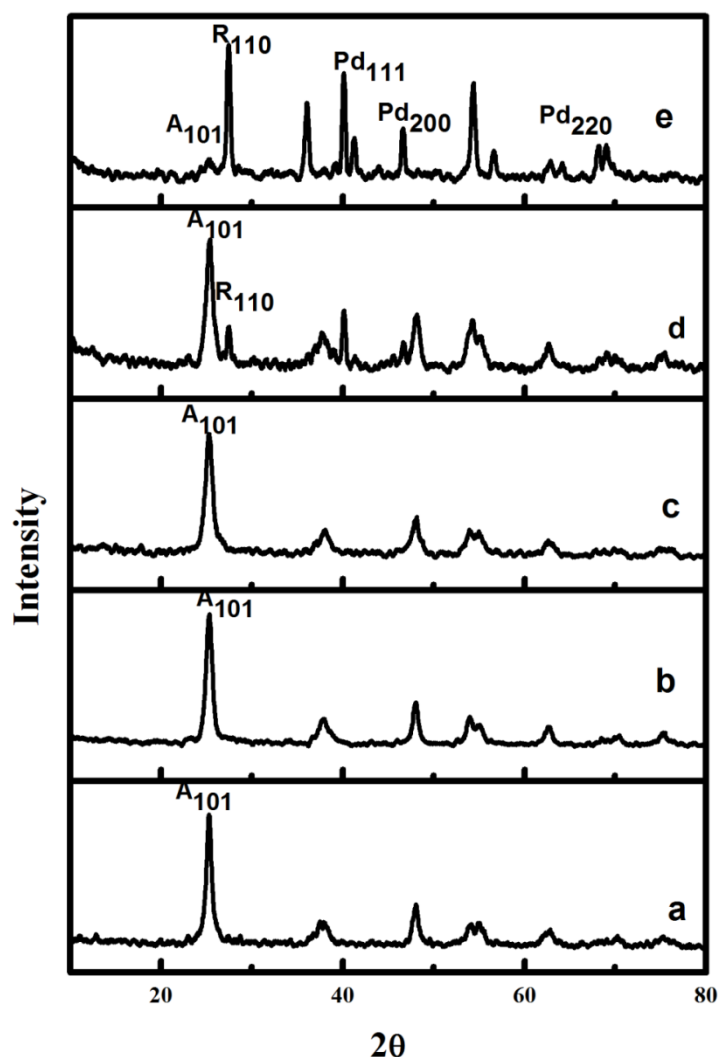


Figure 3.1: XRD pattern of pure and Pd loaded titania nanotube calcined at 400 °C (a) unloaded TNT (b) 0.1Pd (c) 1Pd (d) 5Pd and (e) 10Pd

Raman spectra of the Pd loaded and unloaded titania nanotubes are shown in Figure 3.2. In pure, 0.1Pd and 1Pd samples, phonon modes corresponding to anatase type are present at 144, 197, 399, 513 and 639 cm^{-1} .³¹⁻³² Phonon modes corresponding to the rutile phase of titania are observed for 5Pd and 10Pd samples at 608, 392 and 247 cm^{-1} . Results obtained from the Raman spectra (Figure 3.2) are in conformity with those obtained from XRD.

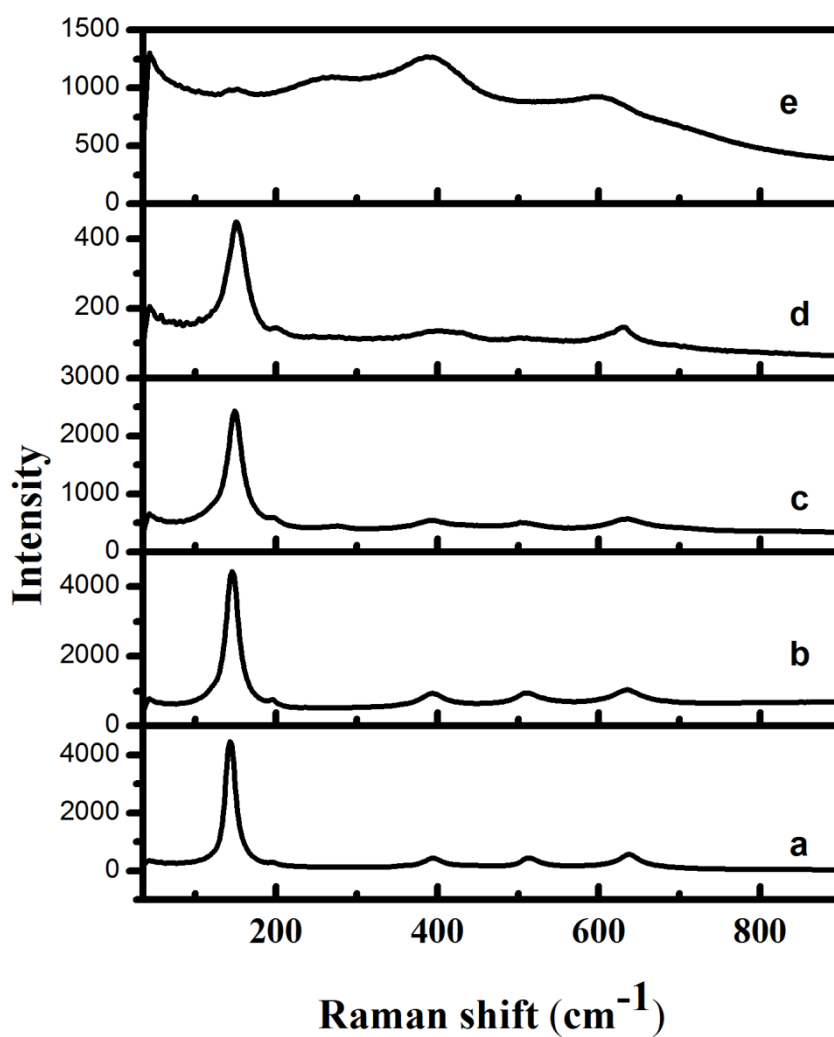


Figure 3.2 Raman spectra of Pd loaded and unloaded titania nanotube (a) unloaded TNT (b) 0.1Pd (c) 1Pd, (d) 5Pd and (e) 10Pd.

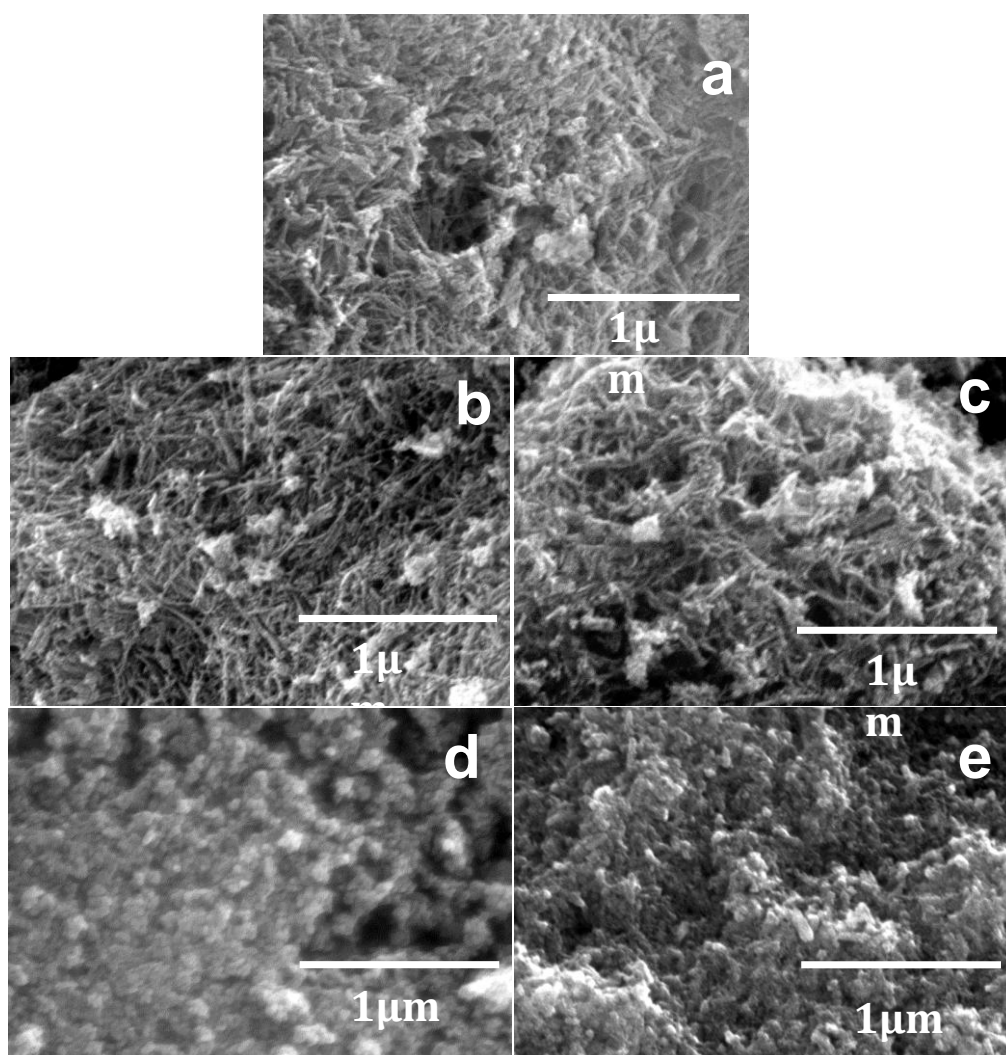


Figure 3.3: SEM images of pure and Pd loaded titania nanotubes calcined at 400 °C (a) NT (b) 0.1Pd (c) 1Pd, (d) 5Pd and (e) 10Pd.

The scanning electron microscope images of the samples indicate a tubular morphology of the titania nanotube samples up to a Pd concentration of 1.0 mol.% (Figures 3.3 a,b,c). As the Pd concentration increases (Figure 3.3 d,e) collapse of the tubular structure in titania nanotubes is observed which is attributed to anatase to rutile phase transformation.³³

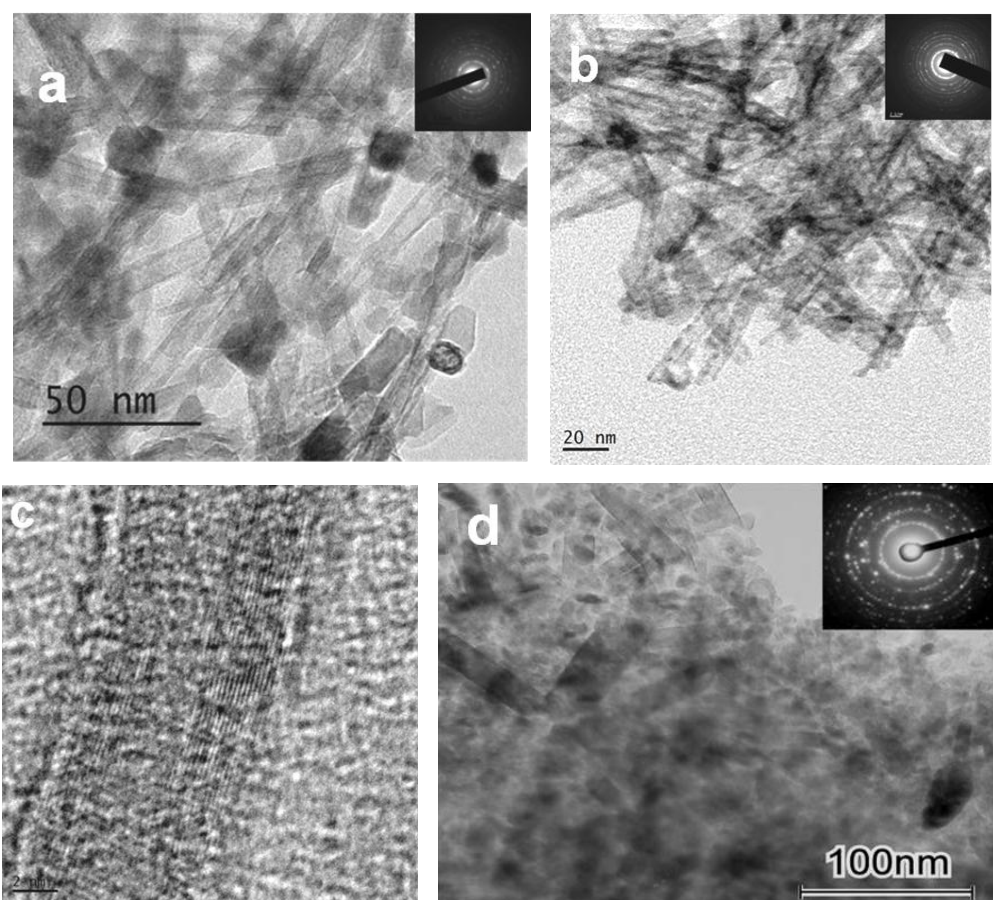


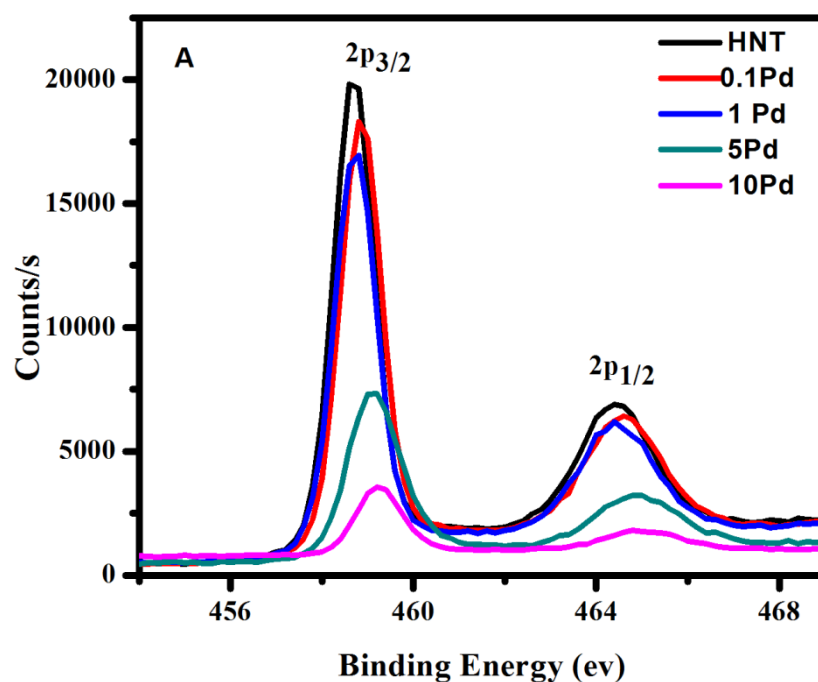
Figure 3.4: TEM images of Pd loaded titania nanotubes calcined at 400 °C (a) 0.1Pd (b,c) 1Pd (d) 5Pd.

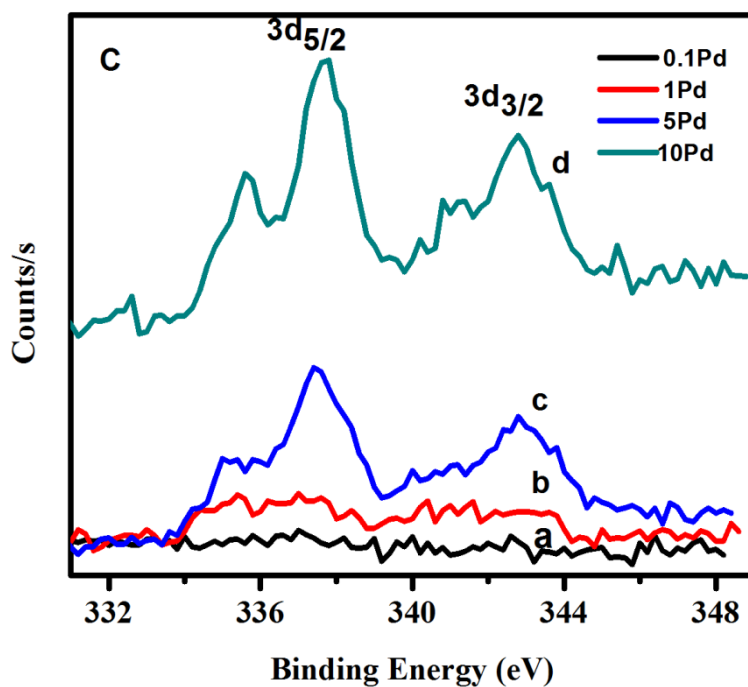
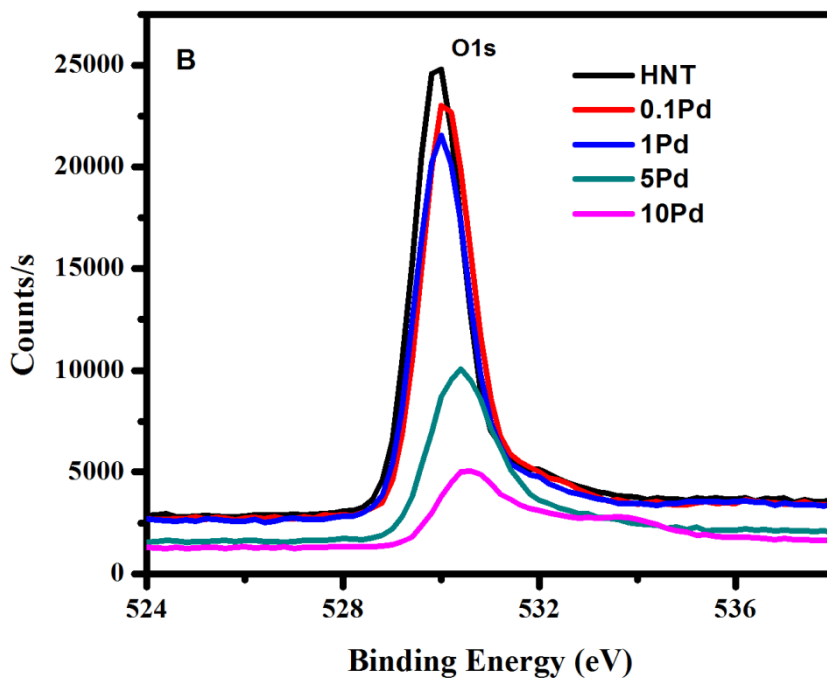
In titania nanotube with 0.1 and 1.0 mol. % Pd, transmission electron microscope images reveal tubular morphology with an average diameter between 10-12 nm (Figures. 3.4 a & b). HRTEM reveals multi wall tube structure that shows signs of scrolling during formation of titania nanotubes synthesised through hydrothermal method (Figure 3.4c).³⁴ Pd particles can be distinguished from the dominant anatase phase because of their dark contrast. The particle size of the Pd particle estimated from TEM micrographs indicate that 0.1Pd and 1 Pd sample have an average particle size of 11 to 13 nm respectively. At higher loading such as 5 mol% of Pd, the nanotubes crumbled

to powder (Figures.3.4 d). The selected area electron diffraction pattern of the samples (insets of Figures 3.4 a,b,d) clearly indicate that the 0.1 and 1Pd samples are less crystalline in nature than the 5 Pd sample, mainly caused by the nanotubes with high aspect ratio. The BET surface area obtained are 240, 261, 228, 167 and 159 m^2g^{-1} for pure and Pd loaded titania nanotube samples such as 0.1Pd, 1Pd, 5Pd 10 Pd respectively. The drastic reduction in the surface area of the 5 and 10Pd samples indicate the collapse of tubular structure of highly Pd loaded samples.

The XPS spectra of the Ti $2p$ peak are provided in the Figure 3.5A. In unloaded TNT's the $2p_{3/2}$ and $2p_{1/2}$ binding energies are obtained at 458.59 eV and 464.31 eV respectively. The Ti $2p_{3/2}$ peak in TiO_2 is reported to be observed at 458.5 eV.³⁵ The binding energy of $2p_{3/2}$ peak of titania is increased from 458.68 to 459.23 when the concentration of Pd increases in the titania matrix. Peak shift is detected which indicates decrease of the coordination number of Ti and the shortening of the Ti-O bond.³⁶ This enhances the anatase to rutile phase transformation in Pd loaded titania nanotube. The $\text{O}1s$ binding energy of TiO_2 has been reported to be observed at 529.9 eV (Figure 3.5B).³⁷ Moreover, the asymmetry in the oxygen peak indicates different chemical states of oxygen. The binding energy of oxygen in PdO is reported to be between 529.8–530.1 eV.³⁸ The XPS spectra of the Pd 3d peak for all of the Pd loaded samples are provided in the Figure 3.5C. The XPS spectra of Pd 3d peak of 10Pd sample are presented in Figure 3.5D, in which the palladium exists in metallic as well as PdO state. The presence of metallic as well as oxidized form (PdO) are characterized by the binding energies at 340.7 eV ($3d_{3/2}$), 335.5 eV ($3d_{5/2}$) for Pd³⁵ where as for PdO, they are at 342.8 eV ($3d_{3/2}$) and 337.7 eV ($3d_{5/2}$).³⁹ According to the XRD data, the

Pd exists in metallic state even though the XPS data show peaks corresponding to oxidized palladium species PdO. This discrepancy can be explained by the low stability of the reduced palladium states. It is reported that PdO particles have been shown to be stabilized by the matrix of other oxides, such as Al₂O₃ and SnO₂.⁴⁰⁻⁴¹ However the X-ray diffraction indicates only the presence of metallic palladium. This discrepancy is likely to arise from the very different depths of analysis between the two techniques. In X-ray diffraction analysis penetration/analysis depth is reported to be of few microns⁴² while XPS has an analysis depth below 10 nm.⁴³ Thus a thin layer of Pd oxide on the surface of Pd will show as a major contribution to the XPS Pd peak and remain undetected, via X-ray diffraction analysis.





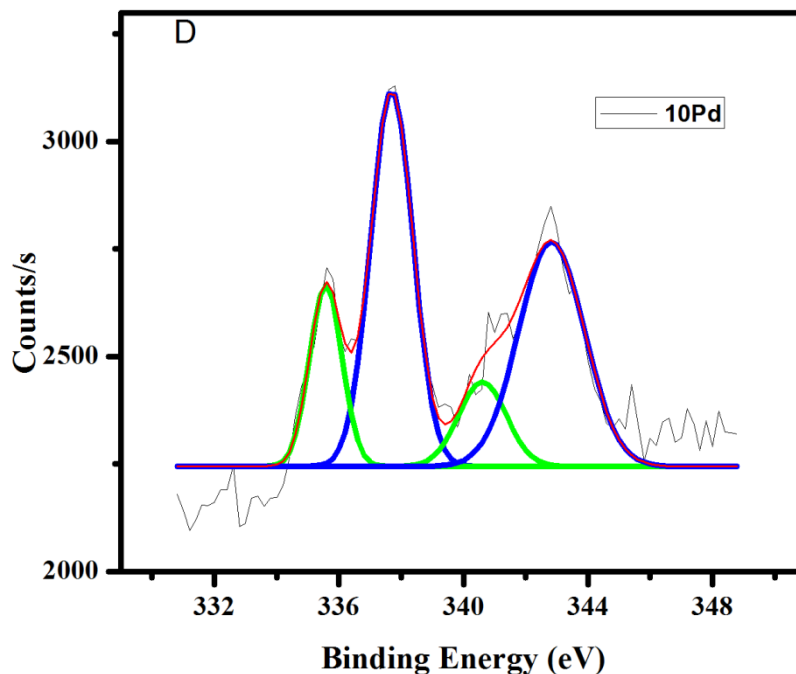


Figure 3.5 XPS spectra of Pd loaded titania nanotube samples (A) Ti 2p (B) O 1s, Pd 3d of (C) Pd loaded titania nanotube and (D) 10Pd sample fitted for Pd and PdO

The catalytic action of Pd loaded titania nanotube were studied using liquid phase reduction of p-nitrophenol by sodium borohydride. The reduction of p-nitrophenol to p-aminophenol using sodium borohydride is usually accelerated in the presence of a metal catalyst.⁴⁴⁻⁴⁵ The reduction pathway is depicted in equation 3.3. The catalytic reduction in presence of excess sodium borohydride has been reported to follow first order kinetics. Figure 3.7A represents a typical plot of the time dependent absorption spectra of p-nitrophenol in presence of Pd loaded titania nanotube. The reduction was monitored from the decrease in the absorption maximum of p-nitrophenol at 400 nm⁴⁶⁻⁴⁷ and the increase in intensity of the peak at 300 nm corresponding to the formation of p-aminophenol. A small reduction in concentration of p-nitrophenol with pure titania nanotube powder was also observed (Figure 3.8).

Which may be due to the adsorption of reactant on titania nanotube surface or the slow reduction of p-nitrophenol by sodium borohydride in the absence of metal catalyst.⁴⁸ This shows that pure titania cannot alone accelerate the catalysis reaction. In order to quantify the catalytic action of different samples, reaction kinetics for the reduction of p-nitrophenol in presence of Pd loaded titania nanotube catalyst are studied. Figure 3.7B shows the typical plot of $-\ln(C_t/C_0)$ against time, where $C(t)$ and $C(0)$ are the concentrations of p-nitrophenol at time t and initial concentration, respectively. From the slope of the linear fit the rate constant k , of the reaction was calculated and tabulated in Table 3.1.

Table 3.1 Comparitive evaluation of catalytic activity of Pd loaded titania nanotube samples

Sample	A/R ratio	Rate constant, k (min^{-1})	Morphology
0.1Pd	100	0.0894	Tubular
1Pd	100	0.7072	Tubular
5Pd	68/32	0.0324	Crumbled tubes
10Pd	15/85	0.0168	Crumbled tubes

The rate constants of the 0.1Pd, 1Pd, 5Pd and 10Pd samples are 0.0894, 0.7072, 0.0324, 0.0168 min^{-1} respectively. The rate constant of the reaction follows the order: 1Pd > 0.1Pd > 5Pd > 10Pd. The presence of Pd particles on titania matrix catalyse the reduction reactions. Even though 5Pd and 10Pd contain higher amounts of palladium, they show lower catalytic reaction. There are two possible mechanisms for the reduction of p-nitrophenol (i) surface mediated electron transfer and (ii) surface mediated hydrogen transfer. In both these mechanisms the reactants are adsorbed on the surface of the metal nanoparticle before the reduction reaction. Hence the surface area of the metal plays a major role in the reduction reaction. The reduction of p-nitrophenol has been reported to be kinetic and diffusion

controlled. In diffusion controlled reactions, since the reactions on the surface of metal particles are significantly faster than diffusion of the reactants, apparent rate constant is determined by the diffusion of the reactants through the solution. The molecular size of the 4-NP, calculated using molecular modeling, is reported to be 0.66 nm by 0.43 nm in the plane of the benzene ring.⁴⁹ The diffusion of p-nitrophenol through TNT is given in Figure 3.6

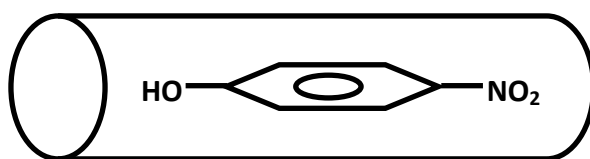


Figure 3.6 The diffusion of p-nitrophenol through titania nanotubes

This indicates that the tubular structure and surface area have very important role in the catalytic reaction. The titania nanotubes synthesized in the present method have inner diameters of 6.0-7.0 nm (Figure.3.4c), which allow the easy diffusion of reactants through the heterogeneous catalysis system. This facilitates the higher rate constant for the system with stable tubular structure containing lower concentration of palladium nanoparticles. The XPS result indicates the formation of Pd and PdO in the samples. Earlier work indicated that both the metallic as well as the oxide form of palladium contribute to the reduction reaction of 4-NP.⁵⁰ Moreover, the reaction rates of different prepared samples reveal that, for a higher catalytic action there is an optimum Pd loading level. In the case of higher loading of Pd in the titania matrix as in the case of 5 and 10Pd samples, even though the variation of particle size is very less, the 5 Pd exhibits a two times higher rate constant than 10Pd sample. This clearly indicate that not only morphology but phase composition of titania matrix also has a significant effect on the reduction of p-nitrophenol. The 10Pd sample contains 85% of rutile whereas 5Pd has 32% rutile phase. It is seen that, in the present case, the 1 mol.% Pd-loaded sample

exhibit the optimum catalytic activity. Above and below this concentration the rate of reaction decreases in Pd loaded titania nanotubes. This can be explained as given below. The smaller particles contain more exposed surface atoms (catalytically active sites) due to high surface to volume ratio. However, it has been reported that intermediate size of catalyst is more catalytically active for the para nitro phenol reduction reaction.⁵¹ Therefore, morphology and the nature of the substrate as well as particle size of Pd have played a major role in the reduction reaction as reported earlier.²⁶

Though size of the metal nanoparticles are known to significantly influence the catalytic activity.⁵²⁻⁵³ In the present case, the morphology as well as the crystalline phase of the host titania nanotube are found to play important roles in their catalytic activity. The comparison of the result with the published literature on catalytic reduction of p-nitrophenol using Pd nanoparticle supported on different substrates is provided in Table 3.2. It is clearly seen that the present method provides an easy and scalable method for the synthesis of Pd supported titania nanotube catalyst for the reduction of p-nitrophenol to p-aminophenol. The product has applications in production of analgesic, antipyretic drugs, photographic developers, corrosion inhibitors and anticorrosion lubricants. The rate of the reaction is comparable with the rate constant reported by other groups using Pd catalyst (Table 3.2). A rate constant of 0.7072 min^{-1} was obtained at a concentration 0.01 M of 4-NP using 1mg of catalyst containing 1 mol% Pd nanoparticle, which is higher than many of the reported values presented in the Table 3.2. Therefore the current method holds promise for the industrial production of an efficient catalyst for the reduction of p- nitrophenol in bulk quantities.

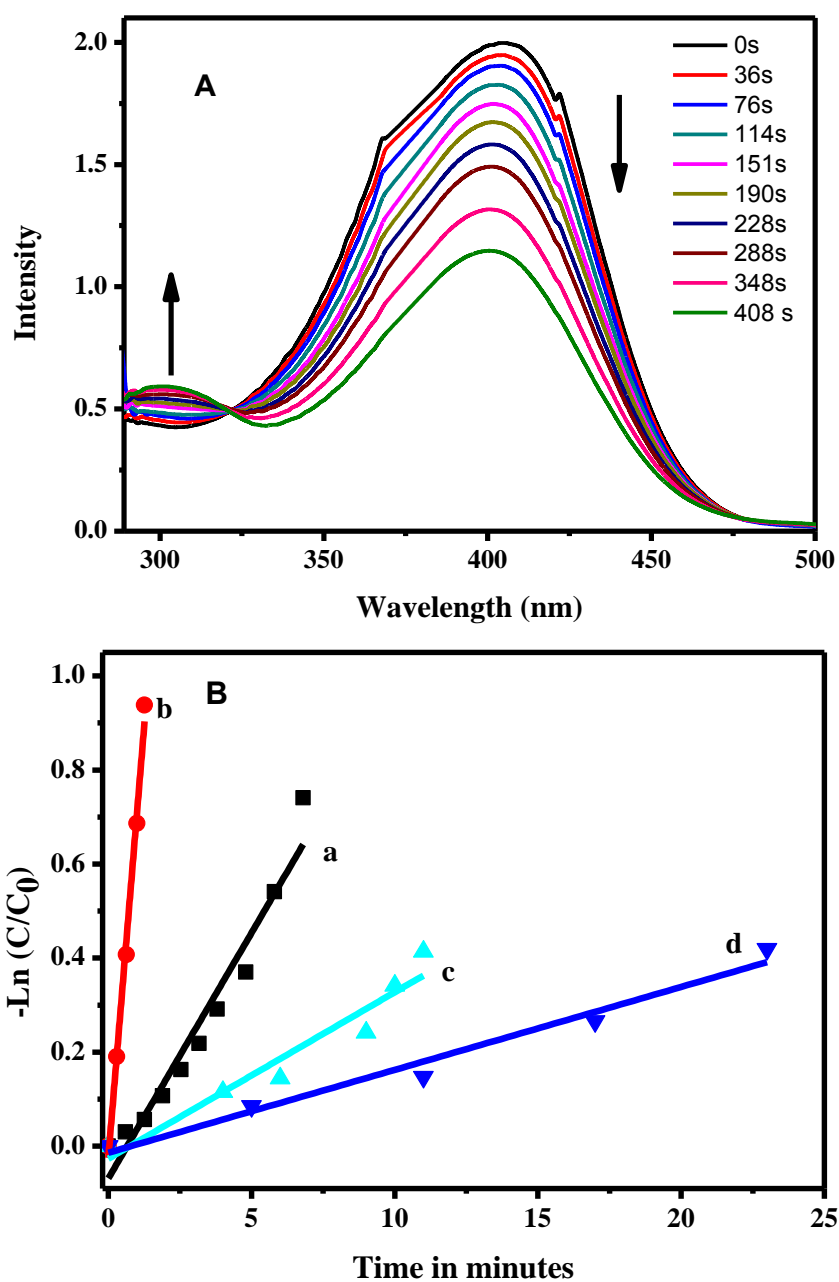


Figure 3.7: (A) Time dependent absorption spectra of the reaction solution in the presence of the Pd loaded titania nanotube (0.1Pd) (B) A typical plot of $-\ln(C/C_0)$ against time for the determination of rate constant for reduction of p-nitrophenol by NaBH₄ in presence of Pd loaded titania nanotube catalyst (a) 0.1Pd (b) 1Pd (c) 5Pd and (d) 10Pd.

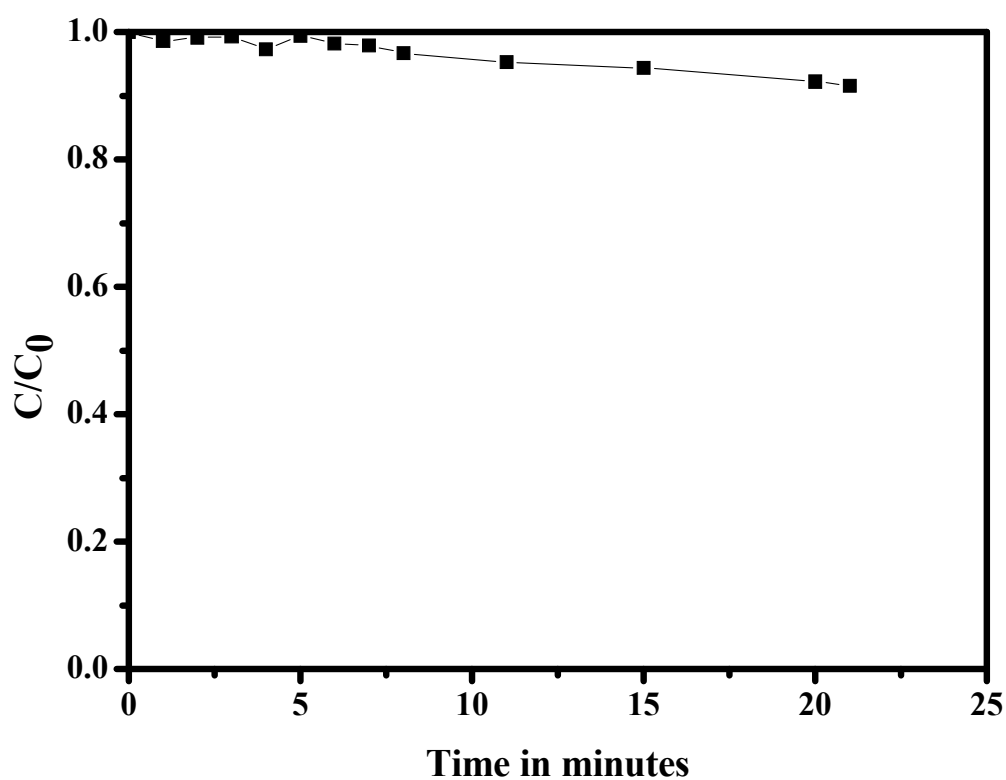
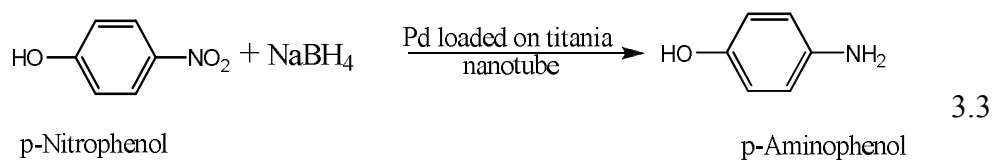


Figure 3.8 Plot of C/C_0 for the catalytic reduction of 4-nitrophenol by sodium borohydride in presence of pure titania nanotube



The recyclability of the catalyst was monitored by repeating the p-nitrophenol reduction reaction for 2nd and 3rd cycle with 1Pd sample. The time dependant absorption spectra of the p-nitrophenol reaction solution in presence of 1Pd catalyst in 2nd and 3rd cycle and their rate constant are provided in the Figures 3.9 and 3.10. After consecutive cycles catalytic activity of p-nitrophenol reduction reaction with 1Pd sample decreased drastically. It was previously noted that the catalytic activity could significantly be reduced in noble metals due to aggregation and leaching of the noble metal in the reaction mixture.⁵⁴ To improve the recyclability a core shell approach has previously been successfully tried with ceria and carbon.⁵⁵⁻⁵⁶ Zhang *et al* reported a high catalytic deactivation for reduced graphene oxide @ Pd catalyst after 10 cycles. They observed that the time required for 100% conversion of p-nitrophenol increases from 25 s in 1st cycle to 420 s after 10th cycle.⁵⁶ In the current investigation a decrease in the rate constant to 0.2641 and 0.1013 min⁻¹ in 2nd and 3rd cycle has been observed. It is due to adsorbed product (p-aminophenol) on the surface hindering the activity in the subsequent cycles. Further investigation is required to improve the recyclability of the catalyst.

Table 3.2 Catalytic activity comparison of Pd nanoparticle supported on different material for the reduction of 4-nitrophenol (4-NP)

Nature of the catalyst	Rate constant	Amount of catalyst	Concentration of 4-nitrophenol (4-NP)	Reference
Pd supported on titania microspheres	0.19 min^{-1}	1 mol% Pd on titania microspheres of wt% 0.02 to 0.7 mg	10^*10^{-3}M	Zhao Jin et al. ²⁶
Pd on partially reduced graphene oxide	$2.40 * 10^{-1} \text{ s}^{-1}$ (14.4 min^{-1})	3 mg of reduced graphene oxide contain a 10mM concentration of Pd	$10^* 10^{-3} \text{ M}$	Min-Quan Yang et al. ²³
Pd immobilized on Multiwalled carbon nanotube bonded with amphiphilic dendrimer	0.0141 min^{-1}	2.5 mg of functionalised multiwalled carbon nanotube containing 17.7 wt% Pd nanoparticle of size 3.8 nm	6^*10^{-5} M	E. Murugan et al. ⁵⁷
Palladium nanoparticles stabilized by glycodendrimers in water	$4^*10^{-3} \text{ S}^{-1}$ (0.24 min^{-1})	0.2 mol% glycodendrimer –Pd contains $1,4^*10^{-4} \text{ M Pd}$	$2.5 * 10^{-4} \text{ M}$	Sylvain Gataud et al. ⁵⁸
PPI dendrimer-palladium nanocomposites	$4074^*10^{-4} \text{ S}^{-1}$ (24.444 min^{-1})	2 mmol of PPI dendrimer containing pd nanoparticle of size 2nm.	$2 * 10^{-3} \text{ M}$	Kunio Esumi et al. ⁵⁹
Current study	0.7072 min^{-1}	1mg of 1 mol% of Pd in titania nanotube matrix.	10^*10^{-3}M	

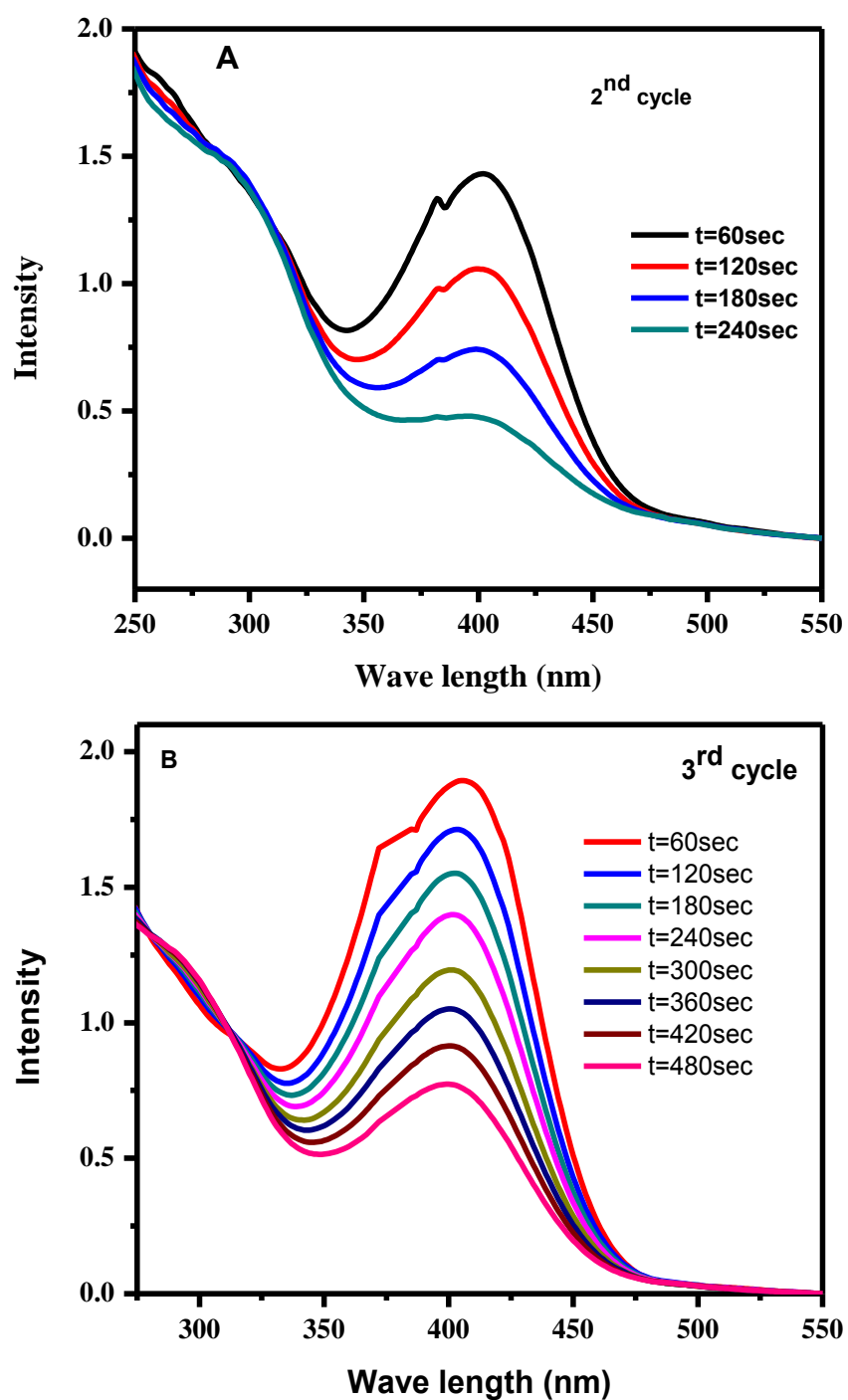


Figure 3.9. Time dependent absorption spectra of the reaction solution in the presence of the 1Pd sample (A) 2nd cycle (B) 3rd cycle

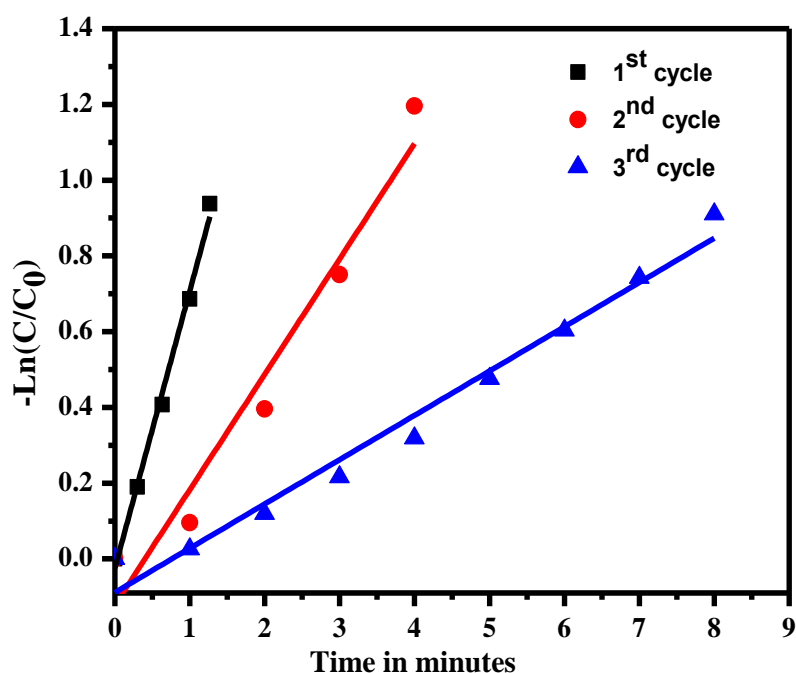


Figure 3.10. A typical plot of $-\ln(C/C_0)$ against time for the determination of rate constant for reduction of p-nitrophenol by NaBH_4 in presence of 1Pd (recyclability) (■) 1st cycle (●) 2nd cycle and (▲) 3rd cycle

3.4 Conclusions

The catalytic performance of palladium loaded titania nanotubes was quantitatively evaluated in the liquid-phase reduction of p-nitrophenol by sodium borohydride. The 1mol% Pd loaded titania nanotubes exhibit maximum catalytic efficiency for the catalytic reduction of p-nitro phenol to p-amino phenol. An apparent rate constant of 0.7072 min^{-1} was observed in the 1Pd sample for the catalytic reduction. This study has revealed that in the case of Pd-loaded TNT's, apart from the particle size of Pd, the morphology as well as the crystalline phase of the titania nanotube are also found to play important roles in their catalytic activity. Though optimum anatase/rutile ratio is good for enhanced catalytic activity, the crumbled morphology destroy the catalytic activity of 5 and 10 Pd samples. Therefore in this case, the tubular morphology plays predominant role in

enhanced catalytic activity. The Pd loaded titania nanotubes will be useful for highly efficient catalysts for industrially important chemical reactions. The recyclability of the catalyst were also monitored and found that the rate constant reduces to 0.2641 and 0.1013 min⁻¹ in 2nd and 3rd cycles respectively. Further studies aimed at improving the catalyst recyclability are in progress.

References

- [1] Wan, K. T.; Davis, M. E. *Nature* **1994**, *370*, 449.
- [2] Shibasaki-Kitakawa, N.; Honda, H.; Kuribayashi, H.; Toda, T.; Fukumura, T.; Yonemoto, T. *Bioresource Technology* **2007**, *98*, 416.
- [3] Uysal, B.; Oksal, B. S. *Research on Chemical Intermediates*, **2013**, *41*, 3893.
- [4] Yamaguchi, K.; Yoshida, C.; Uchida, S.; Mizuno, N. *Journal of the American Chemical Society* **2005**, *127*, 530.
- [5] Zhang, R.; Elzatahry, A. A.; Al-Deyab, S. S.; Zhao, D. *Nano Today* **2012**, *7*, 344.
- [6] Hamilton, J. W. J.; Byrne, J. A.; Dunlop, P. S. M.; Dionysiou, D. D.; Pelaez, M.; O'Shea, K.; Synnott, D.; Pillai, S. C. *The Journal of Physical Chemistry C* **2014**, *118*, 12206.
- [7] Keane, D. A.; McGuigan, K. G.; Ibanez, P. F.; Polo-Lopez, M. I.; Byrne, J. A.; Dunlop, P. S. M.; O'Shea, K.; Dionysiou, D. D.; Pillai, S. C. *Catalysis Science & Technology* **2014**, *4*, 1211.
- [8] Vijayan, B. K.; Dimitrijevic, N. M.; Wu, J.; Gray, K. A. *The Journal of Physical Chemistry C* **2010**, *114*, 21262.
- [9] Vijayan, B.; Dimitrijevic, N. M.; Rajh, T.; Gray, K. *The Journal of Physical Chemistry C* **2010**, *114*, 12994.
- [10] Baiju, K. V.; Shajesh, P.; Wunderlich, W.; Mukundan, P.; Kumar, S. R.; Warriar, K. G. K. *Journal of Molecular Catalysis A: Chemical* **2007**, *276*, 41.
- [11] Baiju, K. V.; Periyat, P.; Pillai, P. K.; Mukundan, P.; Warriar, K. G. K.; Wunderlich, W. *Materials Letters* **2007**, *61*, 1751.

- [12] Banerjee, S.; Dionysiou, D. D.; Pillai, S. C. *Applied Catalysis B: Environmental* **2015**, 176–177, 396.
- [13] Banerjee, S.; Pillai, S. C.; Falaras, P.; O’Shea, K. E.; Byrne, J. A.; Dionysiou, D. D. *The Journal of Physical Chemistry Letters* **2014**, 5, 2543.
- [14] Martínez T, L. M.; Montes de Correa, C.; Odriozola, J. A.; Centeno, M. A. *Journal of Molecular Catalysis A: Chemical* **2006**, 253, 252.
- [15] Kang, T.-G.; Kim, J.-H.; Kang, S. G.; Seo, G. *Catalysis Today* **2000**, 59, 87.
- [16] Hu, F.; Ding, F.; Song, S.; Shen, P. K. *Journal of Power Sources* **2006**, 163, 415.
- [17] Mahmoud, M. H. H.; Ismail, A. A.; Sanad, M. M. S. *Chemical Engineering Journal* **2012**, 187, 96.
- [18] Zheng, S.; Gao, L. *Materials Chemistry and Physics* **2003**, 78, 512.
- [19] Li, Y.; Xu, B.; Fan, Y.; Feng, N.; Qiu, A.; He, J. M. J.; Yang, H.; Chen, Y. *Journal of Molecular Catalysis A: Chemical* **2004**, 216, 107.
- [20] Quisenberry, L. R.; Loetscher, L. H.; Boyd, J. E. *Catalysis Communications* **2009**, 10, 1417.
- [21] Han, C.-H.; Hong, D.-W.; Kim, I.-J.; Gwak, J.; Han, S.-D.; Singh, K. C. *Sensors and Actuators B: Chemical* **2007**, 128, 320.
- [22] Shahreen, L.; Chase, G. G.; Turinske, A. J.; Nelson, S. A.; Stojilovic, N. *Chemical Engineering Journal* **2013**, 225, 340.
- [23] Yang, M.-Q.; Pan, X.; Zhang, N.; Xu, Y.-J. *Crystal Engineering Communication* **2013**, 15, 6819.
- [24] El-Sheikh, S. M.; Ismail, A. A.; Al-Sharab, J. F. *New Journal of Chemistry* **2013**, 37, 2399.
- [25] Pradhan, N.; Pal, A.; Pal, T. *Langmuir* **2001**, 17, 1800.

- [26] Jin, Z.; Xiao, M.; Bao, Z.; Wang, P.; Wang, J. *Angewandte Chemie International Edition* **2012**, *51*, 6406.
- [27] Wong, C. L.; Tan, Y. N.; Mohamed, A. R. *Journal of Environmental Management*, **2011**, *92*, 1669.
- [28] Teranishi, T.; Miyake, M. *Chemistry of Materials* **1998**, *10*, 594.
- [29] Hanaor, D. H.; Sorrell, C. *Journal of Materials Science* **2011**, *46*, 855.
- [30] Hishita, S.; Mutoh, I.; Koumoto, K.; Yanagida, H. *Ceramics International* **1983**, *9*, 61.
- [31] Ohsaka, T.; Izumi, F.; Fujiki, Y. *Journal of Raman Spectroscopy* **1978**, *7*, 321.
- [32] Berger, H.; Tang, H.; Lévy, F. *Journal of Crystal Growth* **1993**, *130*, 108.
- [33] Asthana, A.; Shokuhfar, T.; Gao, Q.; Heiden, P. A.; Friedrich, C.; Yassar, R. S. *Advanced Science Letters* **2010**, *3*, 557.
- [34] Wang, Y. Q.; Hu, G. Q.; Duan, X. F.; Sun, H. L.; Xue, Q. K. *Chemical Physics Letters* **2002**, *365*, 427.
- [35] Moulder, J. F.; Stickle, W. F.; E.'Sobol, P.; Bomben, K. D. *Perkin-Elmer Corporation, Physical Electronics Division, Eden Prairie, United States of America* **1992**, 72.
- [36] Etacheri, V.; Seery, M. K.; Hinder, S. J.; Pillai, S. C. *Advanced Functional Materials* **2011**, *21*, 3744.
- [37] Carley, A. F.; Roberts, J. C.; Roberts, M. W. *Surface Science* **1990**, *225*, L39.
- [38] Westerström, R.; Messing, M. E.; Blomberg, S.; Hellman, A.; Grönbeck, H.; Gustafson, J.; Martin, N. M.; Balmes, O.; van Rijn, R.; Andersen, J. N.; Deppert, K.; Bluhm, H.; Liu, Z.; Grass, M. E.; Hävecker, M.; Lundgren, E. *Physical Review B* **2011**, *83*, 115440.

- [39] Kim, K. S.; Gossmann, A. F.; Winograd, N. *Analytical Chemistry* **1974**, *46*, 197.
- [40] Otto, K.; Haack, L. P.; deVries, J. E. *Applied Catalysis B: Environmental* **1992**, *1*, 1.
- [41] Domashevskaya, É. P.; Ryabtsev, S. V.; Turishchev, S. Y.; Kashkarov, V. M.; Yurakov, Y. A.; Chuvenkova, O. A.; Shchukarev, A. V. *Journal of Structural Chemistry* **2008**, *49*, 80.
- [42] Guinebretiene, R. *X-ray Diffraction by Polycrystalline Materials* Lavoisier **2006**.
- [43] Gilbert, J. B.; Rubner, M. F.; Cohen, R. E. *Proceedings of the National Academy of Sciences of the United States of America* **2013**, *110*, 6651.
- [44] Zeng, J.; Zhang, Q.; Chen, J.; Xia, Y. *Nano Letters* **2009**, *10*, 30.
- [45] Ge, J.; Zhang, Q.; Zhang, T.; Yin, Y. *Angewandte Chemie International Edition* **2008**, *47*, 8924.
- [46] Wu, S.-H.; Tseng, C.-T.; Lin, Y.-S.; Lin, C.-H.; Hung, Y.; Mou, C.-Y. *Journal of Materials Chemistry* **2011**, *21*, 789.
- [47] Endo, T.; Yoshimura, T.; Esumi, K. *Journal of Colloid and Interface Science* **2005**, *286*, 602.
- [48] Singla, M. L.; Negi, A.; Mahajan, V.; Singh, K. C.; Jain, D. V. S. *Applied Catalysis A: General* **2007**, *323*, 51.
- [49] Huang, J.; Yan, C.; Huang, K. *Journal of Colloid and Interface Science* **2009**, *332*, 60.
- [50] Javid, R.; Kawasaki, S.-i.; Suzuki, A.; Suzuki, T. M. *Beilstein Journal of Organic Chemistry* **2013**, *9*, 1156.
- [51] Fenger, R.; Fertitta, E.; Kirmse, H.; Thunemann, A. F.; Rademann, K. *Physical Chemistry Chemical Physics* **2012**, *14*, 9343.

- [52] Johnson, J. A.; Makis, J. J.; Marvin, K. A.; Rodenbusch, S. E.; Stevenson, K. J. *The Journal of Physical Chemistry C* **2013**, *117*, 22644.
- [53] Panigrahi, S.; Basu, S.; Praharaj, S.; Pande, S.; Jana, S.; Pal, A.; Ghosh, S. K.; Pal, T. *The Journal of Physical Chemistry C* **2007**, *111*, 4596.
- [54] Zhang, N.; Xu, Y.-J. *Chemistry of Materials* **2013**, *25*, 1979.
- [55] Yu, T.; Zeng, J.; Lim, B.; Xia, Y. *Advanced Materials* **2010**, *22*, 5188.
- [56] Zhang, Z.; Xiao, F.; Xi, J.; Sun, T.; Xiao, S.; Wang, H.; Wang, S.; Liu, Y. *Scientific Reports* **2014**, *4*, 4053.
- [57] Murugan, E.; Vimala, G. *Journal of Colloid and Interface Science* **2013**, *396*, 101.
- [58] Gatard, S.; Salmon, L.; Deraedt, C.; Ruiz, J.; Astruc, D.; Bouquillon, S. *European Journal of Inorganic Chemistry* **2014**, *2014*, 4369.
- [59] Esumi, K.; Isono, R.; Yoshimura, T. *Langmuir* **2004**, *20*, 237.

PbS sensitised TiO₂ nanotube arrays for visible light photocatalytic applications

● Contents ●	4.1 Introduction
	4.2 Experimental
	4.3 Results and Discussion
	4.4 Conclusion
	References

Some of the contents of this chapter have appeared in the following research publication

- [1] N.B. Rahna, **Vijila Kalarivalappil**, Manoj Nageri, Suresh C. Pillai, Steven J. Hinder, V. Kumar and Baiju K. Vijayan “Stability studies of PbS sensitized TiO₂ nanotube arrays for visible light photocatalytic applications by X-ray photoelectron spectroscopy (XPS)”, *Material Science in Semiconductor Processing*, **42**, (2016) 303

4.1 Introduction

The major factors which resist many practical applications of widely used semiconductor titania are the rapid charge recombination of the electron-hole pairs, thereby suppressing the quantum efficiency, and the wide band gap of the material, which restricts light absorption only to UV region of solar spectrum. In this scenario sensitisation of wide band gap semiconductors with those having a smaller band gap is receiving considerable attention for solar cell and photocatalytic applications.¹⁻² The effective use of the terrestrial solar spectrum is very important for the energy and environmental applications.³ The quantum dots of chalcogenides are effectively used for photovoltaic and photocatalytic applications under solar light due to their absorption characteristics in visible and near infrared region.⁴⁻⁸ Nanostructures of titania receive considerable interest as a wide gap semiconductor for the support of such quantum dots for efficient charge transfer,⁹⁻¹⁰ due to its chemical inertness and appropriate band position. There are different methods used for the sensitisation of titania with quantum dots such as chemical bath deposition (CBD), successive ionic layer adsorption and reaction (SILAR), and attachment of quantum dots by a suitable linker.¹¹ The SILAR method is reported to be advantageous over other methods because of the ability to deposit on inner walls of the nanostructure, higher loading and lower aggregation.¹² Deposition of CdS/PbS on mesoporous titania have been reported to be effectively used for photocatalytic and photovoltaic applications.¹³ The PbS quantum dot coated with CdS solar cell has been reported to exhibit an efficiency of 2.21%.¹⁴ Ordered nanopillars of titania decorated with PbS has been reported to exhibit a power conversion efficiency of 5.6%.¹⁵ Sol-gel titania film decorated with PbS was also tested for enhanced I-V properties.¹¹ The electron injection from PbS quantum dots to the titania nanoparticles were monitored using fluorescence

quenching and rapid fluorescence decay measurements.¹⁶ photoactive nanohybrid structure based on the combination of PbS quantum dots (QDs) as light harvester and one-dimensional TiO₂ nanobelts (NBs) to channel the flow of photogenerated charge carriers is reported by Wang et al. Efficient electron transfer from photoexcited PbS QDs to TiO₂ NBs has been demonstrated and the charge-transfer property was tuned through the size quantization effect of PbS QDs. Further the use of TiO₂ NBs instead of TiO₂ nanoparticles permits a larger critical size of PbS QDs capable of injecting electrons into TiO₂ NBs, which, in turn, extends the absorption of the PbS-QD/TiO₂-NB nanohybrids to a longer wavelength region up to IR region.¹⁷ The size dependant photocatalytic reduction of carbondioxide using PbS sensitised titania were studied by Wang *et al.*¹⁸ They reported five times improvement in the photoreduction of carbon dioxide in PbS sensitised titania. In another investigation, PbS quantum dots attached to the titania nanotube surface using a linker were used for photocatalytic degradation of dyes.¹⁹ Sol-gel synthesised PbS-graphene/ titania composites have been effectively used for the photocatalytic degradation of methylene blue. PbS and graphene not only provide the visible light activity but also excellent photoinduced charge separation and transport properties to the system.²⁰ PbS supported on carbon nanotube was employed for the decomposition of methyl orange.²¹ The photocorrosion of PbS quantum dots in solar cells by polysulfide electrolyte is reported by Lee *et al.*²² The 50% decrease in photocurrent was observed in PbS sensitized solar cell after illuminating the cell for 1h with 1 sun at AM 1.5. The photocorrosion of the PbS sensitized cell was decreased by providing a CdS layer on the surface of PbS.²³ The photostability of the CdS sensitized titania was studied using micro raman analysis.²⁴ The photostability of the PbS nanoparticle play an important role in determining the efficiency of photocatalytic activity and photovoltaic property.

The quantum dots of PbS are effectively used for photovoltaic and photocatalytic applications under solar light due to their absorption characteristics in visible and near infrared region and the property of multiple exciton generation (MEG), a process by which one absorbed photon generates multiple electron–hole pairs. So in the present work titania nanotube prepared through anodisation method was sensitised with PbS nanoparticles using a SILAR method. The SILAR cycle play an important role to tune the photocatalytic and photovoltaic properties of PbS sensitised titania nanotube. The stability and recyclability of the PbS sensitised titania nanotube were also studied through the X-ray photoelectron spectroscopy.

4.2 Experimental

Titania nanotubes were synthesised by potentiostatic anodisation process in ethylene glycol-fluoride electrolyte. In a typical experiment, titania metal sheet (assay 99.7%, Sigma Aldrich) of dimension ($3 \times 1 \times 0.25 \text{ cm}^3$) is potentiostatically anodised under 40 V using platinum counter electrode in an electrolyte consists of 96.5 ml ethylene glycol (assay 99%, Merck), 3.5 ml water and 0.6 g ammonium fluoride (assay 98%, Sigma Aldrich). The resultant amorphous titania nanotube arrays formed on the surface of titanium metal surface is further heated at 400 °C for one hour to form crystalline anatase phase of titania nanotube. These nanotubes are further used for the deposition of PbS quantum dots using SILAR method.

4.2.1 Deposition of PbS on Titania Nanotube

The deposition of PbS was carried out by dipping the titania nanotube substrate in an 0.02 M methanolic solution of PbNO_3 for one minute followed by rinsing in pure methanol to remove excess precursor and dried at 100 °C. The same process was followed for depositing S^{2-} , by treating with 0.02 M

methanolic solution of Na₂S.xH₂O (assay 50%, Merck) and rinsed with pure methanol (assay 99.5%, Spectrochem India) and dried at 100 °C for one minute. Pb²⁺ ions are adsorbed onto the surface of oxide (TiO₂) nanoparticles during the first dipping step in the precursor solution containing the metal salt. After the washing, Pb²⁺ reacts with S²⁻ to form PbS QDs on the TiO₂ surface at the second dipping step in the sulfur precursor solution. This cycle was repeated for several times such as 1, 3, 5 and 10 to increase the amount of PbS deposition on the surface of titania nanotube arrays and the samples were labelled as 1PT, 3PT, 5PT and 10PT.

The stability and oxidation state of the PbS sensitised titania nanotubes before and after photocatalytic reaction were monitored by X-ray photoelectron spectroscopy (XPS). XPS analyses were performed on a ThermoFisher Scientific (East Grinstead, UK) Theta Probe spectrometer. XPS spectra were acquired using a monochromated Al K α X-ray source ($h\nu = 1486.6$ eV). An X-ray spot of ~ 400 μm radius was employed. All spectra were charge referenced against the C1s peak at 285 eV to correct for charging effects during acquisition. Quantitative surface chemical analyses were calculated from the high resolution, core level spectra following the removal of a non-linear (Shirley) background. The manufacturers Avantage software was used which incorporates the appropriate sensitivity factors and corrects for the electron energy analyser transmission function. Crystalline phase of titania nanotube sensitised with PbS was determined using a X-ray diffractometer (D5005, Bruker, Germany). The Kubelka –Monk absorbance of the samples were obtained from the absorbance spectra recorded in diffuse reflectance mode using a UV-Visible Spectrometer (Lambda 35, Perkin Elmer, USA). Surface morphology and elemental analysis of the samples were determined by a Scanning Electron Microscope (SU6600 SEM, Hitachi, Japan).

The photocatalytic activities of the prepared samples were measured by determining the degradation of methylene blue (MB) dye in an aqueous solution. In a typical experiment, titania film of area 0.8 cm^2 was placed in a cuvette containing MB dye solution of concentration $2.7 \times 10^{-5} \text{ M}$. The above cuvette was kept in the dark for 2 hrs in order to acquire adsorption-desorption equilibrium of dye over the film. After this the initial absorption of the dye was recorded followed by irradiation of the solution at different time intervals in a visible light chamber consisting of 1000W mercury lamp (Philips Belgium HPL-N) with polycarbonate sheet as the filter for UV radiation. The polycarbonate with glass sheet filter out all the radiation below 400 nm. The light after filtering the wave length below 400 nm with intensity of $\sim 330 \text{ } \mu\text{W}/\text{cm}^2$ was used for the photocatalytic reaction. The change in concentration of the dye, with respect to the initial concentration, was plotted as a function of time. The reference MB dye solution having the same concentration without the titania thin film did not show any degradation under identical illumination conditions. After the first photocatalytic reaction the same sample is again used for the next photocatalytic reaction (2nd Cycle) using the same procedure as above.

In order to study the photocurrent generation effect in PbS sensitised titania nanotube with an area 0.25 cm^2 were used for the solar cell fabrication. A polysulfide electrolyte consisting of 1M $\text{Na}_2\text{S} \cdot 9\text{H}_2\text{O}$ and 1M sulphur powder dissolved in 1:1 solution of methanol and water was used as the electrolyte. A platinum coated FTO glass plate was used as the counter electrode. The experiments were carried out under AM1.5 sun conditions using a solar simulator (Class AAA Solar Simulators, Model: 91195A) operating at an intensity of 100 mW cm^{-2} . The light intensity was adjusted using a monocrystalline Si reference cell.

4.3 Result and Discussions

The XRD patterns of TiO₂ nanotube arrays sensitised with PbS are given in Figure 4.1. The diffraction peaks obtained at $2\theta=25.32, 38.44, 48.07, 53.90, 62.19, 70.86, 76.28$ correspond to the reflections from (101), (004), (200), (105), (204), (220), (215) planes of tetragonal phase of anatase form of crystalline titania (JCPDS No. 02-1272). The peaks corresponding to the PbS are observed at $2\theta=30.07, 25.96$ and 43.06 can be assigned as the diffraction from (200), (111) and (220) planes of face centered cubic structure of PbS (JCPDS No. 05-0592). The PbS peak are less crystalline than the titania nanotube, as they are not annealed after sensitization of TNT.

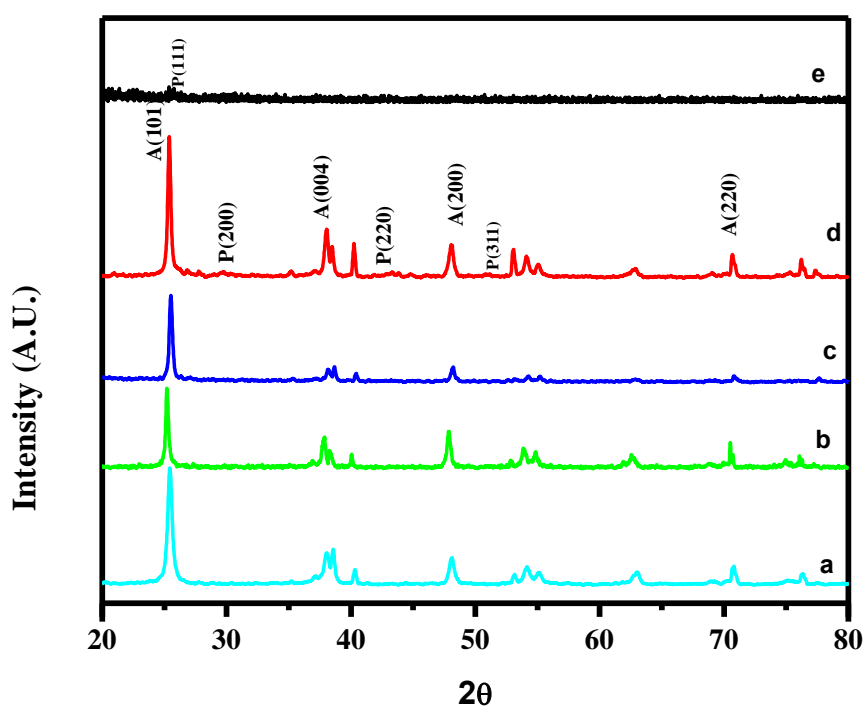


Figure 4.1 XRD patterns of (a) TiO₂ nanotube calcined at 400 °C, PbS sensitised TiO₂ nanotube (b) 1PT (c) 3PT (d) 5PT and (e) 10PT

The SEM images of the unsensitized and PbS-sensitised titania nanotubes are provided in Figure 4.2. The tubular nature of these samples can clearly be observed (Figure 4.2). The average diameter and wall thickness of the titania nanotube were found to be 107 and 22 nm respectively (Figure 4.2A & A1). The small particles of PbS can be observed in the tubular walls of the PbS sensitised titania nanotube arrays (Figure 4.2 B & B1). The percentage of PbS after each cycle is determined using XPS analysis. The percentage of Pb is found to be 0.56, 2.39, 3.98 and 6.89 % for 1, 3, 5 and 10 PT respectively.

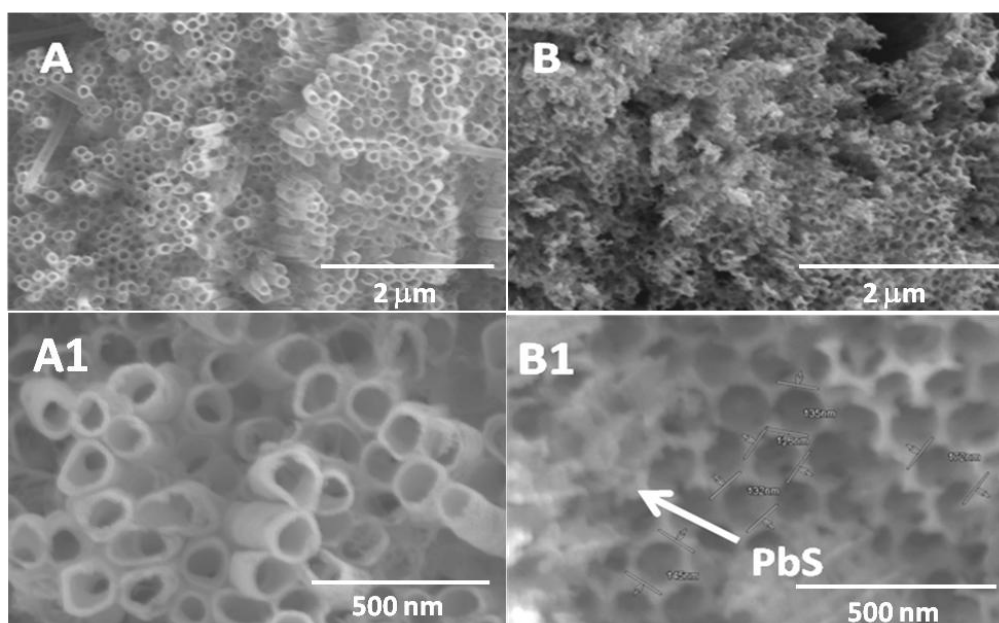


Figure 4.2 SEM images of (A,A1) titania nanotube calcined at 400 °C (B,B1) PbS sensitised titania nanotube

The diffuse reflectance spectra of both the unsensitized and PbS-sensitized nanotube are plotted in Figure 4.3. It is interesting to observe that in the case of titania nanotube sensitized with PbS, absorption shift to the visible region. It has also been observed that when the SILAR cycle was increased the visible light absorption was also increased and further extended to the NIR

spectral region. This can be explained as a result of the PbS incorporation.²⁵ This red shifted absorption is the indirect indication of increase in size of the PbS particle formed on the surface of titania nanotube array. Increase in PbS particle size is attributed to particle coarsening due to agglomeration.

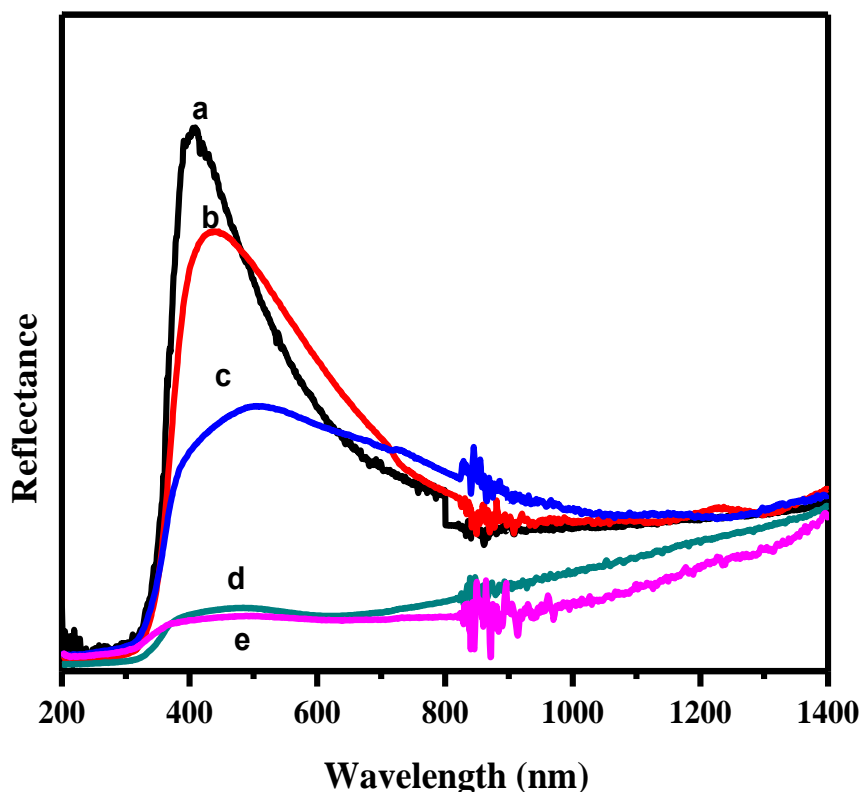


Figure 4.3 Diffuse reflectance spectra of (a) TiO₂ nanotube calcined at 400 °C, PbS sensitised TiO₂ nanotube (b) 1PT (c) 3PT (d) 5PT and (e) 10PT.

The photocatalytic activity of the sample is monitored using methylene blue degradation under visible light irradiation. Photocatalytic degradation of methylene blue under visible light with a freshly prepared PbS sensitized titania nanotube (1st cycle) is shown in Figure 4.4. The PbS sensitised samples show higher photocatalytic activity compared to the unsensitized titania nanotubes. The reaction was found to be following a pseudo first order reaction kinetics as

determined from the plot of $\ln C$ vs time t . The sample with PbS sensitised after 3 cycle exhibits the maximum photocatalytic activity. The photocatalytic activity is found to follow the order of 3PT > 5PT > 10PT > 1PT > TNT. Brahimi et al. reported the PbS/titania heterojunctions are very important in solar cell and photocatalytic degradation due to their increased charge separation and the possibility of multiple exciton generation. They demonstrated the inter particle electron injection from photoactivated PbS to inactivated TiO_2 by the increase of eosin degradation under visible light also they investigated the different parameters affecting the photoactivity such as amount of PbS, concentration of dye and initial pH etc.²⁶

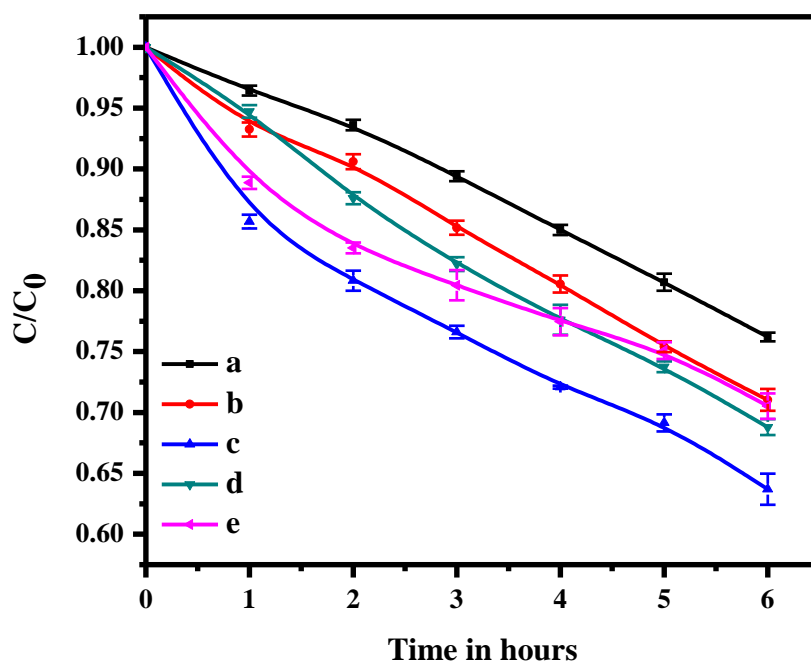


Figure 4.4 Photocatalytic degradation of methylene blue under visible light with freshly prepared PbS sensitized titania nanotube (1st cycle) (a) TiO_2 nanotube calcined at 400 °C, PbS sensitised TiO_2 nanotube (b) 1PT (c) 3PT (d) 5PT and (e) 10PT

The increase in photocatalytic activity with increase in the number of cycles can be better understood by the UV-Visible absorption characteristics. When the coating SILAR cycle increases above the optimum, slight decrease in the photocatalytic activity was observed. For example, 3PT showed a rate constant value of 0.0796 h^{-1} , while 5 PT samples show a value of 0.0626 h^{-1} under similar experimental conditions. This may be due to the aggregation of PbS during the higher cycles of coating. Due to this aggregation, boundaries between PbS-PbS will be created, which increases the loss of electron-hole pairs in the titania PbS system. The photocatalytic recyclability of the samples was tested using fresh methylene blue solution. Photocatalytic degradation of methylene blue under visible light by PbS sensitized nanotube has already been used for the photocatalytic reaction (2nd Cycle) are plotted and shown in Figure 4.5. After the first cycle the photocatalytic activity shows a drastic decrease in the 2nd cycle. The rates of the reaction of 1st and 2nd cycle are plotted in the Figure 4.6 which indicates the instability of PbS sensitised tiania in the heterogeneous based photocatalytic system. In 2nd cycle the 5PT and 10PT shows maximum photocatalytic activity than other samples. The stability of PbS in photocatalytic reaction through X-ray photoelectron spectroscopy were also investigated.

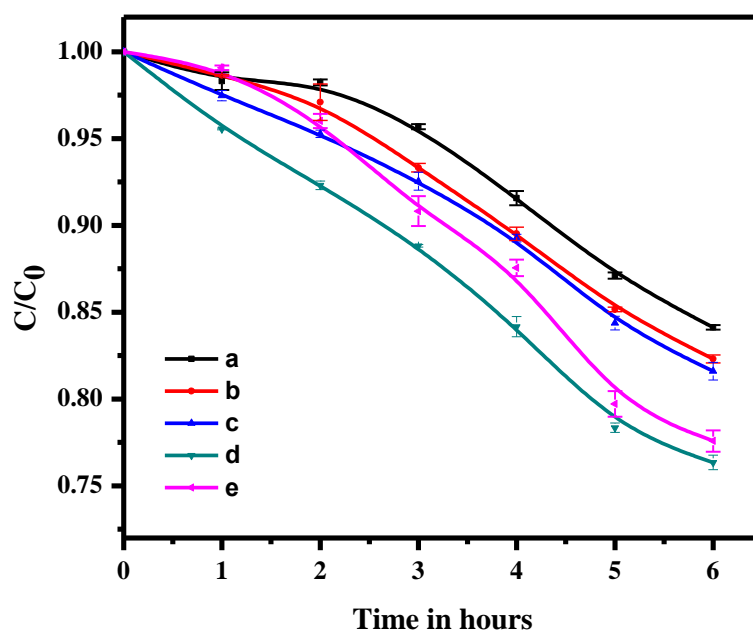


Figure 4.5 Photocatalytic degradation of methylene blue under visible light by PbS sensitized titania nanotube which once used for a photocatalytic reaction (2nd Cycle) (a) TiO₂ nanotube calcined at 400 °C, PbS sensitized TiO₂ nanotube (b) 1PT (c) 3PT (d) 5PT and (e) 10PT

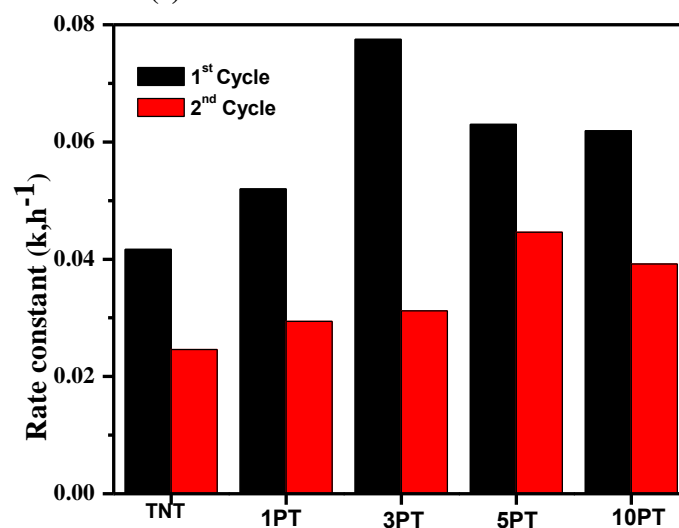


Figure 4.6 Rate constant of methylene blue degradation of PbS sensitized titania nanotube under irradiation with visible light (a) 1st cycle (b) 2nd Cycle.

XPS was used to determine the oxidation and chemical state of the PbS sensitised titania nanotube. The XPS scan of the bare titania nanotube arrays calcined at 400 °C contains the elements in the following atomic percentage Ti (26.35%), O (65.53%) C (6.72%), N (0.50%), F (0.90%), the impurities of nitrogen and fluorine are from the ethylene glycol-water-ammonium fluoride electrolyte used for potentiostatic anodisation process. Nitrogen and fluorine impurities are the reason for the visible light activity of the bare titania nanotube as reported earlier.²⁷⁻²⁸ Ti 2p_{3/2} and 2p_{1/2} peak were observed at 458.98, 464.8 eV respectively (Figure 4.7A). The difference of 5.8 eV in the BE value of the 2 J states indicates that the titania is in the Ti⁴⁺ state in the titania nanotube. The O 1s peak is shown in Figure 4.7B. The peaks located at 529.9 eV and 531.9 eV are assigned to Ti–O in TiO₂ and hydroxyl groups (Ti–OH), respectively.²⁹

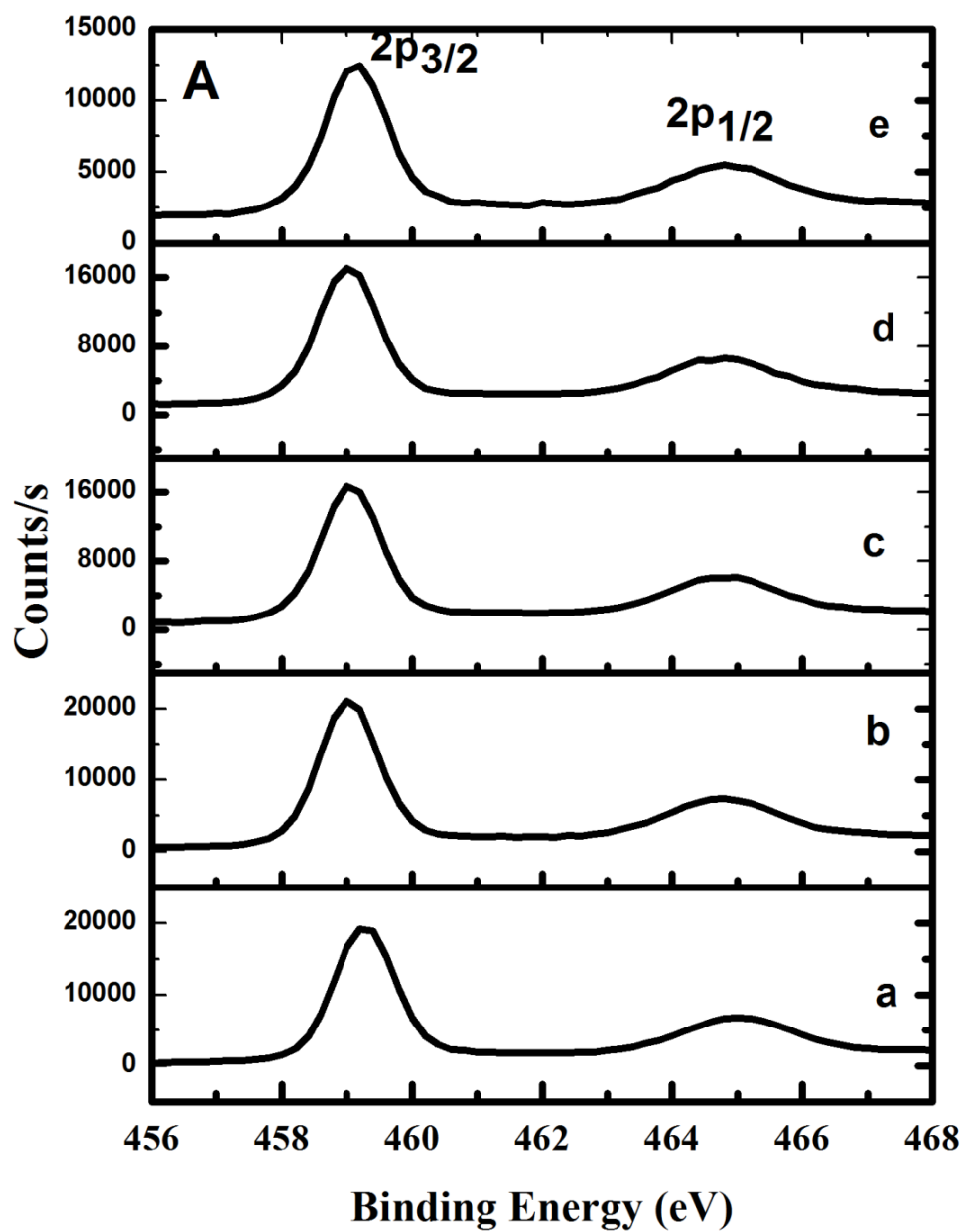


Figure 4.7A. XPS spectra of Ti 2p peak of (a) TiO_2 nanotube calcined at 400 °C, PbS sensitised TiO_2 nanotube (b) 1PT (c) 3PT (d) 5PT and (e) 10PT

The XPS spectra of Pb 4f_{7/2} and 4f_{5/2} peaks are plotted in Figure 4.7C. The peak shows shift from the reference binding energy values of 137.6 and 142.4 eV.³⁰ At higher SILAR cycle such as 5PT, 10 PT the 4f_{5/2} and 4f_{7/2} peak are split into two. In the work of Kovalev *et al* they synthesized crystals of PbS with different sizes by chemical deposition from aqueous solution and has demonstrated that the particle size of PbS can be correlated with observable changes in the binding energies of the Pb XPS peak. They observed growth of binding energies for both donor Pb 4f and acceptor S2p photoelectron lines with decreasing nanocrystal's size. Also they reported the relative integral intensity of the peak depends upon the fraction of particle in the specific region,³¹ which indicate that higher SILAR cycle leads to the formation of fraction of bigger and smaller particles on the surface of titania nanotube. The 4f_{7/2} peak observed at 137.8 and 138.9 eV are due to the presence of PbS having two different particle sizes that are formed in 10PT samples. In case of 4f_{5/2} peak in 10PT two peaks at 142.6 and 143.8 eV are observed. So at higher SILAR cycle the 4f_{7/2} and 4f_{5/2} shows XPS peaks corresponding to the bulk as well as nanoparticle of PbS. The Pb 4f peak fitted for PbS particle of different size of 10PT sample is provided in the Figure 4.7D. In 5PT sample shows a shoulder at 137.8 and 142.6 indicating that a small fraction of bigger particle are also present in 5PTNT samples. This result is clearly in agreement with the red shift of the UV-visible reflectance spectra of the samples with higher SILAR cycles.

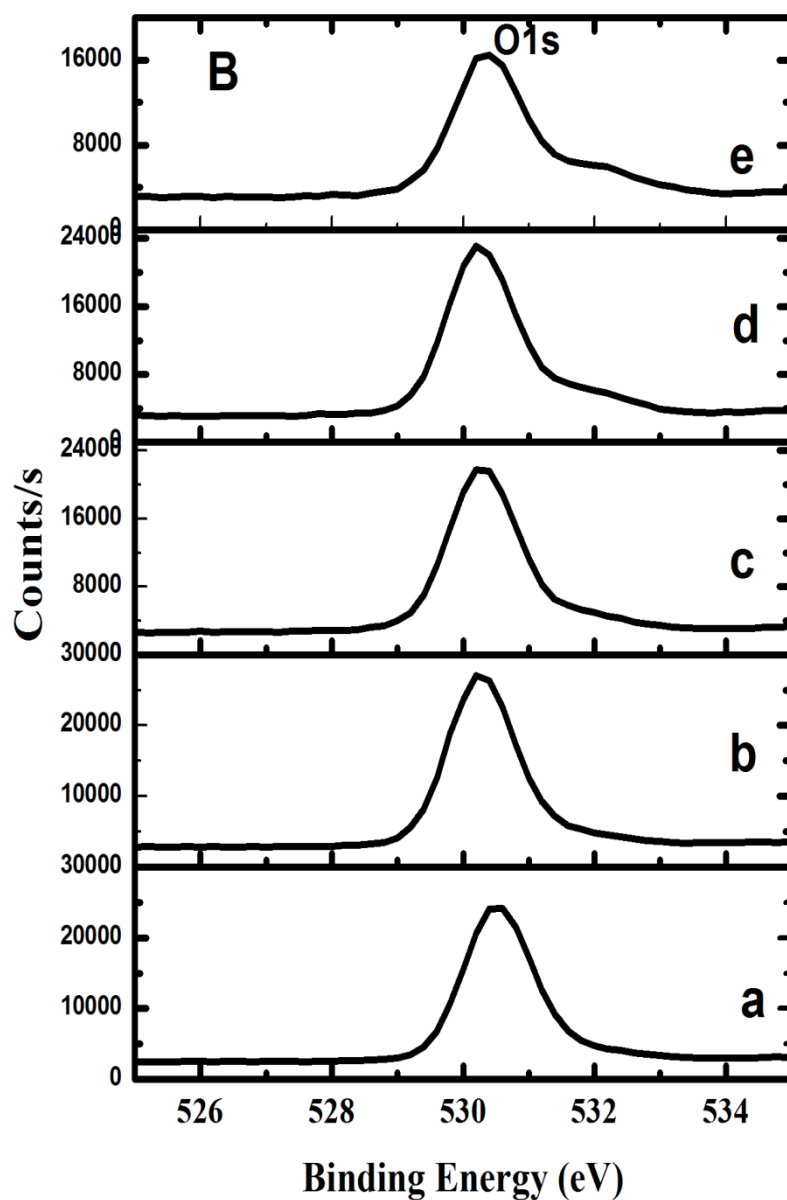


Figure 4.7B. XPS spectra of O 1s peak of (a) TiO₂ nanotube calcined at 400 °C, PbS sensitised TiO₂ nanotube (b) 1PT (c) 3PT (d) 5PT and (e) 10PT

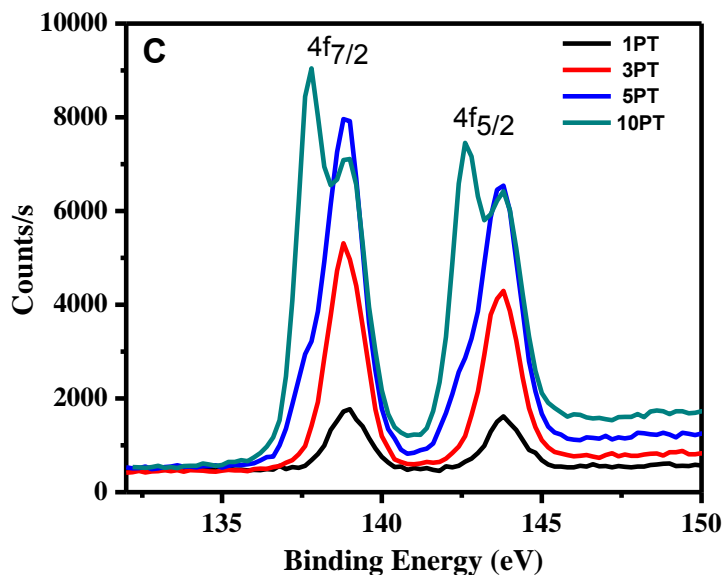


Figure 4.7C. XPS spectra of Pb 4f peak of PbS sensitised TiO₂ nanotube (a) 1PT (b) 3PT (c) 5PT and (d) 10PT

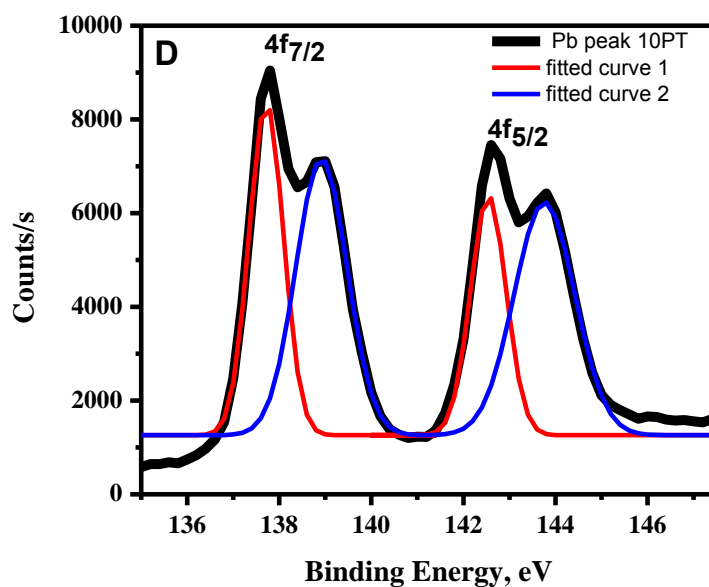


Figure 4.7D. XPS spectra of Pb 4f peak of 10PT fitted for PbS particle with different size

In order to understand the stability of PbS sensitised titania nanotube after photocatalytic reaction, we also carried out XPS analysis on the samples after the photocatalytic degradation studies. It is observed that the relative intensities and the area of Pb $4f_{5/2}$ and $4f_{7/2}$ peaks are decreased drastically after photocatalytic reaction (Figure 4.7E).

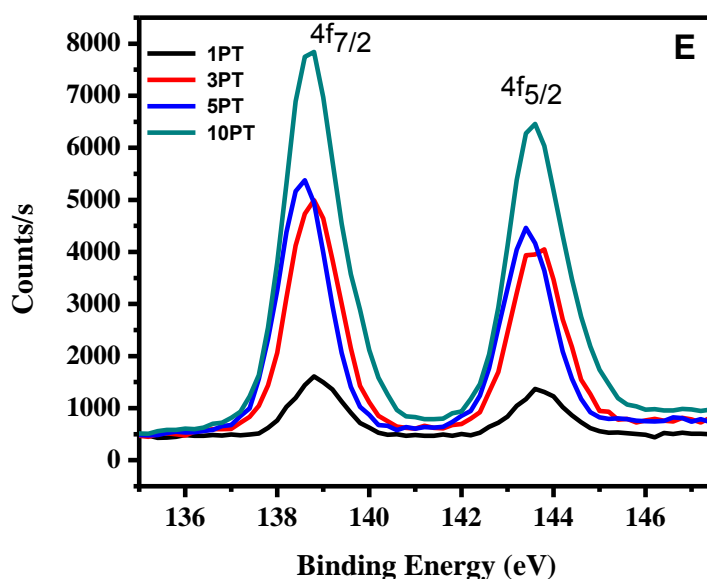


Figure 4.7E. XPS spectra of Pb 4f peak of PbS sensitised TiO₂ nanotube sample after photocatalytic reaction (a) 1PT (b) 3PT (c) 5PT and (d) 10PT

This drastic decrease was more pronounced in 5PT and 10PT samples. Another observation is that the Pb $4f_{5/2}$ and $4f_{7/2}$ peak of 5PT and 10PT are converted to single peak after the photocatalytic reaction. This indicates that after the photocatalytic reaction bigger PbS particle in 5PT and 10PT are dissolved and converted to smaller particle. There are several factors which affect the dissolution mechanism of PbS such as pH, presence of oxygen, light intensity, temperature etc. In presence of dissolved oxygen and H⁺ the possible dissolution mechanism involves protonation of PbS followed by reaction with

adsorbed oxygen to form sulphate ions.³² This clearly has an influence on the photocatalytic activity of the samples in 2nd cycle. In 2nd cycle 5PT and 10PT samples show more activity than the other samples in photocatalytic reaction. After the dissolution PbS particles in the 5PT and 10PT samples are converted to smaller particles which have higher activity as in the case of 3PT sample in the first cycle. In 2nd cycle the photocatalytic activity shows the following order 5PT >10PT >3PT>1PT >TNT. It is already reported that photothermal soaking of PbS quantum dots in air leads to blue shift in the absorption spectra indicating decrease in size of the core of PbS quantumdots.³³ The photocorrosion of PbS highly affect the photoactivity of the system. Zhang et al reported a 43% drop in photocatalytic activity for the PbS sensitized titania for the degradation of pentachlorophenol after photocorrosion.³⁴ The photocorrosion of the PbS nanoparticle leads to its size reduction. The size of the PbS particle play an important role in the photocatalytic reaction.¹⁸ In the current investigation we also observe the size reduction through X-ray photoelectron spectroscopy after the first cycle of photocatalytic reaction. The photocorrosion of the PbS nanoparticles leads to the formation of Pb-O adducts or PbSO₃ as reported earlier. They reported that the accumulated hole after the photoreduction of CO₂ will oxidize the PbS to PbSO₃, PbO and Pb(OH)₂.¹⁸ But in the current study we used methylene blue an organic dye for the photocatalytic degradation study. In this the photoexcited hole and electron simultaneously take part in the photocatalytic reaction.³⁵⁻³⁶ We did not observe any such species in the XPS spectra of Pb. So with the present experiment data it is difficult to propose an exact mechanism for the photocorrosion mechanism of PbS nanoparticle in PbS sensitized titania nanotube samples. The comparison of the photocatalytic property of the PbS sensitized semiconductors are listed in the Table 4.1. We obtain a rate constant of 0.0793 h⁻¹ and 37 % of degradation of methylene blue in 6h using a visible light of intensity ~330 μW/cm² which is comparatively higher for a thin film on the surface of a titanium metal foil.

Table 4.1 Comparison of the photoactivity of PbS sensitised semiconductor system

Nature of Catalysis	Synthesis method	Photocatalytic reaction	Maximum conversion (%)/K _{app} (time ⁻¹), remarks	Lamp used	Reference
ZnO@PbS/ Graphene oxide	Solvothermal method followed by chemical modification	Hydrogen production using methanol as a sacrificing agent	34.48 $\mu\text{mol g}^{-1}\text{h}^{-1}$	500 W Mercury lamp	Shi et al. ³⁷
Graphene oxide-PbS on titania nanotube	Electrodeposition	Degradation of pentachlorophenol	100% degradation of 50 ml 10mgL ⁻¹ pentachlorophenol in 120 min.	500 W Xenon arc lamp	Zhang et al. ³⁴
PbS-titania (10:90) composite	Co-precipitation	Degradation of eosin	0.116 min ⁻¹	2*200W tungsten lamp	Brahimi et al. ²⁶
PbS/titania nanotube	Electrochemical anodisation followed by SILAR and electrodeposition	Degradation of methyloorange	72.44% degradation for 30 ml methyl orange of concentration 5×10^{-5} mol/L in 4 h	300W Xenon arc lamp with intensity 100 mW/cm ²	Kang et al. ³⁸
PbS quantum dot on titania nanotube	Hydrothermal followed by chemical absorption	Degradation of methylene blue, methylene green, Rhodamine B, Rose Bengal, Indigo Carmine	100% degradation for 20ppm dye solution within 30 min. The degradation is more effective in cationic dye methylene blue and methylene green	450 W quartz mercury lamp	Ratanatawanate ¹⁹
PbS/titania nanotube	Electrochemical anodisation with different SILAR cycle	Degradation of methylene blue	0.0793 h ⁻¹ (37% degradation for 4ml methylene blue of concentration 2.7×10^{-5} M)	1000W mercury lamp with polycarbonate and glass sheet as the filter with an intensity $\sim 330 \mu\text{W}/\text{cm}^2$	Current study

The photocurrent density, V_{OC} , fill factor (essentially a measure of quality of the solar cell) and efficiency of the solar cell fabricated using PbS-sensitized TNA are tabulated in Table 4.2. Figure 4.8 shows the photocurrent–voltage (J-V) performance of the PbS sensitised solar cell. It is found that open circuit voltage (V_{OC}) gradually increases to 3 SILAR cycle and then decreases on higher SILAR cycles (5 and 10 cycles). When the coating cycle increases, there will be more PbS with larger crystalline sizes as reported by Baker *et al.* It is also reported that larger nanoparticles can act as an electron-hole recombination center compared to the smaller particles.³⁹ We observed a maximum efficiency of 0.0174% for PbS sensitised (3cycle) titania nanotube photoanode, as observed in the case of photocatalytic activity. The 3SILAR cycle PbS coated titania nanotube (3PT) showed V_{OC} of 0.19V and an efficiency of 0.0174. These values are found to be 4 (for V_{OC}) and 10 times (for efficiency) higher than the other PbS sensitised titania nanotube samples. The lower photo-efficiency may be due to the aggregation or formation of bigger PbS particle at higher SILAR cycle. The photocurrent density under illumination increases with increasing the coating cycle of PbS on the surface of titania nanotube and the optimum SILAR cycle is found to be three. Moreover, the electron transfer from the PbS to titania is highly dependant on the size of PbS.¹⁶ Sambur et al used a photoelectrochemical system composed of PbS nanocrystals of variable size chemically bound to TiO₂ single crystal to assess the efficiency of multiple exciton generation. They observed strong electronic coupling and favourable energy level alignment between PbS nanocrystals and bulk TiO₂ facilitating extraction of multiple exciton more quickly than they recombine, as well as collection of hot electrons from higher quantum dot excited states.⁴⁰ The photo-electrochemical property of the PbS/titania nanotube was monitored by Kang *et al.*³⁸ It was also observed that

the photoelectrochemical property depends upon the SILAR cycles and electrodeposition time. Baker and Kamat studied the effect of SILAR cycle on the growth of CdS particle on the surface of titania.⁴¹ They also reported that small crystals of CdS are much effective in the charge transfer than large crystals for transferring the electron to titania nanostructures.

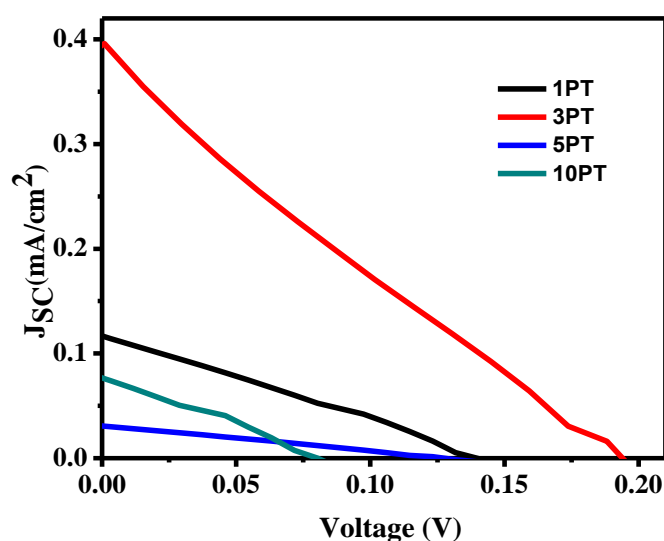


Figure 4.8 J-V curve of PbS sensitised solar cell under 1sun (AM1.5) illumination

Table 4.2 Parameters obtained from J-V curve of the PbS sensitized titania nanotube

Sample	Voc (V)	J _{SC} (mA/cm ²)	Fill Factor	Efficiency
1PT	0.139	0.117	26.69	0.0043
3PT	0.194	0.363	24.70	0.0174
5PT	0.128	0.0308	26.17	0.001
10PT	0.080	0.0766	30.39	0.0019

An overall power conversion efficiency of 3.9% was reported using a CdS (four cycle) /CdSe (seven cycle)/ZnS(one cycle) sensitised TiO₂ electrode, using polysulfide electrolyte and SILAR deposition technique.⁴² Moreover, recent reports shows that Cu₂S counter electrode are more suitable

for the quantum dot sensitised solar cells than the Pt counter electrode.⁴³ Our future work are in the direction to improve the efficiency by changing the counter electrode and by using an additional layer of other Cd and Zn based sulphides.

4.4 Conclusions

The effect of SILAR cycle on the deposition of PbS on the surface of titania nanotube array has been investigated. The PbS sensitised on titania nanotube with three SILAR cycles exhibits maximum photocatalytic activity under visible light with a rate constant of 0.0775 h⁻¹ and optimum photocurrent density. The V_{OC}, photocurrent, fill factor and efficiency of the solar cell (3 SILAR cycle) is found to be 0.194 V, 0.395 mA/cm², 24.7, 0.0174% respectively. The stability of the PbS has been correlated with the photocatalytic activity through X-ray photoelectron spectroscopic studies.

References

- [1] Lee, H. J.; Chen, P.; Moon, S.-J.; Sauvage, F. d. r.; Sivula, K.; Bessho, T.; Gamelin, D. R.; Comte, P.; Zakeeruddin, S. M.; Seok, S. I.; Grätzel, M.; Nazeeruddin, M. K. *Langmuir* **2009**, *25*, 7602.
- [2] Banerjee, S.; Pillai, S. C.; Falaras, P.; O'Shea, K. E.; Byrne, J. A.; Dionysiou, D. D. *The Journal of Physical Chemistry Letters* **2014**, *5*, 2543.
- [3] Keane, D. A.; McGuigan, K. G.; Ibanez, P. F.; Polo-Lopez, M. I.; Byrne, J. A.; Dunlop, P. S. M.; O'Shea, K.; Dionysiou, D. D.; Pillai, S. C. *Catalysis Science & Technology* **2014**, *4*, 1211.
- [4] Zhao, N.; Osedach, T. P.; Chang, L.-Y.; Geyer, S. M.; Wanger, D.; Binda, M. T.; Arango, A. C.; Bawendi, M. G.; Bulovic, V. *ACS Nano* **2010**, *4*, 3743.
- [5] Mora-Seró, I.; Bisquert, J. *The Journal of Physical Chemistry Letters* **2010**, *1*, 3046.
- [6] Gao, J.; Luther, J. M.; Semonin, O. E.; Ellingson, R. J.; Nozik, A. J.; Beard, M. C. *Nano Letters* **2011**, *11*, 1002.
- [7] Synnott, D. W.; Seery, M. K.; Hinder, S. J.; Colreavy, J.; Pillai, S. C. *Nanotechnology* **2013**, *24*, 45704.
- [8] Synnott, D. W.; Seery, M. K.; Hinder, S. J.; Michlits, G.; Pillai, S. C. *Applied Catalysis B: Environmental* **2013**, *130–131*, 106.
- [9] Shalom, M.; Albero, J.; Tachan, Z.; Martínez-Ferrero, E.; Zaban, A.; Palomares, E. *The Journal of Physical Chemistry Letters* **2010**, *1*, 1134.

- [10] Shalom, M.; Dor, S.; Rühle, S.; Grinis, L.; Zaban, A. *The Journal of Physical Chemistry C* **2009**, *113*, 3895.
- [11] Saraidarov, T.; Gevorgian, A.; Reinfeld, R.; Sashchiuk, A.; Bashouti, M.; Lifshitz, E. *Journal of Sol-Gel Science and Technology* **2007**, *44*, 87.
- [12] Shrestha, N. K.; Yoon, S. J.; Lee, D. Y.; Lee, M.; Lim, I.; Sung, M.; Ahn, H.; Han, S.-H. *physica status solidi (RRL) – Rapid Research Letters* **2011**, *5*, 141.
- [13] Stroyuk, O. L.; Rayevska, O. Y.; Shvalagin, V. V.; Kuchmiy, S. Y.; Bavykin, D. V.; Streltsov, E. A.; Poznyak, S. K. *Photochemical and Photobiological Sciences* **2013**, *12*, 621.
- [14] Braga, A.; Giménez, S.; Concina, I.; Vomiero, A.; Mora-Seró, I. n. *The Journal of Physical Chemistry Letters* **2011**, *2*, 454.
- [15] Kramer, I. J.; Zhitomirsky, D.; Bass, J. D.; Rice, P. M.; Topuria, T.; Krupp, L.; Thon, S. M.; Ip, A. H.; Debnath, R.; Kim, H. C.; Sargent, E. H. *Advanced Materials* **2012**, *24*, 2315.
- [16] Hyun, B.-R.; Zhong, Y.-W.; Bartnik, A. C.; Sun, L.; Abruña, H. D.; Wise, F. W.; Goodreau, J. D.; Matthews, J. R.; Leslie, T. M.; Borrelli, N. F. *ACS Nano* **2008**, *2*, 2206.
- [17] Wang, D.; Zhao, H.; Wu, N.; El Khakani, M. A.; Ma, D. *The Journal of Physical Chemistry Letters* **2010**, *1*, 1030.
- [18] Wang, C.; Thompson, R. L.; Ohodnicki, P.; Baltrus, J.; Matranga, C. *Journal of Materials Chemistry* **2011**, *21*, 13452.
- [19] Ratanatawanate, C.; Tao, Y.; Balkus, K. J. *The Journal of Physical Chemistry C* **2009**, *113*, 10755.

- [20] Ullah, K.; Meng, Z.-D.; Ye, S.; Zhu, L.; Oh, W.-C. *Journal of Industrial and Engineering Chemistry* **2014**, *20*, 1035.
- [21] Hamadani, M.; Jabbari, V.; Shamshiri, M.; Asad, M.; Mutlay, I. *Journal of the Taiwan Institute of Chemical Engineers* **2013**, *44*, 748.
- [22] Lee, H.; Leventis, H. C.; Moon, S.-J.; Chen, P.; Ito, S.; Haque, S. A.; Torres, T.; Nüesch, F.; Geiger, T.; Zakeeruddin, S. M.; Grätzel, M.; Nazeeruddin, M. K. *Advanced Functional Materials* **2009**, *19*, 2735.
- [23] Lai, L.-H.; Protesescu, L.; Kovalenko, M. V.; Loi, M. A. *Physical Chemistry Chemical Physics* **2014**, *16*, 736.
- [24] Sfaelou, S.; Kontos, A. G.; Falaras, P.; Lianos, P. *Journal of Photochemistry and Photobiology A: Chemistry* **2014**, *275*, 127.
- [25] Kontos, A.; Likodimos, V.; Vassalou, E.; Kapogianni, I.; Raptis, Y.; Raptis, C.; Falaras, P. *Nanoscale Research Letters* **2011**, *6*, 266.
- [26] Brahim, R.; Bessekhoud, Y.; Bouguelia, A.; Trari, M. *Journal of Photochemistry and Photobiology A: Chemistry* **2008**, *194*, 173.
- [27] Wu, Y.; Liu, H.; Zhang, J.; Chen, F. *The Journal of Physical Chemistry C* **2009**, *113*, 14689.
- [28] Czoska, A. M.; Livraghi, S.; Chiesa, M.; Giamello, E.; Agnoli, S.; Granozzi, G.; Finazzi, E.; Valentin, C. D.; Pacchioni, G. *The Journal of Physical Chemistry C* **2008**, *112*, 8951.
- [29] Yu, J.; Yu, J. C.; Ho, W.; Jiang, Z. *New Journal of Chemistry* **2002**, *26*, 607.

- [30] Moulder, J. F.; Stickle, W. F.; Sobol, P. E.; Bomben, K. D. *Hand book of X-ray Photoelectron Spectroscopy*, Perkin Elmer corporation, Physical Electronics Division, Eden Prairie, United States of America **1992**.
- [31] Kovalev, A. I.; Wainstein, D. L.; Rashkovskiy, A. Y.; Osherov, A.; Golan, Y. *Surface and Interface Analysis* **2010**, *42*, 850.
- [32] Hsieh, Y. H.; Huang, C. P. *Journal of Colloid and Interface Science* **1989**, *131*, 537.
- [33] Ihly, R.; Tolentino, J.; Liu, Y.; Gibbs, M.; Law, M. *ACS Nano* **2011**, *5*, 8175.
- [34] Zhang, X.; Tang, Y.; Li, Y.; Wang, Y.; Liu, X.; Liu, C.; Luo, S. *Applied Catalysis A: General* **2013**, *457*, 78.
- [35] Hoffmann, M. R.; Martin, S. T.; Choi, W.; Bahnemann, D. W. *Chemical Reviews* **1995**, *95*, 69.
- [36] Xu, C.; Rangaiah, G. P.; Zhao, X. S. *Industrial & Engineering Chemistry Research* **2014**, *53*, 14641.
- [37] Shi, X.-F.; Xia, X.-Y.; Cui, G.-W.; Deng, N.; Zhao, Y.-Q.; Zhuo, L.-H.; Tang, B. *Applied Catalysis B: Environmental* **2015**, *163*, 123.
- [38] Kang, Q.; Liu, S.; Yang, L.; Cai, Q.; Grimes, C. A. *ACS Applied Materials & Interfaces* **2011**, *3*, 746.
- [39] Yang, L.; Luo, S.; Liu, R.; Cai, Q.; Xiao, Y.; Liu, S.; Su, F.; Wen, L. *The Journal of Physical Chemistry C* **2010**, *114*, 4783.
- [40] Sambur, J. B.; Novet, T.; Parkinson, B. A. *Science* **2010**, *330*, 63.

- [41] Baker, D. R.; Kamat, P. V. *Advanced Functional Materials* **2009**, *19*, 805.
- [42] Lee, H. J.; Bang, J.; Park, J.; Kim, S.; Park, S.-M. *Chemistry of Materials* **2010**, *22*, 5636.
- [43] Zhao, K.; Yu, H.; Zhang, H.; Zhong, X. *The Journal of Physical Chemistry C* **2014**, *118*, 5683.

CdS sensitized TiO₂ nanotubes arrays for enhanced photocatalytic applications

● Contents ●	5.1 Introduction
	5.2 Experimental
	5.3 Results and Discussion
	5.4 Conclusion
	References

Some of the contents of this chapter have appeared in the following research publication

- [1] **Vijila Kalarivalappil**, Suresh C. Pillai, Steven J. Hinder, V. Kumar and Baiju K. Vijayan “Stability studies of CdS sensitized TiO₂ nanotubes prepared using the SILAR method”, *Journal of Environmental Chemical Engineering*, **6** (2018) 1404.

5.1 Introduction

Well aligned titania nanotubes are gaining considerable interest in a variety of applications such as photocatalysis, batteries and sensors.¹⁻⁴ For the effective utilization of solar light the electronic structure of TiO₂ nanotube arrays are modified in several ways including noble metal loading, metal doping, non metal doping, semiconductor composite/heterostructures and sensitization with suitable semiconductors. An important strategy is the fabrication of heterostructures with a visible light active semiconductor having a more negative cathodic potential than TiO₂.

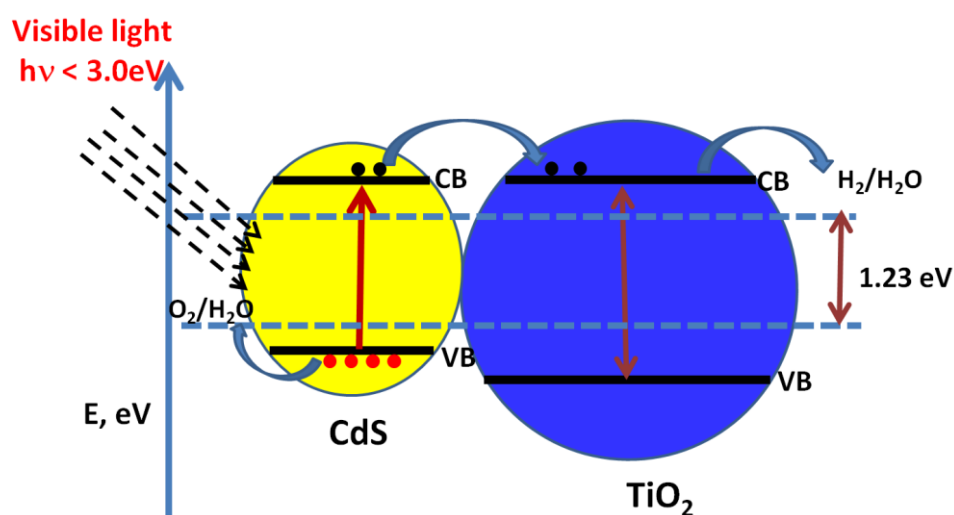


Figure 5.1 The band alignment of CdS sensitized titania nanotube and charge carrier separation

Quantum dot chalcogenides are used widely for the sensitisation of nanostructures for solar cell and photocatalytic applications.⁵⁻⁶ Semiconductor quantum dots are strongly dependent upon the size of the bandgap and hence their ability to create multiple excitons by the absorption of photons with energies greater than the bandgap.⁷ CdS is reported to be one of the most studied chalcogenides due to its small band gap (2.4 eV), its easy tunability

and its relatively high absorption coefficient in the visible region of the spectrum.⁸ Also the CdS/TiO₂ nanocomposite configuration has attracted a great deal of interest because of the positions of their band-gap edges relative to each other (Figure 5.1). In the physical and chemical method employed in quantum dot deposition the SILAR method has advantages over other techniques due to its simplicity and the low cost of equipment required for the deposition. Therefore the SILAR method is widely used in photocatalytic and solar cell applications.⁹⁻¹⁰ A combination of CdS-ZnS coated on the surface of a titania nanoparticle based solar cell is reported to have exhibited an efficiency of 0.66%, however the more costly spiro-OMeTAD (2,2',7,7'-Tetrakis[N,N-di(4-methoxyphenyl)amino]-9,9'-spirobifluorene) material was employed as the hole transport medium.¹¹ Nanorods of CdS-CdSe and CdS₂Se have been deposited on titania nanorods by chemical vapour deposition.¹² Titania nanotubes arrays sensitized with Mn and Co doped CdS were used for photoelectrochemical applications.¹³ Hydrothermal synthesis of titania nanowires sensitized with CdS using chemical bath deposition has been used effectively for the photocatalytic degradation of methyl orange.¹⁴ A sequential chemical bath deposition technique was employed for the deposition of CdS nanoparticles on the surface of titania nanotubes by Qorbani *et al.*¹⁵ Nanocrystalline titania sensitized with optimized compositions of ZnS, CdS and CdSe with CoS and CuS counter electrodes were used to make solar cells with an efficiency of 2.7%.¹⁶ CdS sensitized on vertically aligned single crystalline titania nanorods has been used to fabricate solar cell with an efficiency of 1.8% incorporating a ZnS passivation layer.¹⁷ The layer by layer assembly of titania nanosheet and CdS nanoparticles has been shown to enhance photocurrent generation.¹⁸ Commercially available Hombifine N and Degussa P25 nanoparticles were deposited with CdS nanoparticle and used for

ethanol under visible light irradiation.¹⁹ Sonoelectrochemical anodisation and sonoelectrochemical deposition were used for the preparation of short titania nanotubes deposited with a CdS electrode for photocatalytic generation of hydrogen. The CdS/titania electrode generates hydrogen at a rate of $30.3 \mu\text{mol h}^{-1}\text{cm}^{-2}$ which is nearly 13 times greater than that of a pure titania nanotube electrode.²⁰ A Degussa P25 titania electrode decorated with CdS is reported to have been used for the photocatalytic generation of hydrogen from an ethanol-water mixture.²¹ Titania nanosheets intercalated with CdS were studied using visible light in the degradation of rhodamine B dye by Tian *et al.*²² Chemical bath deposited CdS particles on the titania nanotubes, have been studied for solar cell efficiency by Sun *et al.*²³

The present study describes the deposition of CdS nanoparticle with more negative cathodic potential, on the surface of titania nanotubes, employing the SILAR method, for the effective utilization of solar radiation thereby improving the quantum efficiency. By controlling the number of SILAR cycles, it is possible to tune the optical properties of the material. The stability of the CdS nanoparticles formed on the surface of titania nanotubes is monitored using XPS analysis. It is found that the photocatalytic activity and the solar cell efficiency of the material are highly dependent on the number of SILAR cycles used for the deposition of CdS nanoparticles.

5.2 Experimental

Titania nanotubes were synthesised by potentiostatic anodisation process in ethylene glycol-fluoride electrolyte. In a typical experiment, titania metal sheet (assay 99.7%, Sigma Aldrich) of dimension ($3 \times 1 \times 0.25 \text{ cm}^3$) is potentiostatically anodised under 40 V using platinum counter electrode in an electrolyte consists of 96.5 ml ethylene glycol (assay 99%, Merck), 3.5 ml

water and 0.6 g ammonium fluoride (assay 98%, Sigma Aldrich). The resultant amorphous titania nanotube arrays formed on the surface of titanium metal surface is further heated at 400 °C for one hour to form crystalline anatase phase of titania nanotube.²⁴ These nanotubes were then used as a substrate for the deposition of CdS quantum dots using the SILAR method. The deposition of CdS was carried out by dipping the titania nanotube substrate in a 0.02 M methanolic solution of Cd(NO₃)₂ for one minute followed by rinsing with pure methanol for one minute to remove excess precursor, finally the samples were dried at 60° C for five minute. The same process was followed for depositing S²⁻ by treatment with a 0.02 M methanolic solution of Na₂S and washing in pure methanol. This cycle was repeated 1, 3, 5, 10, 15, 20 and 30 times so as to increase the amount of CdS deposited on the surface of the titania nanotubes arrays.

These samples are labelled T1, T3, T5, T10, T15, T20 and T30. X-ray photoelectron spectroscopy (XPS) was used to determine the stability and oxidation state of the CdS sensitized titania nanotubes before and after the photocatalytic reaction. XPS analyses were carried out using a ThermoFisher Scientific (East Grinstead, UK) K-Alpha⁺ spectrometer with a monochromated Al K α X-ray source ($h\nu = 1486.6$ eV). All spectra were charge referenced against the C1s peak at 285 eV to correct charging effects during acquisition. Quantitative surface chemical analyses were carried out from the high resolution, core level spectra following the removal of a non-linear (Shirley) background. The appropriate sensitivity factors and corrects for the electron energy analyser transmission function are incorporated using manufacturer's Advantage software.

X-ray diffractometer (D5005, Bruker, Germany) was used to determine the crystalline phase of titania nanotubes and CdS sensitized titania nanotubes.

X-ray diffractometer (D5005, Bruker, Germany) was used to determine the crystalline phase of titania nanotubes and CdS sensitized titania nanotubes. The Kubelka–Munk reflectance of the samples were obtained from the Diffuse Reflectance Spectra recorded using a UV-Visible Spectrometer (Lambda 35, Perkin Elmer, USA). The band gap of the samples was calculated by Tauc plot method. The absorption coefficient (α) and incident photon energy ($h\nu$) of the samples are related through the equation 5.1.²⁵⁻²⁶

$$(\alpha h\nu)^2 = A (h\nu - E_g) \quad (5.1).$$

where E_g is the optical band gap of the samples and A is a constant. The optical band gap can be calculated by extrapolating the straight linear portion of the plots between $(\alpha h\nu)^2$ and $h\nu$ to the energy axis. Scanning Electron Microscopy (SU6600 SEM, Hitachi, Japan) and Transmission Electron Microscopy (FEI -TECHNAI FEG30, 300 kV) was used to understand the morphology of CdS sensitized titania nanotubes. Raman spectra of the samples were acquired using a Micro Raman spectroscope (ThermoFisher Scientific DXR 2, USA) using a laser of wavelength 532 nm with 2 mW power.

A methylene blue (MB) dye degradation study was performed so as to evaluate the photocatalytic activity of each of the prepared samples. In a typical experiment, titania samples of 0.8 cm^2 were dipped in a cuvette containing MB dye solution at a concentration of $2.7 \times 10^{-5} \text{ M}$. In order to achieve an adsorption-desorption equilibrium of the dye over the sample the cuvette was kept in the dark for 2 hrs. After 2 hrs the adsorption of the methylene blue on the surface of the samples are monitored. After adsorption-desorption equilibrium, the initial absorption of the methylene blue in the cuvette is monitored, followed by irradiation of the solution over different time intervals in a visible light chamber consisting of a 1000 W mercury lamp

(Philips Belgium HPL-N) with a polycarbonate sheet and glass as the UV radiation filter. The polycarbonate and glass filter out all the radiation below 400 nm and the light after filtration having intensity of $\sim 330 \mu\text{W}/\text{cm}^2$ was used for the photocatalytic reaction. The change in concentration of the dye, with respect to the initial concentration, was plotted as a function of time. The reference MB dye solution having the same concentration but without any titania thin film did not show any degradation under identical illumination conditions. After the first photocatalytic reaction was complete the same sample was used for the next cycle of the photocatalytic reaction (2nd Cycle) using the same procedure as described above. The formation of OH radical in presence of CdS sensitized titania nanotubes under visible light irradiation was monitored by coumarin fluorescence probe method using a PL spectrometer (Agilent Carry Eclipse Fluorescence spectrophotometer).²⁷⁻²⁸ In a typical experiment 10 ml of 0.5 mM solution of coumarin in presence of CdS sensitised titania nanotube (0.25 cm²) samples is irradiated in visible light photocatalytic chamber for 2 hrs. The OH radical formed upon irradiation interact with coumarin to form umbelliferone (Figure 5.2). Upon the excitation at 332 nm, coumarin and umbelliferone show the fluorescence peaks centered at 398 and 455 nm, respectively. The increase in the intensity of the fluorescence peak centered at 455 nm after irradiation indicate the formation of OH radical in the photocatalytic reaction.

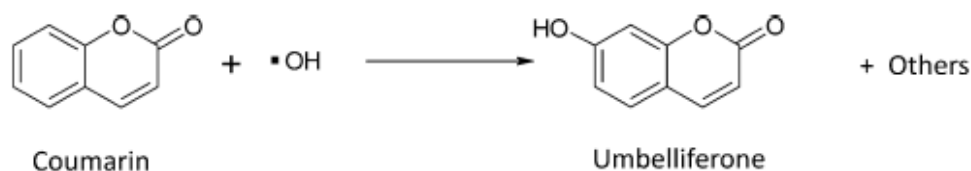


Figure 5.2 Reaction of Coumarin with OH radical to form umbelliferon

[Source: Nakabayashi et.al. *The Journal of Physical Chemistry C* 2013 ,117, 23832]

and 1M of sulphur (in powder form) were dissolved in a 1:1 solution of methanol and water which was used as the electrolyte. A platinum coated FTO glass plate was used as the counter electrode. The experiments were carried out under AM1.5 sun conditions using a solar simulator (Class AAA Solar Simulators, Model: 91195A) operating at an intensity of 100 mW cm^{-2} . The light intensity was calibrated using a monocrystalline Si reference cell.

5.3 Results and Discussion

The SILAR method was adopted for the deposition of CdS particles on the surface of titania nanotube array(TNA) synthesized via a potentiostatic anodisation process. The SILAR technique is a versatile method for the deposition of nanoparticles on to the surface of titania.²⁹ The X-ray diffraction (XRD) pattern of CdS sensitized titania nanotube array are shown in Figure 5.3. After each SILAR cycle the number of CdS particles deposited on the surface of the titania nanotubes increases which can be inferred from the increase in the intensity of the CdS peaks in the XRD pattern. The diffraction peaks observed at $25.32, 38.44, 48.07, 53.90, 62.19, 70.86$ and 76.28 2θ correspond to reflections from the (101), (004), (200), (105), (204), (220), (215) planes of the tetragonal phase of the anatase form of crystalline titania (JCPDS No. 02-1272). In CdS sensitized titania nanotubes the peaks observed at two theta values $24.8, 26.3, 28.1, 44.0, 48.2, 51.4$ and 52.1 correspond to the (100), (002), (101), (110), (103), (112) and (201) planes of hexagonal phase CdS (JCPDS 65-3414).

The scanning electron microscope images of the titania nanotubes and the nanotubes sensitized with CdS (T15) using 15 SILAR cycles are shown in Figure 5.4. The tubular nature of the aligned titania nanotubes are clearly observed in the scanning electron microscope image in Figure 5.4A. The average diameter and wall thickness of the titania nanotubes were found to be 107 and 22 nm respectively. In the CdS sensitized sample the pore wall and mouth are covered with deposited CdS nanoparticles. This is clearly visible in the SEM image in Figure 5.4B. Transmission electron microscope image of the T15 and T30 is shown in the Figure 5.5. It is clearly observed that CdS nanoparticles are deposited on inner and outer surface of titania nanotubes (Figure 5.5A&B). Also figure 5.5B clearly indicates large aggregates of CdS nanoparticle formed at higher SILAR cycle (T30). HRTEM image of the T15 and T30 are shown in Figure 5.5 C & D clearly indicate that large CdS particles are formed at higher SILAR cycle on T30.

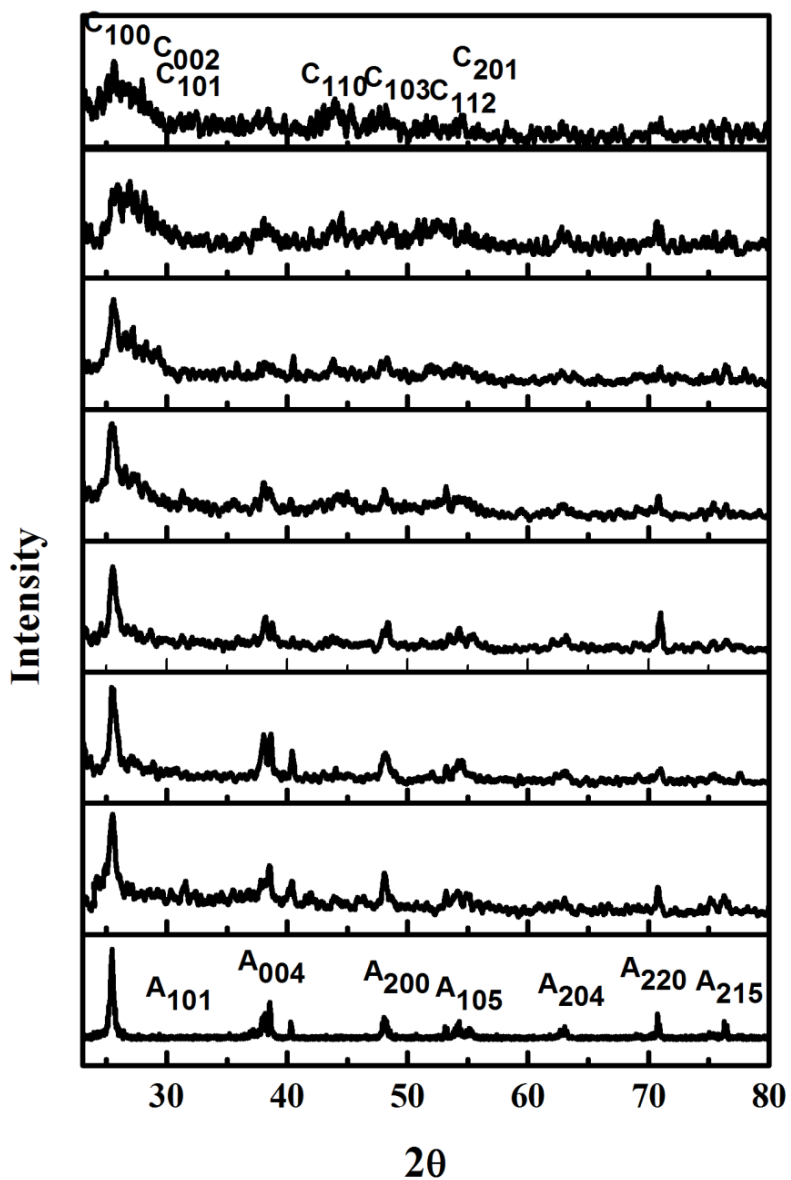


Figure 5.3 X-ray diffraction pattern of (a) TNT (b) T1 (c) T3 (d) T5 (e) T10 (f) T15 (g) T20 and (h) T30 .

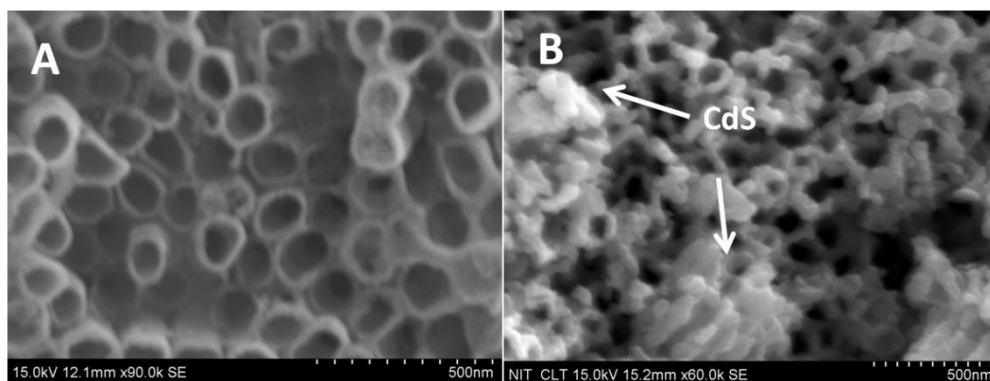


Figure 5.4 SEM images of (A) Unsensitized TNT (B) T15

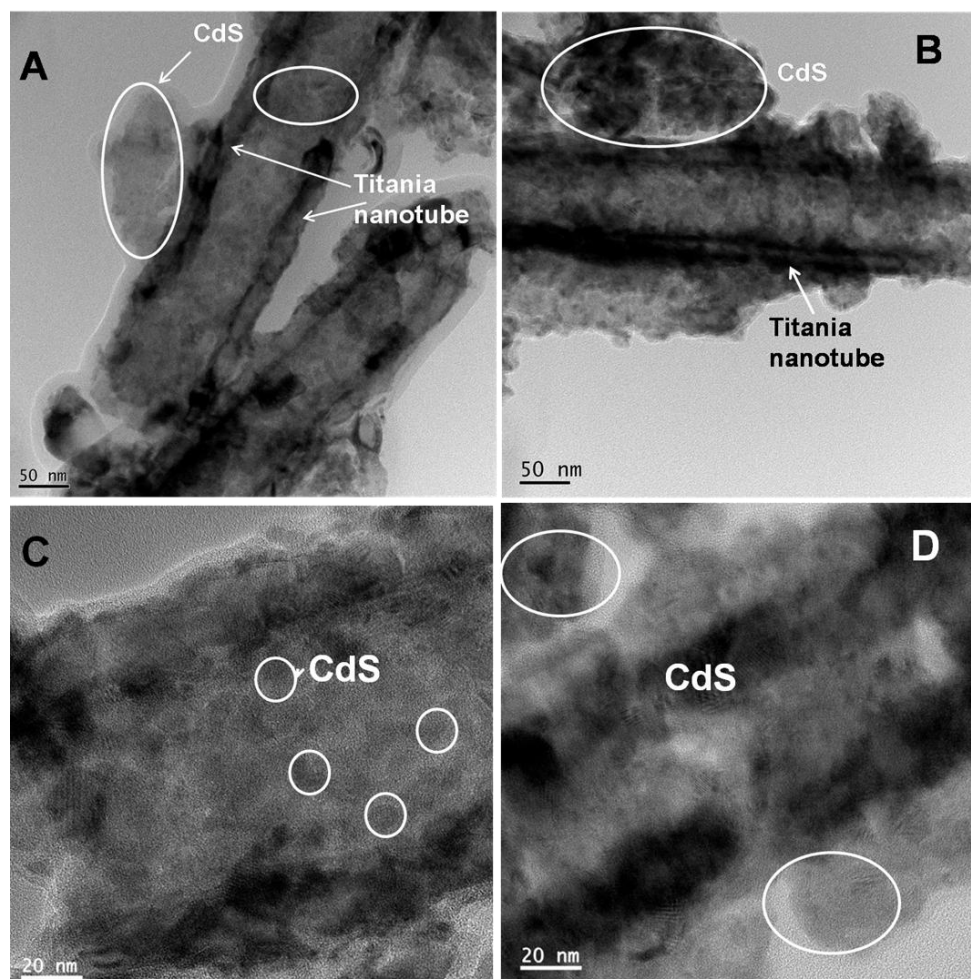


Figure 5.5 TEM and HRTEM images of (A, C) T15 (B, D) T30

The Raman spectra of the unsensitized titania nanotubes and CdS sensitized titania nanotubes were acquired using an excitation wavelength of 532 nm with a laser power of 2 mW. The Raman spectra of the samples are shown in Figure 5.6. The characteristic peaks for anatase phase titania are observed at 144, 197, 399, 513, 519 and 639 cm^{-1} corresponding to the $A1g+2B1g+3Eg$ modes of vibration.³⁰ The first (1LO) and second (2LO) order longitudinal optical (LO) phonon modes of single crystal of bulk CdS are observed at 305 and 600 cm^{-1} respectively.³¹ In this work the CdS nanoparticle sensitized on the surface of titania nanotubes exhibits the 1LO phonon peak at 300 cm^{-1} . This red shift in the 1LO peak of CdS nanoparticles is due to the phonon confinement. The relative intensity of the 1LO and 2LO peaks changes with the increase in the particle size of CdS.³² As the size of the CdS particles increases the 2LO peak increases in intensity with respect to the 1LO peak, this is observed in the Raman spectra. The samples with the greatest number of SILAR cycles exhibit an intense 2LO peak at 597.5 cm^{-1} and also possess the largest particle sizes.

The Kubelka-Munk reflectance spectra of the CdS sensitized titania nanotubes are provided in Figure 5.7. It is interesting to note that the reflectance spectra of the samples is red shifted as the number of SILAR cycles employed increases, a corresponding visible colour change in the samples is clearly observed as can be seen in the inset of Figure 5.7. The reflectance in the visible region leads to a band gap shift from the UV to the visible region of the spectrum in the CdS sensitised titania nanotubes. There are two phenomena evident from the reflectance spectra for the samples which received a higher number of SILAR cycles; (i) there is an increase in the CdS concentration on the surface of the titania nanotubes, (ii) and the redshift observed in the bandgap of the CdS nanoparticles with larger size.

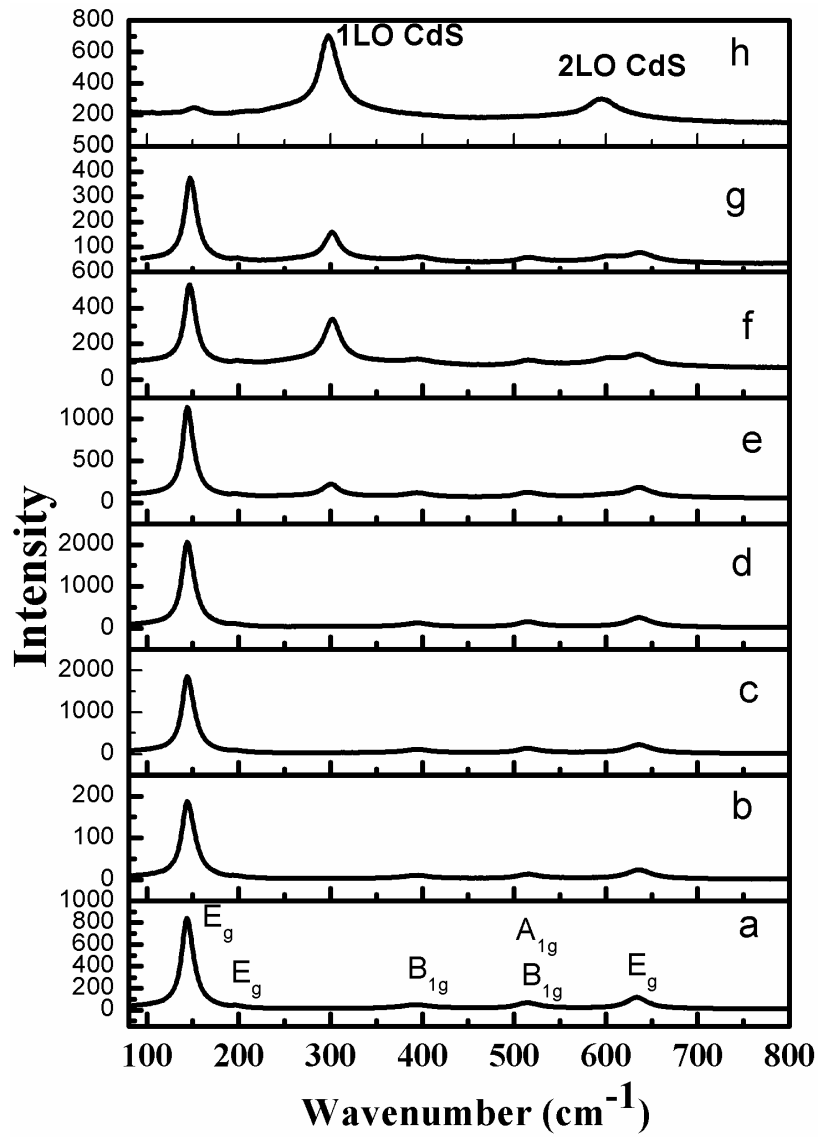


Figure 5.6 Raman spectra of (a) unsensitized TNT (b) T1 (c) T3 (d) T5 (e) T10 (f) T15 (g) T20 and (h) T30.

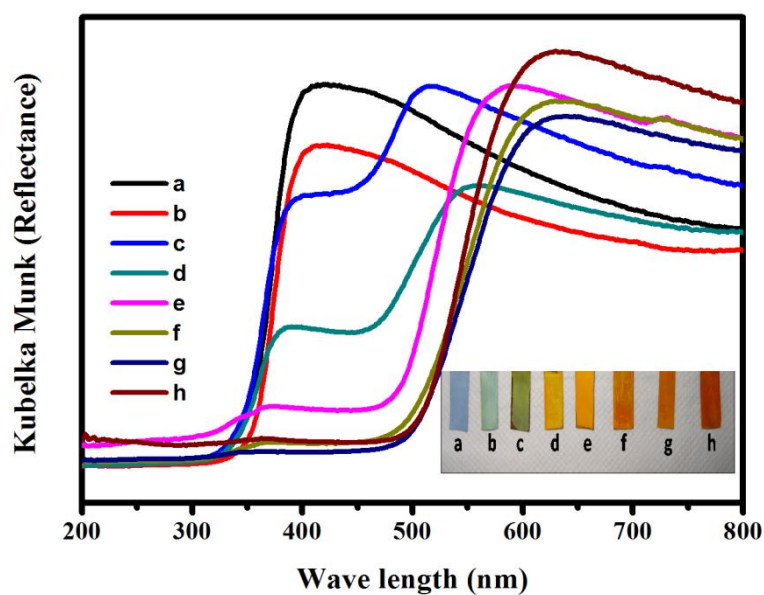


Figure 5.7 Diffuse reflectance spectra of (a) TNT (b) T1 (c) T3 (d) T5 (e) T10 (f) T15 (g) T20 and (h) T30.

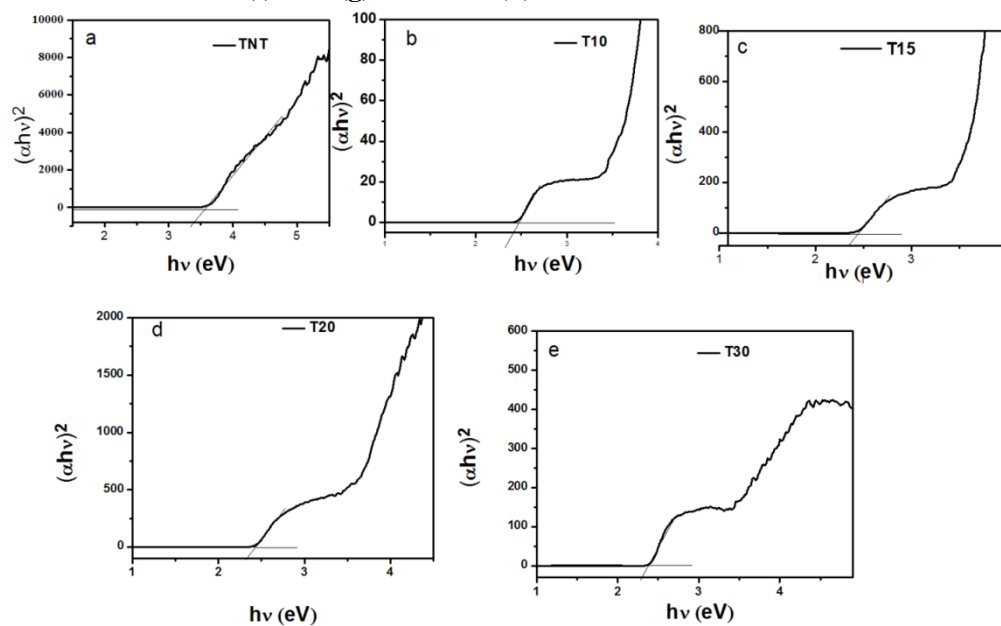


Figure 5.8 Tauc plot of titania nanotubes and CdS sensitized titania nanotubes (a) TNT (b) T10 (c) T15 (d) T20 and (e) T30

Two band edges are observed for CdS sensitized titania nanotubes which correspond to the band gap of titania as well as the band gap of the CdS nanoparticles. The band gap of the titania nanotubes and CdS sensitized titania nanotubes has been calculated by Tauc plot method (Figure 5.8). They are found to be 3.49, 2.47, 2.45, 2.43 and 2.40 eV for TNT, T10, T15, T20 and T30 samples respectively. As the size of the CdS particle decreases the bandgap increases, this is due to the quantum size effect and similar band gap narrowing has been reported for different semiconductor materials.³³⁻³⁵

The presence of intense peaks due to Cd3d, S2p, Ti2p and O1s are clearly observed in the XPS survey scan of the T15CdS sample shown in Figure 5.9. The concentration (in atomic percent) of Cd was estimated using XPS narrow scans acquired on CdS sensitized titania nanotubes samples and was found to be 0.35, 2.31, 2.66, 4.72, 12.18, 17.26 and 25.63 atomic % for the T1, T3, T5, T10, T15, T20 and T30 samples respectively. The Cd to sulphur ratio is found to vary between 1.2 and 1.6 up to 10 SILAR cycles. This indicates that up to T10 the CdS particles on the titania nanotubes are Cd rich species. In solution based processes it has been reported that it is a normal phenomenon to form such Cd rich species.^{15,36} It is interesting to note that at higher SILAR cycles the Cd/S ratio decreases to 1.0. As previously reported the Cd/S ratio is highly dependent on the cadmium precursor used for the CdS SILAR deposition.³⁷ The isoelectric point of a titania surface is reported to be 6 but it depends significantly on the preparation conditions employed.³⁸ In the present work, at lower SILAR cycles the pristine titania possesses a greater concentration of surface hydroxyl groups which enhances the adsorption of Cd²⁺ ions more than S²⁻ ions. However as the number of SILAR cycles increases the already formed CdS quantum dot on the surface of the titania nanotubes do not favour the adsorption of more Cd²⁺ since the isoelectric point

of CdS is reported to be between pH 1 and pH1.5.³⁹ Recently, it has been reported that the deposition rate and distribution of CdS on titania can be improved by the addition of sodium acetate in the SILAR cycle.⁴⁰

Figure 5.10 contains XPS narrow scan spectra for Cd, S and O. The XPS narrow scan spectra of Cd3d_{5/2} and 3d_{3/2} are plotted and presented in Figure 5.10A. The doublet observed for the Cd peak is due to spin-orbit splitting resulting in 3d_{5/2} and 3d_{3/2} peaks being observed with a peak separation of 6.7 eV.⁴¹⁻⁴² The Cd 3d_{5/2} and 3d_{3/2} peak are observed at high Cd binding energies in the case of lower SILAR cycles, which indicates that Cd possesses a higher oxidation state when a lower number of SILAR cycles are employed.⁴³ The S2p peak is observed in two different regions of the S2p spectrum (see Figure 5.10B), the peak observed at 161.6 eV corresponds to S²⁻ species while the peak observed at 169.0 eV is attributed to SO₄²⁻ species.⁴⁴ This indicates the presence of sulphate type species, i.e. the formation of CdSO₄. At lower SILAR cycles i.e. up to T5, the S2p peak corresponding to SO₄²⁻ species is more pronounced than that for sulphide (S²⁻) species⁴⁵, this clearly indicates that the smaller CdS particles, formed using a lower number of SILAR cycles, are more prone to form oxidised species than the larger particles formed at higher SILAR cycle numbers. The O1s peaks for the titania nanotubes and CdS sensitized titania nanotubes are provided in Figure 5.10C. It is noted that the oxygen peak is composed of 2 sub-components peaks in the case of CdS sensitized titania nanotubes. The peak corresponding to the O1s peak of Ti-O is observed at 530 eV.⁴⁶ In addition to this peak, in CdS sensitized samples an O1s peak corresponding to the oxygen in the CdSO₄ moiety is observed at 531.8 eV for all CdS sensitized samples, even though T15, T20 and T30 do not show a peak corresponding to a sulphate (SO₄²⁻) species in their S2p spectra (see Figure 5.10B).

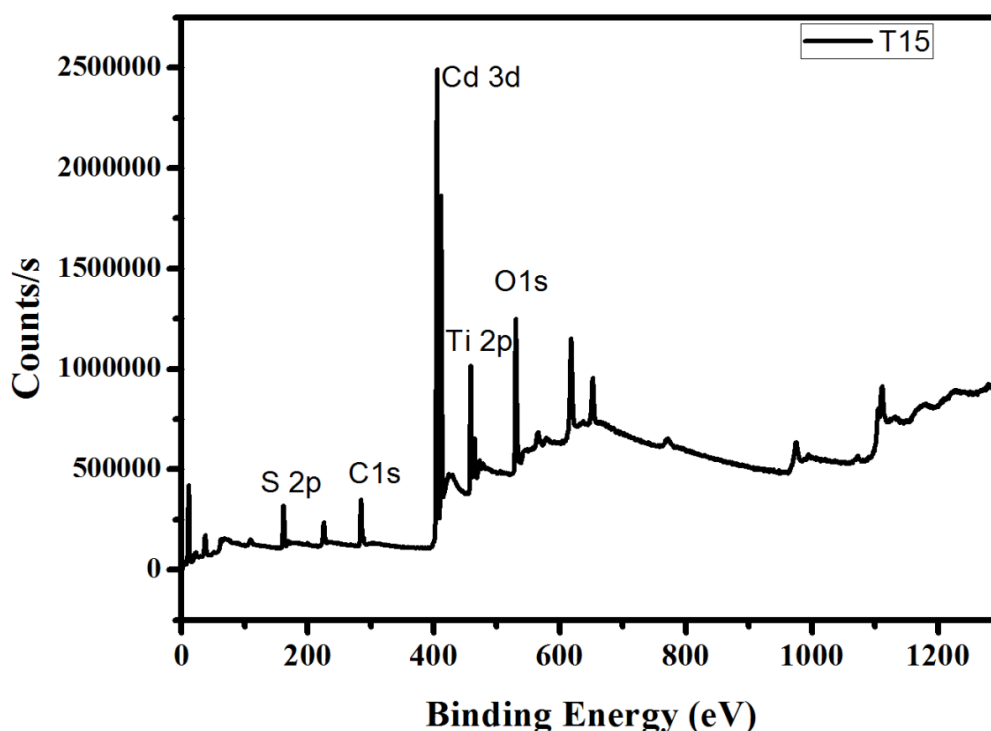


Figure 5.9 XPS survey scan of T15

The O1s peaks for all CdS sensitized titania nanotubes contain two sub-component peaks attributed to TiO₂ and CdSO₄, this clearly indicates the formation of an oxidation layer at the surface of the CdS nanoparticles which confirms the formation of CdSO₄ in all of the CdS sensitized samples. XPS data for the S2p peaks shows that at higher SILAR cycle there is more sulphide present than sulphate. This clearly indicates that the CdS particle sensitized on titania nanotubes surfaces is oxidized to a different extent in these samples. The larger CdS particle formed at higher SILAR cycle are more resistant to oxidation than the smaller CdS particles formed at lower SILAR cycles. Lin *et al* observed that the number of surface atoms in a CdS particle will dominate the number of internal atom when the nanoparticles are near to or less than 5 nm in diameter.⁴⁷ They also reported that the electroluminescence spectrum was

highly dependent on the oxidation state of the 5 nm sized CdS particle. Similar sulfide to sulphate oxidation was reported for CdS deposited on titania nanotubes when using a hydrothermal method.⁴⁸ Therefore, depending on the number of cycles used for SILAR deposition of CdS on TNA, the nature of the chemical species present, especially on the surface, also vary.

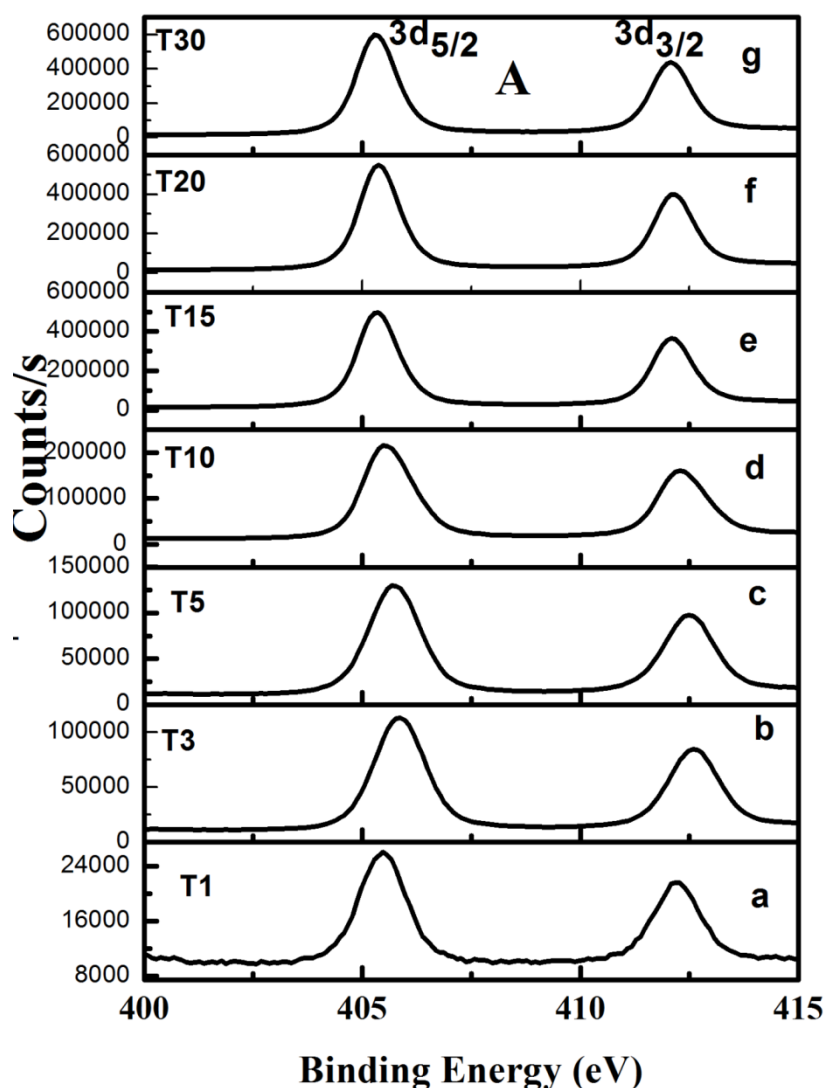


Figure 5.10A XPS spectra of Cd 3d peak of CdS sensitized titania nanotubes (a) T1 (b) T3 (c) T5 (d) T10 (e) T15 (f) T20 and (g) T30

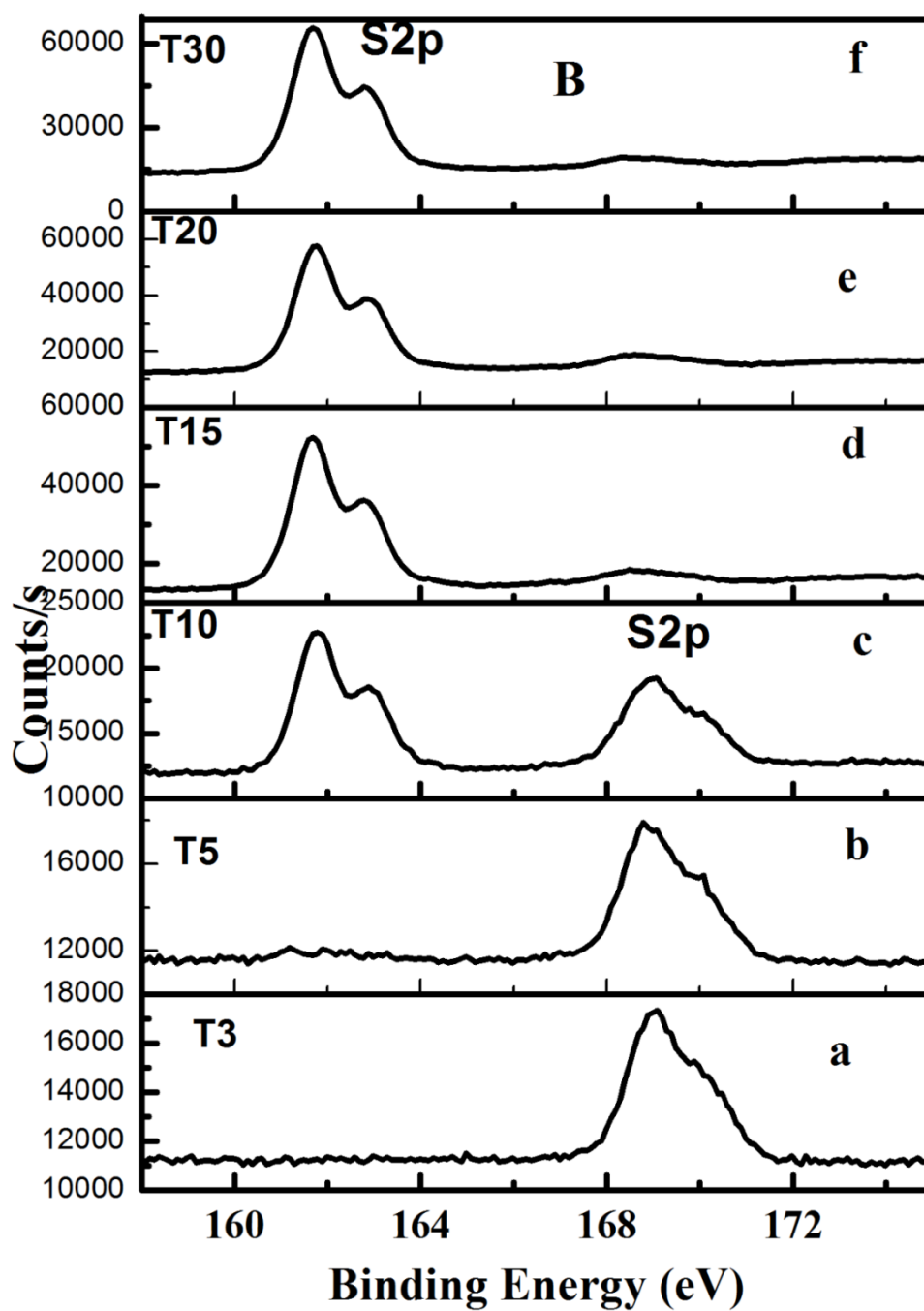


Figure 5.10B. XPS spectra of S 2p peak of CdS sensitized titania nanotubes (a) T3 (b) T5 (c) T10 (d) T15(e) T20 and (f) T30

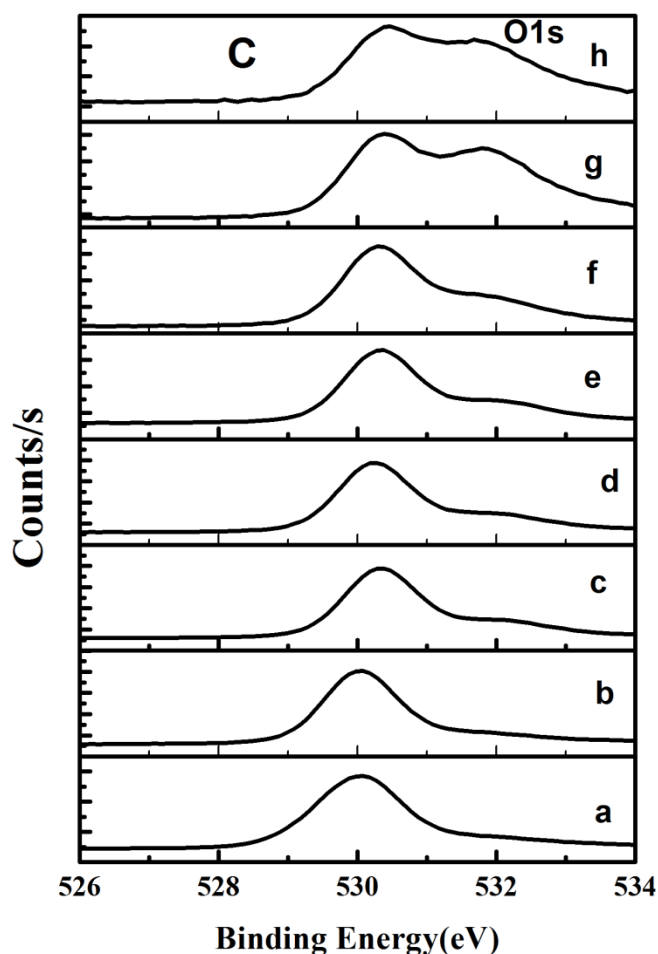


Figure 5.10C. XPS spectra of O 1s peak of CdS sensitized titania nanotubes (a) TNT (b) T1 (c) T3 (d) T5 (e) T10 (f) T15 (g) T20 and (h) T30.

The photo activity of the samples was monitored via the degradation of methylene blue under visible light irradiation as shown in Figure 5.11A. This degradation follows first order kinetics and the rate of the reaction is plotted as a bar chart in Figure 5.12. At higher SILAR cycles the photoactivity is found to increase, this is attributed to the increase in the concentration of CdS on the surface of the titania nanotubes. It is also interesting to note that after 15 SILAR cycle (T15) the photoactivity is seen to decrease (see Figure 5.11A). Lui *et al*

observed that the Cd/Ti ratio in the CdS-TiO₂ composite play an important role in the photocatalytic degradation of gaseous benzene. They also observed that when the ratio of Cd/Ti increased from 0.057 to 0.225 the rate of photocatalytic degradation of benzene decreased from 9 to 1.7 $\mu\text{mol min}^{-149}$. Li *et al* reported that the photocatalytic efficiency of methyl orange degradation is highly dependent on the sequential chemical bath deposition (SCBD) cycle used to create CdS sensitized titania nanowires.¹⁴ The 4-SCBD cycle has been reported to show the highest photocatalytic activity compared to other samples. Higher numbers of SCBD cycles were reported to lower the rate of photocatalytic degradation of methyl orange. Antoniadou *et al.* observed that the photocatalytic and photoelectrocatalytic production of hydrogen by a CdS-ZnS system was highly dependent on the CdS-ZnS composition. A composition of 75 wt.% CdS and 25 wt.% ZnS coupled to titania is reported to have exhibited the maximum rate of hydrogen production.⁵⁰ ZnS/CdSe/CdS quantum dots coupled to titania were shown to be even more effective for hydrogen production than single component CdS sensitized titania is for the photoelectrocatalytic production of hydrogen.⁵¹ CdS deposited on titania nanotubes using a chemical bath deposition method enhanced the photocatalytic production of hydrogen, $3.35 \pm 0.03 \text{ ml cm}^{-2}$ was produced after 3h irradiation.⁵² Earlier reports by many research groups stressed the necessity of micro-heterostructures at the interface for the photooxidation reaction in CdS/TiO₂ coupled semiconductor system.⁵³⁻⁵⁴ In the present work T15 is shown to exhibit maximum photocatalytic activity for the degradation of methylene blue. At higher SILAR cycles (15cycl <) due to the aggregation of CdS particle the interface area between CdS and titania nanotubes may be lowered this in turn results in the decreased photocatalytic activity observed (see Figure 5.11A and B). It has also been reported that the efficient harnessing of the photo-generated charge carriers is highly dependent

on the morphological features (size, shape, grain boundary, and interconnection of particles) of the CdS particles deposited on titania.^{48,55}

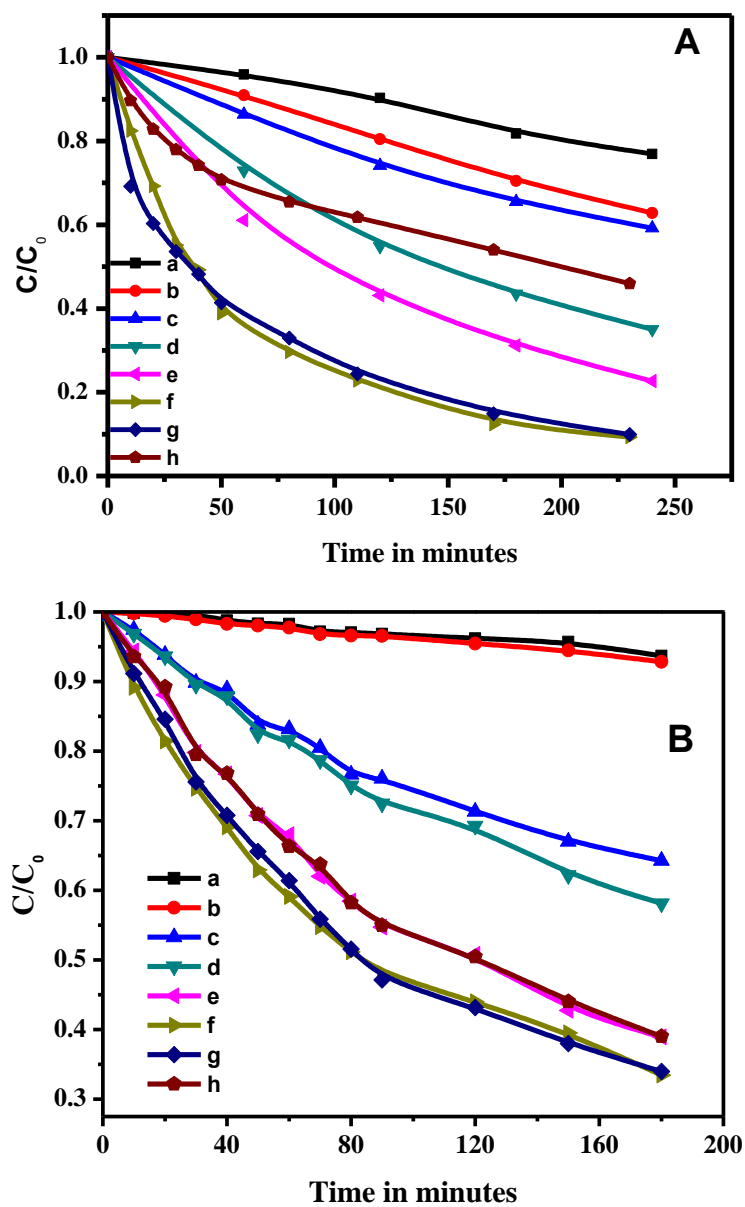


Figure 5.11 Photocatalytic degradation of methylene blue under visible light (a) TiO₂ nanotubes calcined at 400 °C, CdS sensitized TiO₂ nanotubes (b) T1 (c) T3 (d) T5 (e) T10 (f) T15 (g) T20 and (h) T30 (A) 1st cycle (B) 2nd Cycle

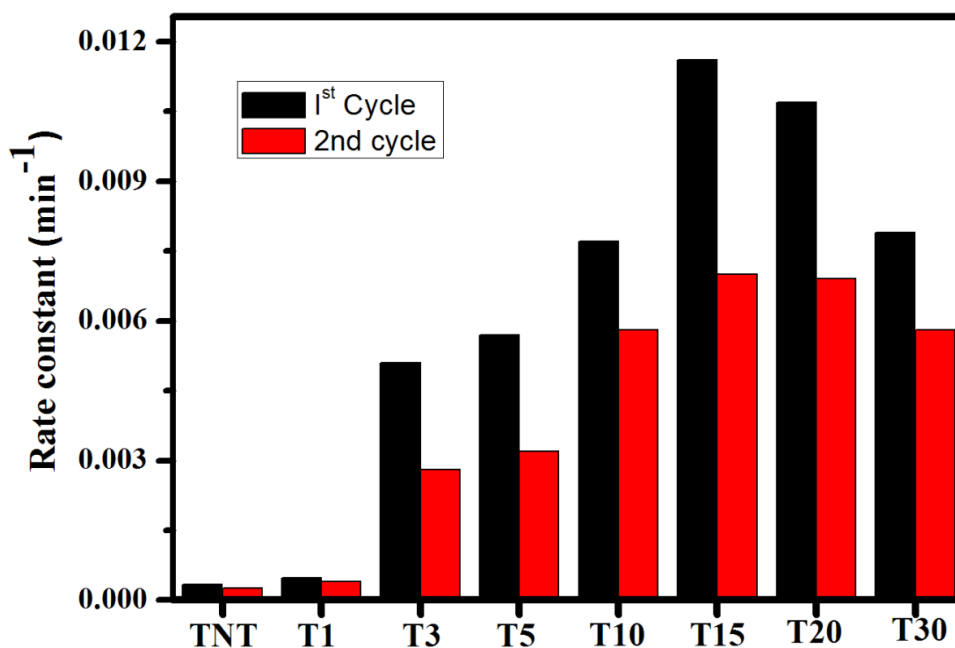


Figure 5.12 Rate constant of methylene blue degradation of CdS sensitized titania nanotubes under irradiation with visible light (a) 1st cycle (b) 2nd Cycle

After a second cycle of the photocatalytic reaction was performed, it was found that the activity was drastically reduced and that the photocatalytic activity pattern followed the same behavior as that observed in the first cycle. CdS nanoparticles are reported to be photocorroded when irradiated with visible light. The excited electron in the CdS nanoparticle after visible light irradiation is transferred to titania and the hole remains in the CdS. The photogenerated holes in the valence band (VB) of CdS react with H₂O or OH⁻ to produce •OH radicals which can directly degrade the methylene blue molecule. The results of coumarin fluorescence probe study confirm the formation of •OH radicals in photocatalytic reaction as revealed by the umbelliferone formation in CdS sensitized titania nanotube samples after irradiation (Figure 5.13). The hole can also interact with the CdS particle and oxidize S²⁻ to S⁶⁺. The sulphide anion in the CdS will readily be susceptible to oxidation by the photogenerated holes.⁵⁶⁻⁵⁷ The spectrum for

S_{2p_{3/2}} and S_{2p_{1/2}} peaks contains more sulphate species than S²⁻ species (Figure 5.14). This indicates that the CdS nanoparticles following the 1st cycle are more oxidized than the fresh sample. The photocorrosion of CdS is reported to effect the photocatalytic efficiency of CdS sensitized titania.⁵⁸⁻⁵⁹ This higher concentration of sulphate species in the samples after the 1st cycle is due to the oxidation of the CdS surface during the photocatalytic reaction. The X-ray diffraction pattern of the sample after 1st cycle of photocatalytic reaction is also recorded and provided in Figure 5.15. The relative intensity of CdS peak intensity is reduced with respect to the titania peak compared to the freshly prepared sample (Figure 5.3e and figure 5.15e). There is no evidence of CdSO₄ moiety in XRD pattern, therefore it is possible that the CdSO₄ layer formed on the surface of CdS nanoparticles may be undetected by X-ray diffraction analysis.

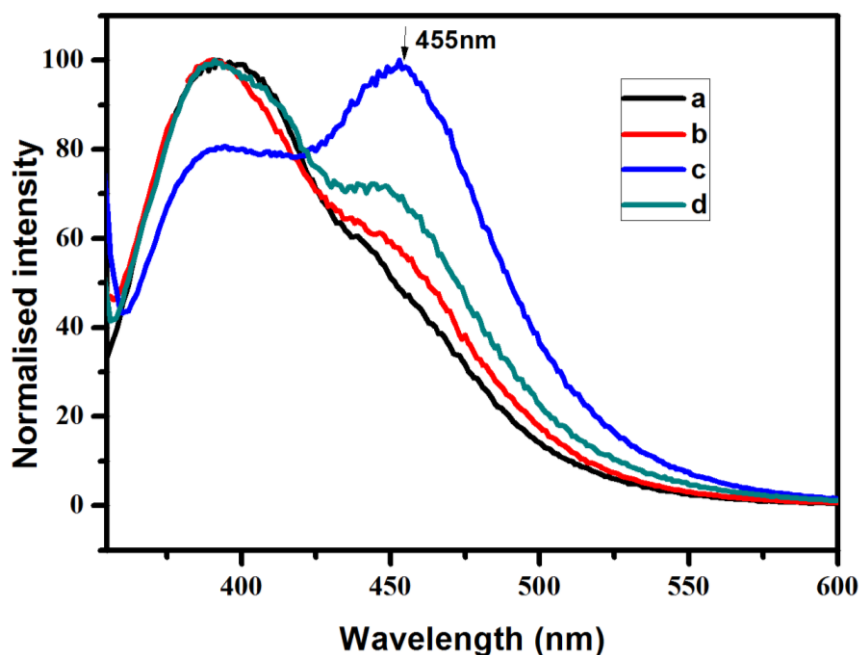


Figure 5.13 Fluorescence spectra for (a) 0.5 mM coumarin solution, after visible light irradiation in presence of (b) T5 (c) T15 (d) T30

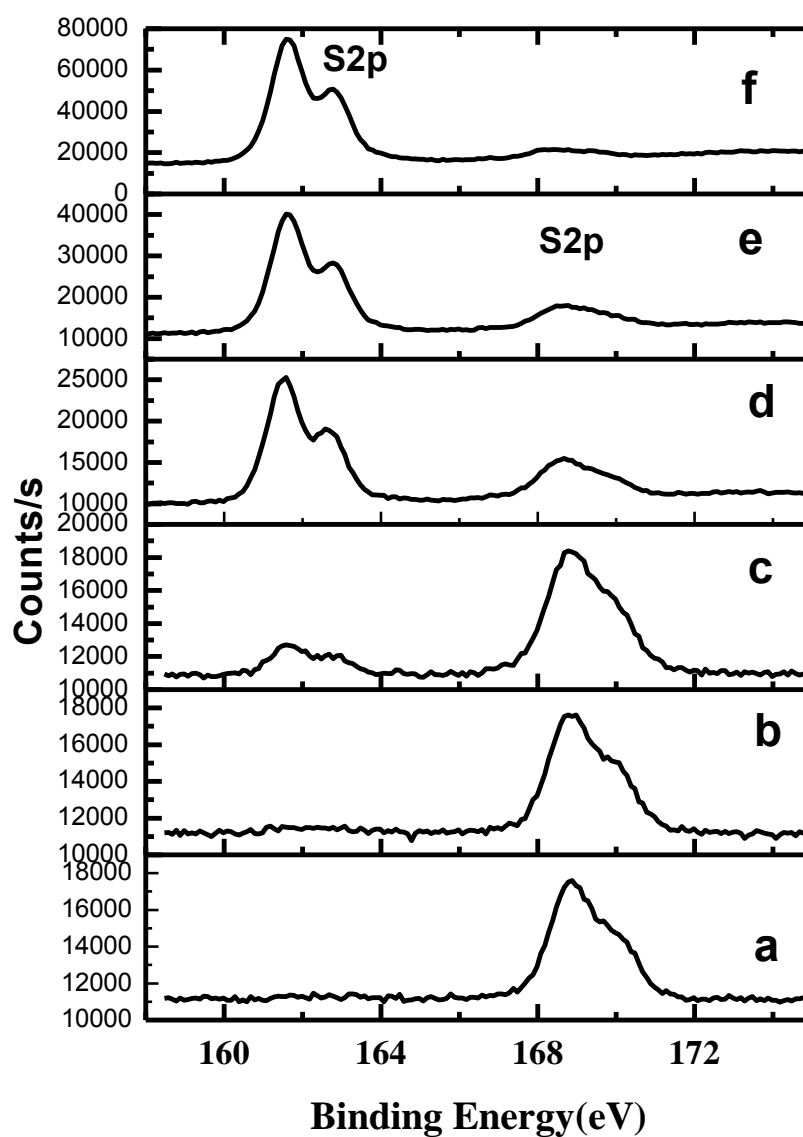


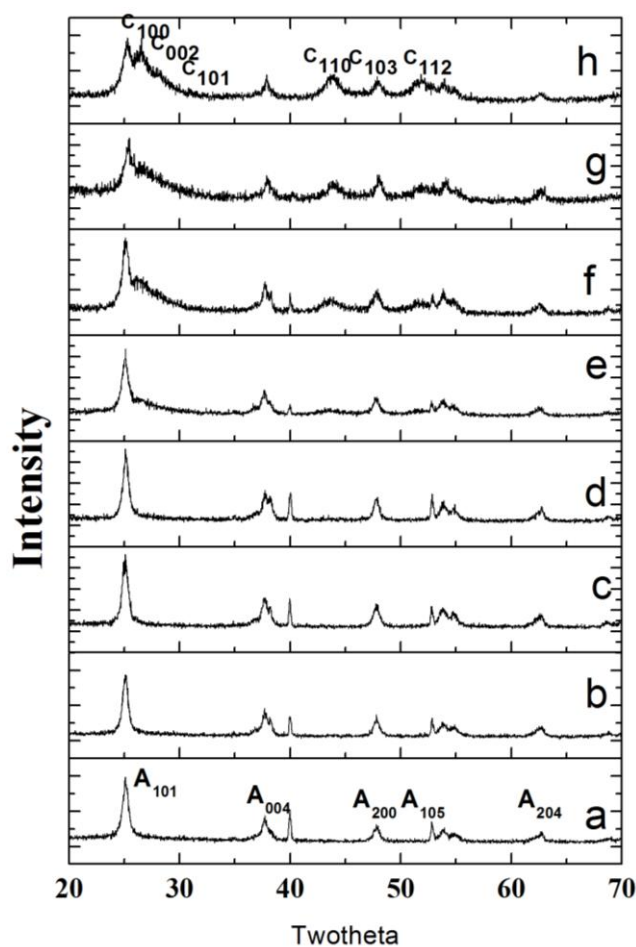
Figure 5.14 XPS spectra of S 2p peak of CdS sensitized titania nanotubes (a) T3 (b) T5 (c) T10 (d) T15 (e) T20 and (f) T30 after first cycle.

The prepared CdS sensitized titania nanotube photocatalyst were used for the fabrication of solar cell. J-V curves for the CdS sensitized titania nanotubes are provided in Figure 5.16 while solar cell efficiency data for the CdS sensitized titania nanotubes are provided in Table 5.1. It is interesting to

note that the solar cell efficiency increased up to 15 SILAR cycles (T15) and then decreases again. The greater loading of CdS on the surface of the titania nanotubes (with SILAR cycles) increases the density of carriers on the sample surface and hence increases the current density.⁶⁰ Increasing the number of SILAR cycles also increases the particle size of CdS on the surface of the titania nanotubes which results in the red shift in the absorption edge of the photoelectrode.⁶¹ It also results in the aggregation of CdS particles which reduces the light absorbance capacity.⁶² Fu *et al* correlate the CdS layer thickness, deposited by an electrochemical method on the titania nanotubes, affecting the Voc and Jsc of the solar cell. It is observed that a higher solar cell efficiency is obtained at an optimum thickness of 25 nm.⁶³ The Voc in the quantum dot sensitized solar cell is the potential difference between the CB of titania and the redox potential of the polysulphide electrolyte. The redox potential of the polysulphide electrolyte is highly dependent on concentration, pH and temperature.⁶⁴ The Ecb of the CdS increases when the number of SILAR cycles is increased, this will affect the injection of electrons from CdS into titania. In the present work the highest solar cell efficiency of 0.1123% was exhibited by the T15 sample. It has been reported that the Voc and photoefficiency are highly dependent on the number of SILAR cycles employed in the formation of the CdS/CdSe system, in these experiments a passive layer of ZnS was deposited prior to the CdS layer deposition.⁶⁵ In the current work CdS nanoparticles on the surface of titania nanotubes have been developed. When the number of SILAR cycle employed increases, the energy difference between the conduction band of TiO₂ and CdS increases, which enhances the driving force for electron injection. Hence, in the present scenario the optimum number of SILAR cycles is found to be fifteen (T15 sample) for both photovoltaic and photocatalytic reactions.

Table 5.1 Parameters obtained from J-V curve of the CdS sensitized titania nanotubes

Sample	V _{oc} (V)	J _{sc} (mA/cm ²)	Fill Factor	Efficiency
T1	0.0575	0.3018	21.22	0.0037
T3	0.4529	0.6658	17.55	0.0529
T5	0.3698	1.2810	16.44	0.0779
T10	0.4106	0.5064	24.51	0.0510
T15	0.4272	1.4910	17.64	0.1123
T20	0.3958	0.6155	22.08	0.0538
T30	0.5106	0.3791	17.11	0.0331

**Figure 5.15** X-ray diffraction pattern of after first cycle (reused for photocatalysis) (a) TNT (b) T1 (c) T3 (d) T5 (e) T10 (f) T15 (g) T20 and (h) T30 .

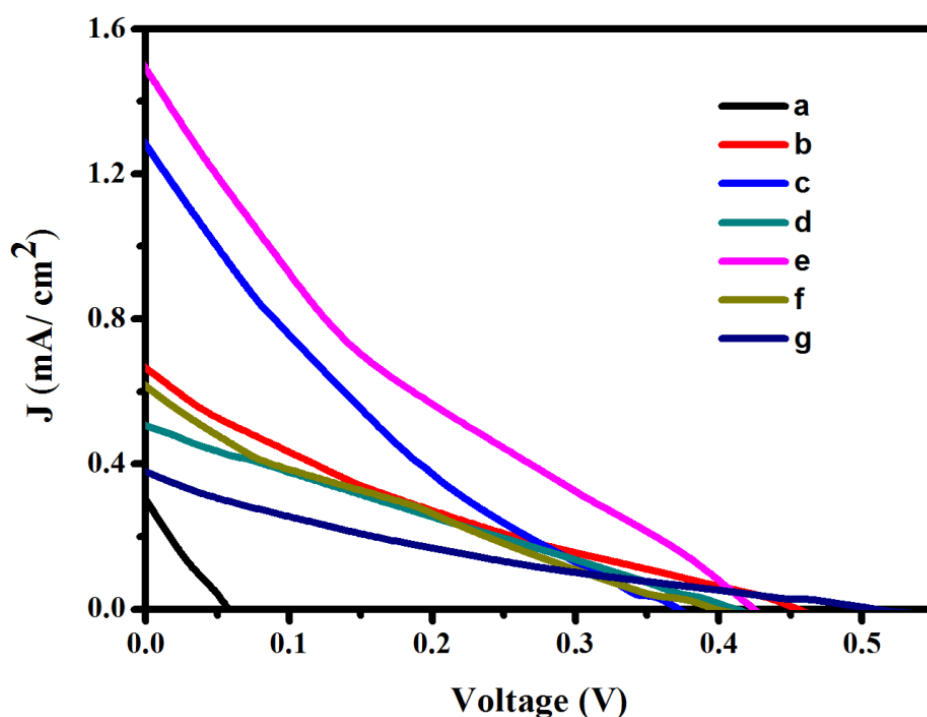


Figure 5.16 J-V curve of CdS sensitized solar cell under 1sun (AM1.5) illumination (a)T1 (b)T3 (c)T5 (d)T10 (e) T15 (f) T20 (g) T30

The electron injection efficiency and the onset potential are dependent on the conduction band level in the semiconductor systems which can affect the photocatalytic activity and solar cell efficiency of CdS sensitized titania nanotubes. Valence band XPS (VBXPS) was used to determine the valence band maximum (VBM) of the titania and CdS sensitized titania nanotubes. The VBM of the material is determined using an extrapolation method on the VBXPS spectra for each of the samples, the VBXPS spectra are presented in Figure 5.17. The VBM is found to be 2.74, 1.70, 1.611, 1.58 and 1.50 eV below the Fermi level for TNT, T10, T15, T20 and T30 respectively. From the valence band maximum and the band gap of the titania and CdS sensitized titania the conduction band minimum (CBM) of the samples can be measured, a schematic band diagram of the samples are provided in Figure 5.18. The E_{cb}

of CdS is shifted upwards when an increasing number of SILAR cycles are employed. The band position affects the electron injection efficiency of the CdS into the titania nanotubes. Hence a combined effect of particle size, band potential and aggregation tuned by the number of SILAR cycle employed plays a major role in the photocatalytic and solar cell efficiency of the CdS sensitized titania nanotubes.

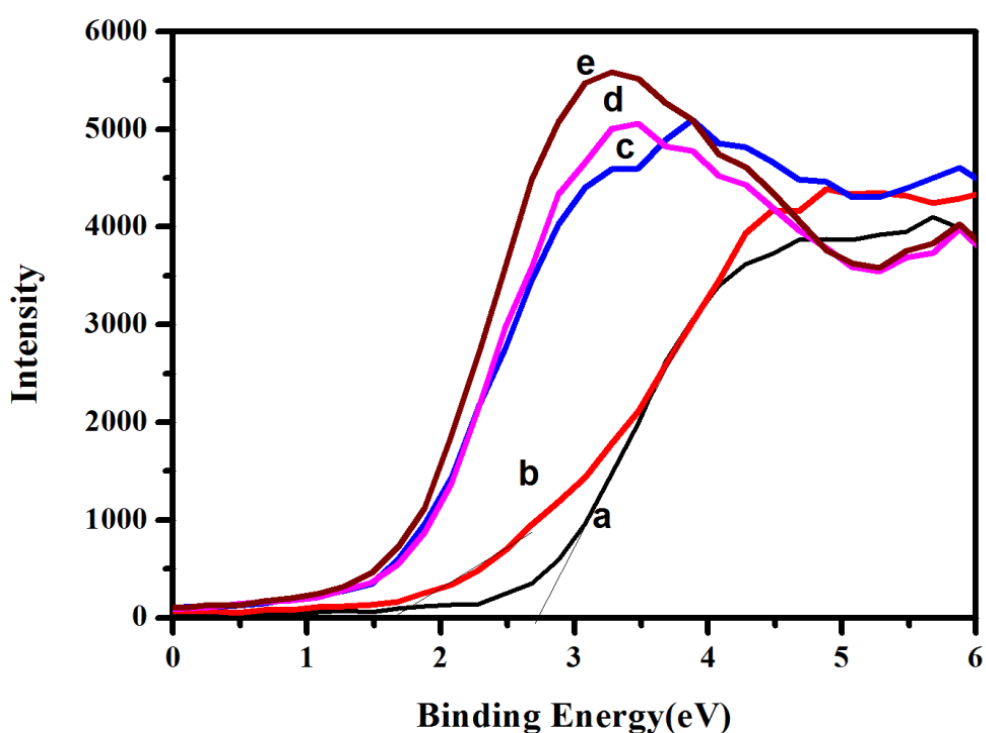


Figure 5.17 XPS valence band spectra of the samples (a) TNT (b) T10 (c) T15 (d) T20 and (e) T30

Vs. Fermi level (eV)

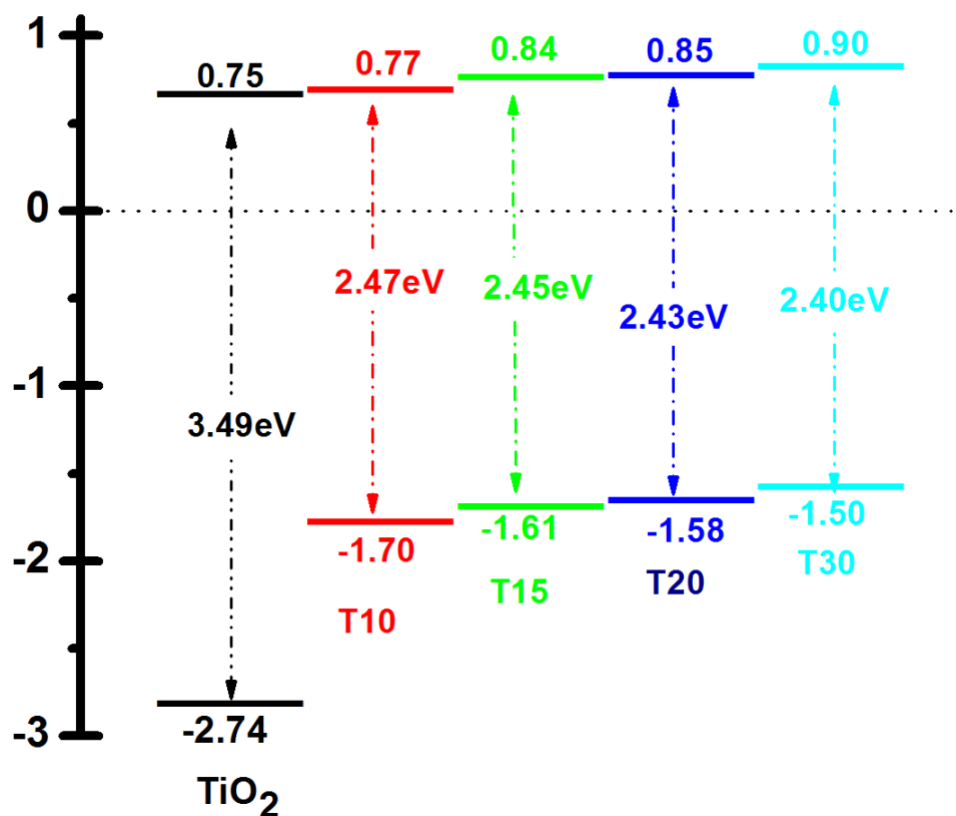


Figure 5.18 Band diagram versus Fermi level, valence band positions with reference to their Fermi levels are labelled

5.4 Conclusions

In the CdS sensitized TNA, the photocatalytic and solar cell efficiency is dependent upon the number of SILAR cycle used for the CdS sensitization of the surface of titania nanotubes. CdS sensitized on titania nanotubes using fifteen SILAR cycles (T15) exhibits the maximum photocatalytic activity under visible light irradiation with a rate constant of 0.0116 min^{-1} . Fifteen SILAR cycles is also found to give the maximum solar cell efficiency of 0.1123%. The CdS nanoparticles on the surface of titania nanotubes are prone

to oxidation and the formation of a CdSO₄ layer is confirmed by XPS analysis. The band potential of the CdS was determined using VBXPS analysis which can affect the electron injection efficiency. Hence the band potential, particle size and aggregation behavior all depend on the number of SILAR cycles employed which effectively determines the photocatalytic and solar cell efficiencies of the CdS sensitized titania nanotubes.

References

- [1] Kwon, Y.; Kim, H.; Lee, S.; Chin, I.-J.; Seong, T.-Y.; Lee, W. I.; Lee, C. *Sensors and Actuators B: Chemical* **2012**, *173*, 441.
- [2] Podporska-Carroll, J.; Panaitescu, E.; Quilty, B.; Wang, L.; Menon, L.; Pillai, S. C. *Applied Catalysis B: Environmental* **2015**, *176*, 70.
- [3] Garvey, M.; Panaitescu, E.; Menon, L.; Byrne, C.; Dervin, S.; Hinder, S. J.; Pillai, S. C. *Journal of Catalysis* **2016**, *344*, 631.
- [4] Xiong, H.; Slater, M. D.; Balasubramanian, M.; Johnson, C. S.; Rajh, T. *The Journal of Physical Chemistry Letters* **2011**, *2*, 2560.
- [5] Kamat, P. V. *The Journal of Physical Chemistry Letters* **2013**, *4*, 908.
- [6] Kandi, D.; Martha, S.; Parida, K. M. *International Journal of Hydrogen Energy* **2017**, *42*, 9467.
- [7] Semonin, O. E.; Luther, J. M.; Choi, S.; Chen, H.-Y.; Gao, J.; Nozik, A. J.; Beard, M. C. *Science* **2011**, *334*, 1530.
- [8] Lee, Y.-L.; Chi, C.-F.; Liao, S.-Y. *Chemistry of Materials* **2010**, *22*, 922.
- [9] Fujishima, M.; Nakabayashi, Y.; Takayama, K.; Kobayashi, H.; Tada, H. *The Journal of Physical Chemistry C* **2016**, *120*, 17365.
- [10] Lv, P.; Fu, W.; Yang, H.; Sun, H.; Chen, Y.; Ma, J.; Zhou, X.; Tian, L.; Zhang, W.; Li, M.; Yao, H.; Wu, D. *CrystEngComm* **2013**, *15*, 7548.
- [11] Hu, W.; Liu, T.; Guo, Y.; Luo, S.; Shen, H.; He, H.; Wang, N.; Lin, H. *Journal of The Electrochemical Society* **2015**, *162*, H747.
- [12] Luo, J.; Ma, L.; He, T.; Ng, C. F.; Wang, S.; Sun, H.; Fan, H. J. *The Journal of Physical Chemistry C* **2012**, *116*, 11956.

- [13] Smith, Y. R.; Gakhar, R.; Merwin, A.; Mohanty, S. K.; Chidambaram, D.; Misra, M. *Electrochimica Acta* **2014**, *135*, 503.
- [14] Li, Y.; Zhang, L.; Wu, W.; Dai, P.; Yu, X.; Wu, M.; Li, G. *Nanoscale Research Letters* **2014**, *9*, 270.
- [15] Qorbani, M.; Naseri, N.; Moradlou, O.; Azimirad, R.; Moshfegh, A. *Z. Applied Catalysis B: Environmental* **2015**, *162*, 210.
- [16] Balis, N.; Dracopoulos, V.; Bourikas, K.; Lianos, P. *Electrochimica Acta* **2013**, *91*, 246.
- [17] Hsu, S.-H.; Hung, S.-F.; Chien, S.-H. *Journal of Power Sources* **2013**, *233*, 236.
- [18] Kameyama, T.; Okazaki, K.-i.; Takagi, K.; Torimoto, T. *Electrochemistry* **2011**, *79*, 776.
- [19] Kozlova, E. A.; Kozhevnikova, N. S.; Cherepanova, S. V.; Lyubina, T. P.; Gerasimov, E. Y.; Kaichev, V. V.; Vorontsov, A. V.; Tsybulya, S. V.; Rempel, A. A.; Parmon, V. N. *Journal of Photochemistry and Photobiology A: Chemistry* **2012**, *250*, 103.
- [20] Liu, Y.; Zhou, H.; Zhou, B.; Li, J.; Chen, H.; Wang, J.; Bai, J.; Shangguan, W.; Cai, W. *International Journal of Hydrogen Energy* **2011**, *36*, 167.
- [21] Strataki, N.; Antoniadou, M.; Dracopoulos, V.; Lianos, P. *Catalysis Today* **2010**, *151*, 53.
- [22] Tian, Y.; Fu, J.; Chang, B.; Xi, F.; Dong, X. *Materials Letters* **2012**, *81*, 95.

- [23] Sun, W.-T.; Yu, Y.; Pan, H.-Y.; Gao, X.-F.; Chen, Q.; Peng, L.-M. *Journal of the American Chemical Society* **2008**, *130*, 1124.
- [24] Rahna, N. B.; Kalarivalappil, V.; Nageri, M.; Pillai, S. C.; Hinder, S. J.; Kumar, V.; Vijayan, B. K. *Materials Science in Semiconductor Processing* **2016**, *42*, 303.
- [25] Chang, P.; Cheng, H.; Li, W.; Zhuo, L.; He, L.; Yu, Y.; Zhao, F. *Physical Chemistry Chemical Physics* **2014**, *16*, 16606.
- [26] Zhang, M.; Xu, Y.; Gong, Z.; Tao, J.; Sun, Z.; Lv, J.; Chen, X.; Jiang, X.; He, G.; Wang, P.; Meng, F. *Journal of Alloys and Compounds* **2015**, *649*, 190.
- [27] Zhang, J.; Nosaka, Y. *The Journal of Physical Chemistry C* **2013**, *117*, 1383.
- [28] Ohguri, N.; Nosaka, A. Y.; Nosaka, Y. *Electrochemical and Solid-State Letters* **2009**, *12*, B94.
- [29] Shrestha, N. K.; Yoon, S. J.; Lee, D. Y.; Lee, M.; Lim, I.; Sung, M.; Ahn, H.; Han, S.-H. *physica status solidi (RRL) – Rapid Research Letters* **2011**, *5*, 141.
- [30] Choi, H. C.; Jung, Y. M.; Kim, S. B. *Vibrational Spectroscopy* **2005**, *37*, 33.
- [31] Tell, B.; Damen, T. C.; Porto, S. P. S. *Physical Review* **1966**, *144*, 771.
- [32] Zeiri, L.; Patla, I.; Acharya, S.; Golan, Y.; Efrima, S. *The Journal of Physical Chemistry C* **2007**, *111*, 11843.

- [33] Nedeljkovic, J. M.; Nenadovic, M. T.; Micic, O. I.; Nozik, A. J. *The Journal of Physical Chemistry* **1986**, *90*, 12.
- [34] Haase, M.; Weller, H.; Henglein, A. *The Journal of Physical Chemistry* **1988**, *92*, 4706.
- [35] Kavan, L.; Stoto, T.; Graetzel, M.; Fitzmaurice, D.; Shklover, V. *The Journal of Physical Chemistry* **1993**, *97*, 9493.
- [36] Lin, C. J.; Yu, Y. H.; Liou, Y. H. *Applied Catalysis B: Environmental* **2009**, *93*, 119.
- [37] Sfaelou, S.; Sygellou, L.; Dracopoulos, V.; Travlos, A.; Lianos, P. *The Journal of Physical Chemistry C* **2014**, *118*, 22873.
- [38] Jiang, J.; Oberdörster, G.; Biswas, P. *Journal of Nanoparticle Research* **2009**, *11*, 77.
- [39] Guindo, M. C.; Zurita, L.; Durán, J. D. G.; Delgado, A. V. *Materials Chemistry and Physics* **1996**, *44*, 51.
- [40] Liu, I. P.; Chen, L.-Y.; Lee, Y.-L. *Journal of Power Sources* **2016**, 325, 706.
- [41] Kumar, A.; Mandale, A. B.; Sastry, M. *Langmuir* **2000**, *16*, 9299.
- [42] Khomane, R. B.; Manna, A.; Mandale, A. B.; Kulkarni, B. D. *Langmuir* **2002**, *18*, 8237.
- [43] Okotrub, A. V.; Asanov, I. P.; Larionov, S. V.; Kudashov, A. G.; Leonova, T. G.; Bulusheva, L. G. *Physical Chemistry Chemical Physics* **2010**, *12*, 10871.
- [44] Mandrino, D.; Vrbancic, D.; Jenko, M.; Mihailovic, D.; Pejovnik, S. *Surface and Interface Analysis* **2008**, *40*, 1289.

- [45] Periyat, P.; Pillai, S. C.; McCormack, D. E.; Colreavy, J.; Hinder, S. J. *The Journal of Physical Chemistry C* **2008**, *112*, 7644.
- [46] Yu, J.; Yu, J. C.; Ho, W.; Jiang, Z. *New Journal of Chemistry* **2002**, *26*, 607.
- [47] Ching-Fuh, L.; Eih-Zhe, L.; Sheng-Ming, S.; Wei-Fang, S. *Japanese Journal of Applied Physics* **2003**, *42*, L610.
- [48] Johan, R. G.-M.; Yunier, G.-B.; Maria Luiza, M. R.; Marcelo, B. P.; Jefferson, L. P.; Luciano, C. A.; Carlos, M. A.; Denis, G. F. D.; Antonio Ferreira da, S.; Giovanna, M. *Nanotechnology* **2016**, *27*, 285401.
- [49] Liu, Z.; Fang, P.; Wang, S.; Gao, Y.; Chen, F.; Zheng, F.; Liu, Y.; Dai, Y. *Journal of Molecular Catalysis A: Chemical* **2012**, *363–364*, 159.
- [50] Antoniadou, M.; Daskalaki, V. M.; Balis, N.; Kondarides, D. I.; Kordulis, C.; Lianos, P. *Applied Catalysis B: Environmental* **2011**, *107*, 188.
- [51] Antoniadou, M.; Sfaelou, S.; Dracopoulos, V.; Lianos, P. *Catalysis Communications* **2014**, *43*, 72.
- [52] Bai, J.; Li, J.; Liu, Y.; Zhou, B.; Cai, W. *Applied Catalysis B: Environmental* **2010**, *95*, 408.
- [53] Bessekhoud, Y.; Robert, D.; Weber, J. V. *Journal of Photochemistry and Photobiology A: Chemistry* **2004**, *163*, 569.
- [54] Shi, J.-w.; Yan, X.; Cui, H.-J.; Zong, X.; Fu, M.-L.; Chen, S.; Wang, L. *Journal of Molecular Catalysis A: Chemical* **2012**, *356*, 53.

- [55] Kamble, A.; Sinha, B.; Agawane, G.; Vanalakar, S.; Kim, I. y.; Kim, J. Y.; Kale, S. S.; Patil, P.; Kim, J. H. *Physical Chemistry Chemical Physics* **2016**, *18*, 28024.
- [56] Xie, Y. P.; Yu, Z. B.; Liu, G.; Ma, X. L.; Cheng, H.-M. *Energy & Environmental Science* **2014**, *7*, 1895.
- [57] Wu, K.; Chen, Z.; Lv, H.; Zhu, H.; Hill, C. L.; Lian, T. *Journal of the American Chemical Society* **2014**, *136*, 7708.
- [58] Wu, L.; Yu, J. C.; Fu, X. *Journal of Molecular Catalysis A: Chemical* **2006**, *244*, 25.
- [59] Kudo, A.; Miseki, Y. *Chemical Society Reviews* **2009**, *38*, 253.
- [60] Mora-Seró, I.; Bisquert, J. *The Journal of Physical Chemistry Letters* **2010**, *1*, 3046.
- [61] Lan, Z.; Wu, W.; Zhang, S.; Que, L.; Wu, J. *Ceramics International* **2016**, *42*, 8058.
- [62] Jeong, M.-S.; Son, M.-K.; Kim, S.-K.; Park, S.; Prabakar, K.; Kim, H.-J. *Electronic Materials Letters* **2014**, *10*, 621.
- [63] Fu, H.; Liu, H.; Shen, W. *Nanoscale Research Letters* **2014**, *9*, 631.
- [64] Lessner, P. M.; McLarnon, F. R.; Winnick, J.; Cairns, E. J. *Journal of The Electrochemical Society* **1993**, *140*, 1847.
- [65] Zhang, Y.; Zhu, J.; Yu, X.; Wei, J.; Hu, L.; Dai, S. *Solar Energy* **2012**, *86*, 964.

HIGHLIGHTS OF THE PRESENT WORK

In this study titania nanotube array (TNA) have been effectively surface modified with quantum dots of chalcogenides and metal particles for enhanced photocatalytic applications.

- Pd loaded titania nanotubes (Pd@TiO_2) synthesized by a hydrothermal method have been successfully used for the effective catalytic reduction of p-Nitrophenol. A systematic study of Pd loading and its effect on the morphological stability of the underlying titania and catalytic reduction of p-nitrophenol have also been carried out.
- In Pd-loaded TNT's, this study has revealed the effect of the particle size of Pd and the morphology as well as the crystalline phase of the titania nanotube in their catalytic activity. The recyclability of the catalyst were also monitored and found that the rate constant is reduced in the successive cycles. Further studies aimed at improving the catalyst recyclability are in progress.
- PbS sensitised titania (PbS@TiO_2) nanotube array were synthesised using anodisation followed by successive ionic layer adsorption and reaction (SILAR) method. The SILAR cycle was found to play an important role to tune the photocatalytic and photovoltaic properties of PbS sensitised titania nanotube. The stability and recyclability of the PbS sensitised titania nanotube have been correlated with the photocatalytic activity through detailed X-ray photoelectron spectroscopic studies.
- In the CdS sensitized TNA (CdS@TiO_2) the photocatalytic and solar cell efficiency is dependent upon the number of SILAR cycles used for the CdS sensitization of the surface of titania nanotubes. CdS sensitized on

titania nanotubes using fifteen SILAR cycles have been found to exhibit maximum photocatalytic activity under visible light irradiation.

- The number of SILAR cycles employed was also found to determine the band potential, particle size and aggregation behaviour, which in turn determines the photocatalytic and solar cell efficiencies of the CdS sensitized titania nanotubes.
- Future work is aimed at improving the stability of chalcogenides by core-shell approaches, by adopting different morphologies and making effective coupling between semiconductors.

LIST OF RESEARCH PUBLICATIONS

1. **Vijila Kalarivalappil**, Suresh C. Pillai, Steven J. Hinder, V. Kumar and Baiju K. Vijayan “Stability studies of CdS sensitized TiO₂ nanotubes prepared using the SILAR method”, *Journal of Environmental Chemical Engineering*, **6** (2018) 1404
2. **Vijila Kalarivalappil**, C.M.Divya, W.Wunderlich, Suresh C. Pillai, Steven J. Hinder, Manoj Nageri, V. Kumar and Baiju K. Vijayan “Pd Loaded TiO₂ Nanotubes for the Effective Catalytic Reduction of p-Nitrophenol”, *Catalysis Letters*, **146** (2016) 474
3. Manoj Nageri, **Vijila Kalarivalappil**, Baiju K. Vijayan and V. Kumar “Titania nanotube arrays surface-modified with ZnO for enhanced photocatalytic applications”, *Material Research Bulletin*, **77** (2016) 35
4. N.B. Rahna, **Vijila Kalarivalappil**, Manoj Nageri, Suresh C. Pillai, Steven J. Hinder, V. Kumar and Baiju K. Vijayan “Stability studies of PbS sensitized TiO₂ nanotube arrays for visible light photocatalytic applications by X-ray photoelectron spectroscopy (XPS)”, *Material Science in Semiconductor Processing*, **42**, (2016) 303

Conference Papers

1. **Vijila Kalarivalappil**, Suresh C. Pillai, Steven J. Hinder, V. Kumar and Baiju K. Vijayan “Solar Cell and Photocatalytic Applications of Chalcogenide sensitized Titania Nanotube and It’s Stability” International Conference on Advanced Nanostructures, held at Catholicate College, Pathanamthitta, Kerala during March 12-14 2018

2. **Vijila Kalarivalappil**, Suresh C. Pillai, Steven J. Hinder, V. Kumar and Baiju K. Vijayan “Stability studies of Chalcogenide sensitized titania nanotube” International Seminar on Organic Molecules for Material Applications, held at Government College for Women, Thiruvananthapuram during September 19-22, 2017.
3. **Vijila Kalarivalappil**, Baiju K. Vijayan., Kumar V, “Titania films with anatase/rutile interface by simple sol-gel method for enhanced photocatalytic applications” Indo-US workshop on Nano-Structured Electronic Materials: Challenges & Relevance to Electronics & Energy Research (IUSWNM-2013), held at Thrissur, India March 8-11, 2013.
4. Manoj N., Aparna P. M. , **Vijila Kalarivalappil**, Baiju K. Vijayan, Kumar V., “Facile aqueous synthesis of ZnO nanorods and its photocatalytic studies” Indo-US workshop on Nano-Structured Electronic Materials: Challenges & Relevance to Electronics & Energy Research (IUSWNM-2013), held at Thrissur, India, March 8-11, 2013.
